The Pennsylvania State University

The Graduate School

Investigation of Various Factors Affecting Noise Emission from Roller Element Bearings

A Thesis in

Mechanical Engineering

Submitted in Partial Fulfillment
of the Requirements
for the Degree of

Master of Science

May 2021

The thesis of Jacob Elston was reviewed and approved the following:

Issam Abu-Mahfouz
Professor of Mechanical Engineering
Thesis Advisor
School of Science, Engineering, and Technology Program Chair

Amit Banerjee
Professor of Mechanical Engineering

Abdallah Ramini
Professor of Mechanical Engineering

Richard C. Ciocci
Associate Professor of Mechanical Engineering
Professor-in-Charge of Mechanical Engineering

ABSTRACT

A vast amount of research has gone into interpreting vibrational signals emitted from roller element bearings of various designs. Most of this research is dedicated to detecting bearing faults in damaged bearing or predicting the end of useful life for a worn bearing. There is little research dedicated to the exploration of the vibration signals emitted from new bearings operating under various conditions. This paper aims to document the result of scientific experiments, using the scientific method to the greatest extent possible, where bearing parameters are varied and compared. Although many types of roller bearing designs exist, all bearings tested in this paper were spherical roller element type bearings. All tested bearing were composed of only the inner race, outer race, balls, and cage; no bearings were tested with integral mounting block, retaining devices, etc. All bearings had any seals and manufacturer provided lubricant removed. Standard ball bearings, deep groove ball bearings, and 'low quality' ball bearings were tested at varied loads, with varied speeds, and different viscosity lubricants. Statistical data (kurtosis, skewness, crest factor, and standard deviation) was collected and compared, along with frequency domain data (FFT, and Burg), and wavelets. The same data was also collected and analyzed for a load cell placed between the test bearing and the hydraulic cylinder used to generate the radial load. The raw data was processed by Matlab and exported to Excel where a multitude of figures were generated that allowed for the easy comparison of data. Conclusions were drawn based on the comparisons made. The goal is to provide additional information to engineers and equipment designers, for selecting the most appropriate bearing, when it is desired to minimize vibrations emissions from operating equipment.

TABLE OF CONTENTS

LIST OF FIGURES

ACKNOWLEDGMENT

I would like to offer my most sincere gratitude to my advisor Dr. Issam Abu Mahfouz and the committee members Dr. Banerjee, and Dr. Rimini. My experience undergraduate experience with the Pennsylvania State University, and Specifically with Dr. Abu Mahfouz, greatly influence my decision to return to academia. I'm fortunate that my career path and the expertise of Dr. Abu Mahfouz aligned and allowed for the deeper exploration of the topic of this paper. The topic of the paper is bearing, but the knowledge and knowledge related to sensors, data acquisition, signal processing, programming, etc. were of equal value.

I'd also like to thank my employer for the partial funding of the project, and specifically the Engineering Director for the scheduling flexibility provided; without it, this would never be possible.

The Air Force Reserves, specifically the commander of the 514LRS, for maximizing the schedule flexibility associated with training evolutions.

Lastly, the greatest sacrifices made for this thesis were my two young children and wife. The time spent away from them, while on campus and in the local library, is time children were without a father and a wife without a husband. I beg your forgiveness with the hope that my master's degree will allow me to provide you a better life.

CHAPTER 1

INTRODUCTION

Mechanical equipment usually involves the motion of one, or more, components relative to a stationary base. The motion may be rotary, linear, or some combination of the two. The stationary component will necessarily have to support and transmit the forces associated with the moving components. There is no ideal combination of material, lubricant, and design suitable for all situations where a moving component must be supported. Therefore, careful consideration must be given to the areas in contact experiencing relative motion or a tribological failure will occur, usually resulting in equipment failure. Areas in contact and experiencing relative motion are usually equipped with a bearing or bushing made from carefully selected materials with appropriate lubricants. The material and lubrication selections made are based on consideration of variables such a: type of motion (rotary, linear, or some combination), radial loading, axial lading, relative speeds, available space, maintenance, cost, cycles to failure, etc. Depending on the circumstances, some of these variables will be of primary concern while others are of little concern. Another variable of concern is the vibration signature of the equipment as a whole. Depending on the type of equipment, a significant portion of the vibration generated could be related to the bearings and bushings as a moving component rotates or translates relative to the stationary component supporting it. Much research has gone into understating the mechanism of vibration generation in bushings and roller element bearings with efforts to reduce it. Reducing vibration has several benefits to include, greater efficiency, longer component life, reduced noise pollution and more favorable

ergonomics. V. Bucinskas explains how noise is considered a technical problem and its effects on machinery are always negative [1]

Bushing are generally reserved for operating conditions characterized by high load and low relative velocities and are not the subject of this paper. This paper focuses on roller element bearings where the roller elements are spherical. It should be noted that roller elements come in a variety of alternative geometries with tapered rollers, cylindrical, and needle rollers being very popular. Spherical roller element bearings come in a variety of designs based on their applications. Standard spherical ball bearings are traditionally used in applications where the bearing will predominantly experience radial loads with very little axial load. Deep groove ball bearings are used where radial loads are the dominant load but can tolerate some degree of axial load without significantly reducing bearing life. Offset groove ball bearings are designed to transmit moderate amounts of both radial and axial loads. Bearings often work in sets; an example is a duplex arrangement. In a duplex arrangement two offset groove ball bearings can be assembled in series on a rotating shaft with the offset being in opposite directions. In the sense, both bearings share responsibility for supporting radial load and one bearing supports axial load in one direction and the other supports axial load when the direction of axial load is reversed. Some bearings come are 'self-aligning', meaning they can automatically reposition within their housing so that the bore of the bearing is parallel with the outside diameter (OD) of the shaft it supports.

The past several decades have seen a wide variety of studies aimed at understanding bearing vibration and analyzing it for signs of bearing failure onset. H. Qiu conducted experiments using wavelet filters to detect the decaying ringing sound associated with failure

[2]. Y. Lei proposed improvements to kurtosis and kurtograms to assist in fault diagnostics in roller element bearings [3]. D. Fernandez-Fracos reports this type of research is frequently geared towards bearing that are late in life or newer bearings ‘seeded’ with a fault [4]. This paper aims to employ existing bearing analysis techniques with the purpose of manipulating bearing variables to identify the circumstances under which a rotating component can be properly supported with minimal vibration from healthy bearings.

Chapter 2

Spherical Ball Bearing Model

Rollers in roller element bearings can be fabricated from a variety of materials with plastic, bearing steel and ceramic being the most popular. Plastic bearings are excluded from this paper due to their inability to support high loads. Also, plastic bearing have limited operations speeds due to the heat generated from friction and plastics inability to tolerate elevated temperatures. V. Bucinskas, X. T. Bai, and V. K. Augustaitis have conducted extensive research into noise emission from bearings with roller elements composed of ceramic and report elevated noise emission due to the increased stiffness ceramic offers as a material [1, 5, and 6]. Ceramic bearings, either full ceramic or hybrid ceramic, with their increased stiffness tend to emit strong vibrations. This is especially true when operating at high rotational speeds. Seeing as how this paper is aimed at identifying spherical roller bearing designs that emit the least vibration energy, ceramic bearings were excluded.

Spherical ball bearings have four main components; inner race, outer race, spherical balls, and cage. The races, inner and outer, act as intermediaries between the balls and housing / rotor. Without the races, indentation of the balls would cause localized deformation of the housing / rotor and the surface would fail in short order. The races are fabricated from a hard material capable of resisting indentation assuming load limits are respected. The balls are generally fabricated from bearing steel, a hard material also capable of resisting deformation. The presence of the balls allows for rolling friction as opposed to sliding friction, with rolling friction having a much lower coefficient of friction than sliding friction. The cage keeps the balls physically separated from one another. All bearings are fabricated with a clearance such that

the outside diameter of the inner race plus two times the outside diameter of the balls is less than the inside diameter (ID) of the outer race. This is necessary to allow for thermal expansion.

There are several known sources of vibration in a roller bearing for a given design. According to H. T. Shi, the dominant noise source is the transition of load from one or several balls as one ball exits the load bearing region of the bearing and another enters the load bearing region [7]. This paper and the design of the test rig used, assumes the shaft is mated to the inner race and is rotating and a stationary housing containing the outer race; although the opposite is also possible. The extent of loading is closely related to the amplitude of the emitted vibration energy. Y. Wang, while discussing the advantages of wavelet analysis, and R. B. Randal, while attempting to decompose total system vibration into individual component vibration, emphasize the relationship between shaft speed and how it directly relates to the frequency of the emitted noise energy [5, 9]. The emitted noise associated with balls entering and exiting the loaded region is greatly influenced by the homogeneity of ball diameter. For instance, an oversized ball entering the loaded zone will abruptly assume a large load and result in increased vibration and noise. Conversely, an undersized ball will leave the shaft unsupported in a manner allowing it to 'fall', likely onto an incoming bearing and result in increased vibration as described by H. T. Shi and J. Liu [7, 10]. While studying sound emission of roller bearings under radial load, J. Ban shows that even a theoretical bearing with perfect dimensions would still be expected to generate noise as a result of elastic deformation [11]. Noise is also generated as unloaded bearings either roll or skid along the inside diameter of the outer race, assuming rotational speed is sufficient for centrifugal force to keep the balls in contact with the outer race. At low shaft speeds (low centrifugal force) H. T. Shi and Y. Zhao

both report an impact between the roller element and inner race. If rotational speed is insufficient to keep the ball in contact with the outer race, they will generate noise as gravity pulls the ball through the bearing clearance and into contact with the inner race [7, 12]. H. T. Shi's research shows how loaded and unloaded balls regularly loose and make contact with the race as the bearing assembly makes its way through a complete revolution [7]. Although other sources of noise exist inside of a bearing, these are considered most significant.

J. Bans research on radial bearings operating under various loads shows that for a given bearing design, operating conditions also influence sound and vibration [11]. H. T. Shi's research into noise emission of ceramic bearings with varying amounts of lubricant, some containing friction modifiers, concluded the amount and type of lubricant impact noise emission [7]. A lubrication film is known to increase stiffness as it take up some of the bearings design clearance and supports the load to the extent allowed by its viscosity. W. Jacobs used electrical resistance to measure bearing lubrication film thickness and could show that the existence of an oil film increases bearing dampening [13]. High rotational speeds combined with high viscosity lubricants result in highly pressurized lubricant at the leading edge of the interface of the ball and race. J. Ban used models to prove high pressure lubricant can result in elastic deformation of the balls and races. These results in a thicker oil film, increased dampening, and reduced vibration [11]. High speed and high load conditions can lead to localized areas of low pressure in the lubricating film. At a sufficiently low pressure, gases dissolved in the lubricant diffuse out of solution and create a gas void between a ball and race. The gas void leaves the ball locally and temporarily unsupported. This loss and reacquisition of support leads to vibration and emitted noise energy. M. J. Braun modeled the fluid film of

bearings and concluded that if speed and load are further sufficiently increased, the lubricants will cavitate. Several types of cavitation have been noted; traveling, fixed, vortex, and vibratory. Cavitation occurs at the area of lowest film thickness adjacent to the stationary surface and results in a film rupture [14].

F. Immovilli conducted experiments to investigate the influence of shaft radial load on bearing fault signatures. He concluded that the inner race, outer race, and balls will deform as load is increased [15]. W. Jacobs showed this deformation will allow more balls to support the load and bearing stiffness increases [13]. He also predicts each bearing component will have its own thermal response due to changing operational speed. The inner race is known to heat up more due to its lower thermal capacitance and therefor expand more [13].

Chapter 3

Experimental Equipment

Test apparatus description

A bearing test apparatus was designed and fabricated to facilitate bearing analysis. CAD models and photographs of the test rig can be found in images 1 through Figure 3. Photos of the test ring can be found in Figure 4 through Figure 6. The test apparatus is capable of varying; shaft speed, load, bearing type, and lubricant. Speed variations were accomplished via a ½ horse power 220V motor powered by a variable frequency drive (VFD). The shaft was chosen for sufficient rigidity and was supported by two 'mid-bearings'. The mid-bearings were chosen to have a significantly higher load capacity than the test bearings. This kept the mid-bearings in a low load condition regardless of the load put on the test bearing. The intent was to keep the noise contribution of the mid-bearings relatively constant for all tests. The mid bearing closest to the bearing being tested was outfitted with an accelerometer. The motor shaft was coupled to the test shaft via a flexible jaw coupling. The bearing being tested was installed in fixture that produced a radial load as a hydraulic cylinder was extended. A piezo electric load cell was installed between the hydraulic cylinder and fixture to record radial load. The test rig produced radial loads on the test bearing; axial loads were not produced or measured. The bearing fixture was outfitted with an accelerometer and placed inside of a sump containing a thermocouple that could be filled with various oils. All of this was mounted on a heavy and rigid steel base. The shaft and bearing fixture were sized to allow testing of a variety of bearing types with minimal exchange of test apparatus parts. The test rig had two configurations. The first configuration allowed for the testing of 'small' bearings with a 1" ID and 2" OD, of which a high

quality standard bearing, low quality standard bearing, and deep groove bearing were tested, see Figure 7. The second configuration allowed for testing of a ‘large’ bearing with a 72mm OD and 53mm ID, of which a high quality standard bearing, low quality standard bearing, and deep groove bearing were tested, see Figure 8. Most bearing arrived from the distributor sealed and lubricated. All seals were removed and the bearing cleaned of the manufacturers’ lubricant before being installed in the bearing fixture and immersed in the oil sump.

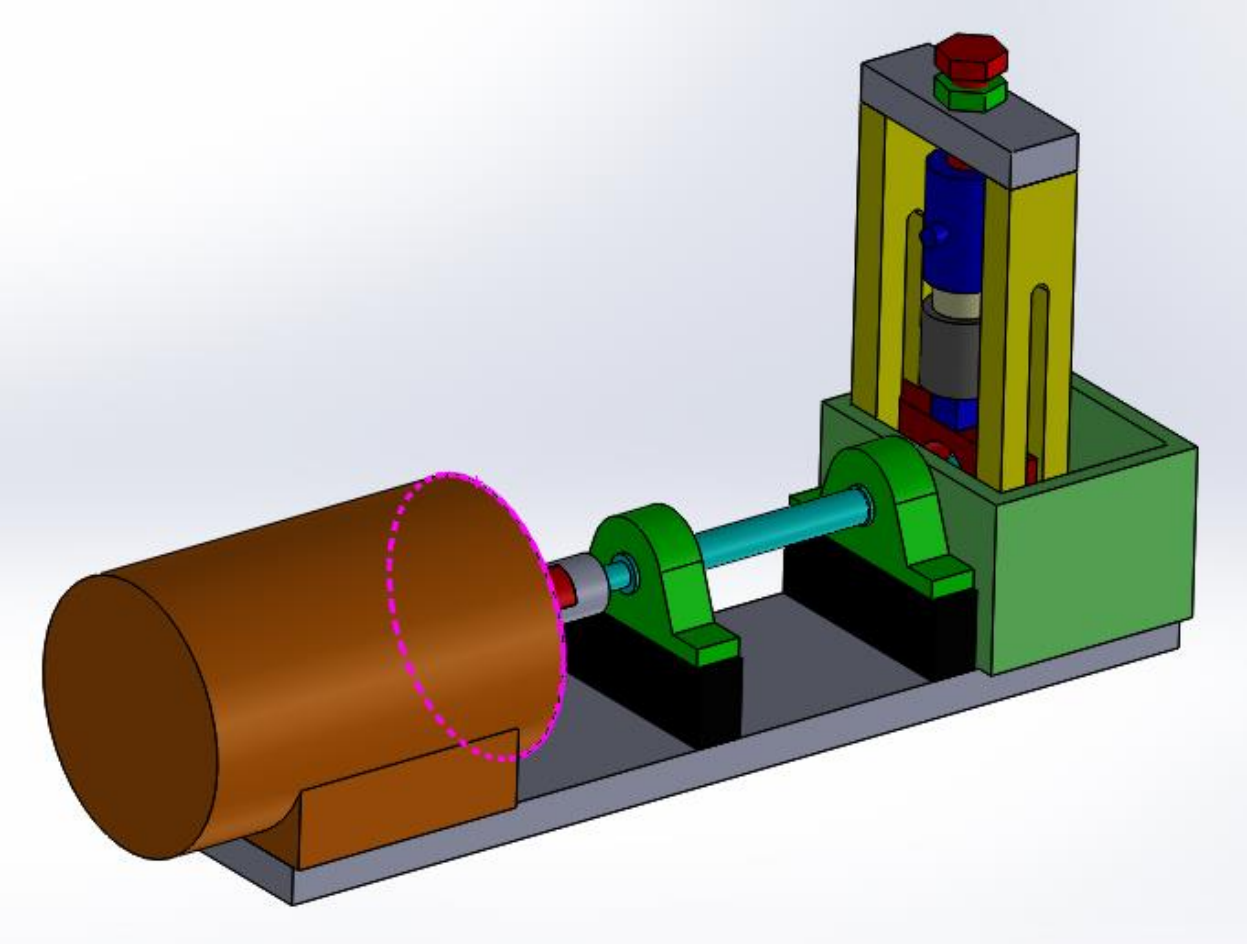

Figure 1: CAD image from top left corner of test rig

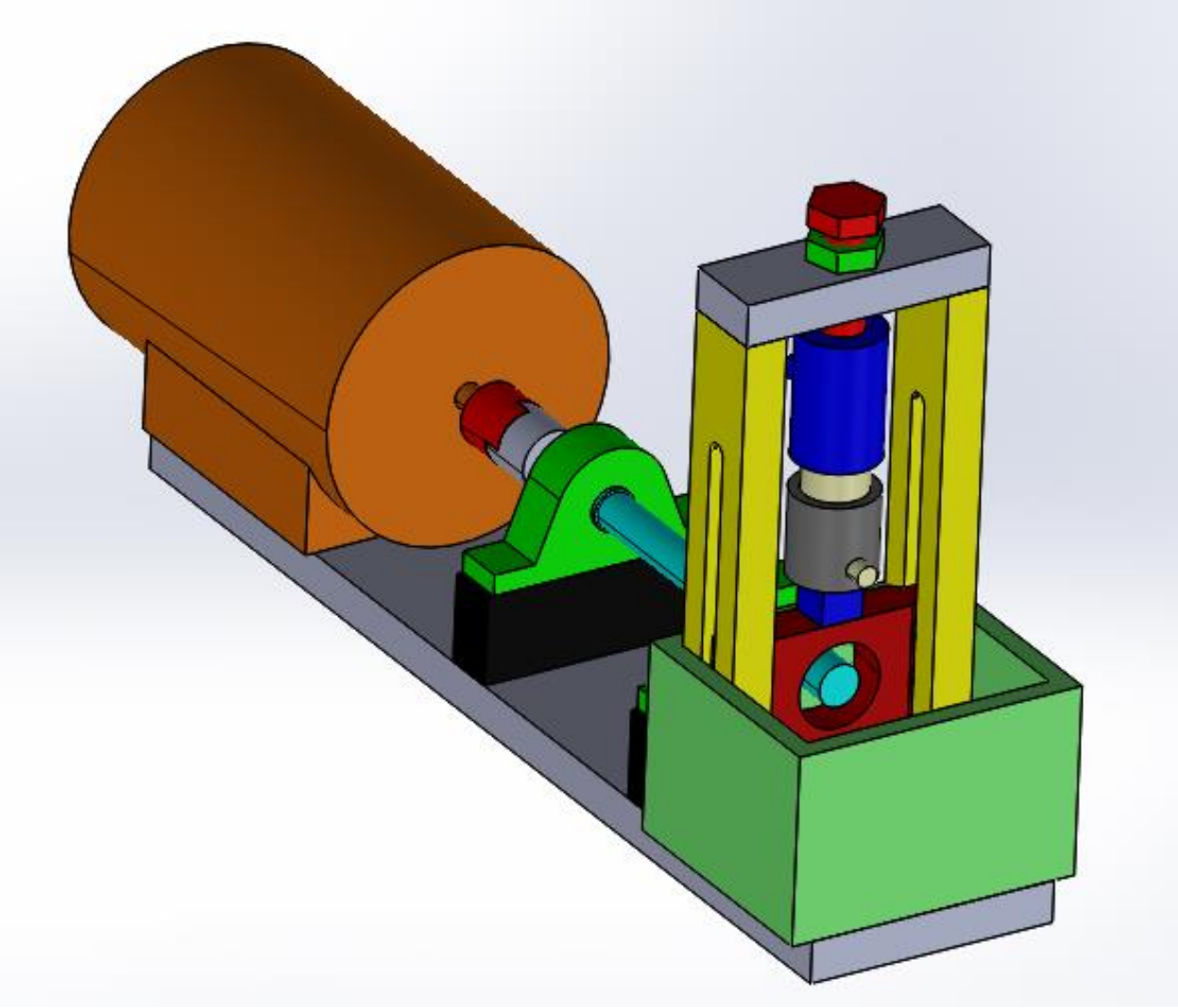

Figure 2: CAD image from top right corner of test rig

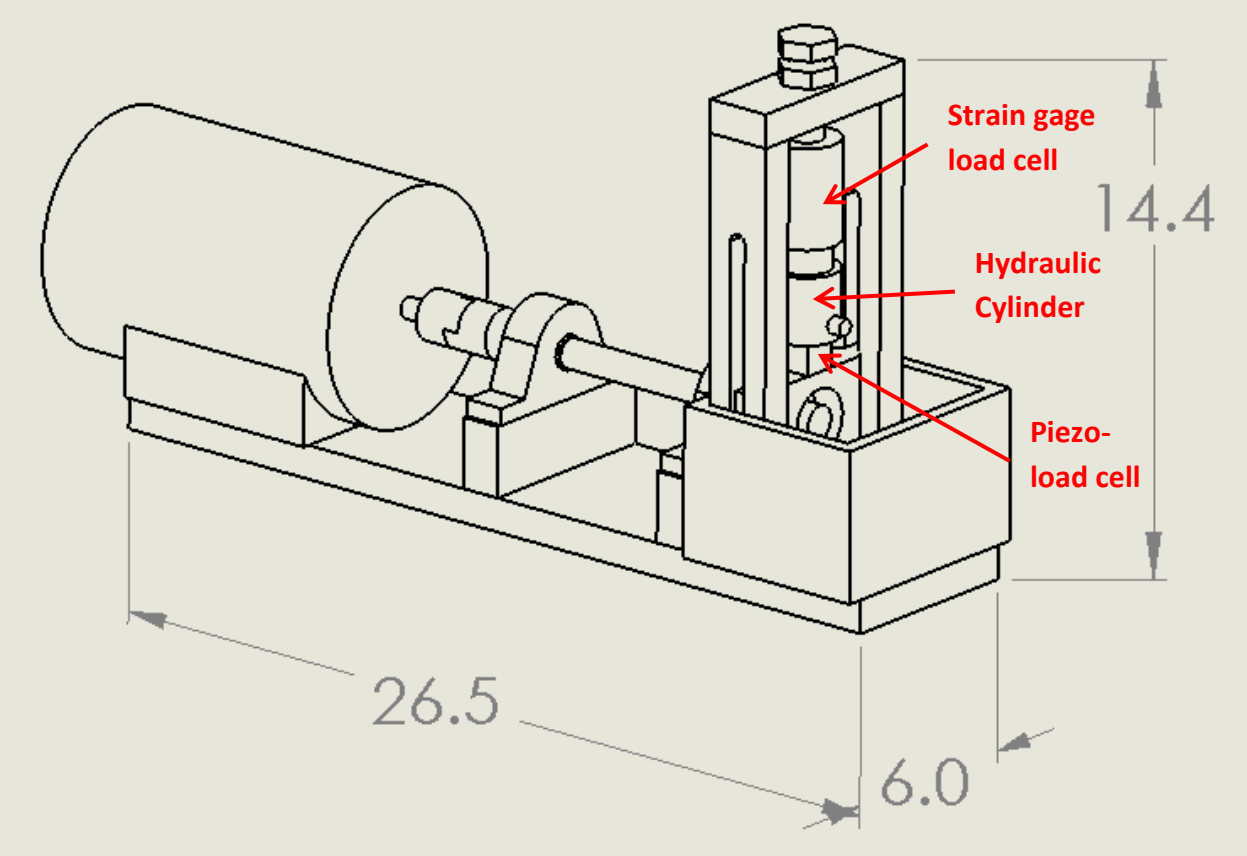

Figure 3: Test rig drawing with overall dimensions

Figure 4: Arial view containing the equipment used in testing (minus data acquisition)

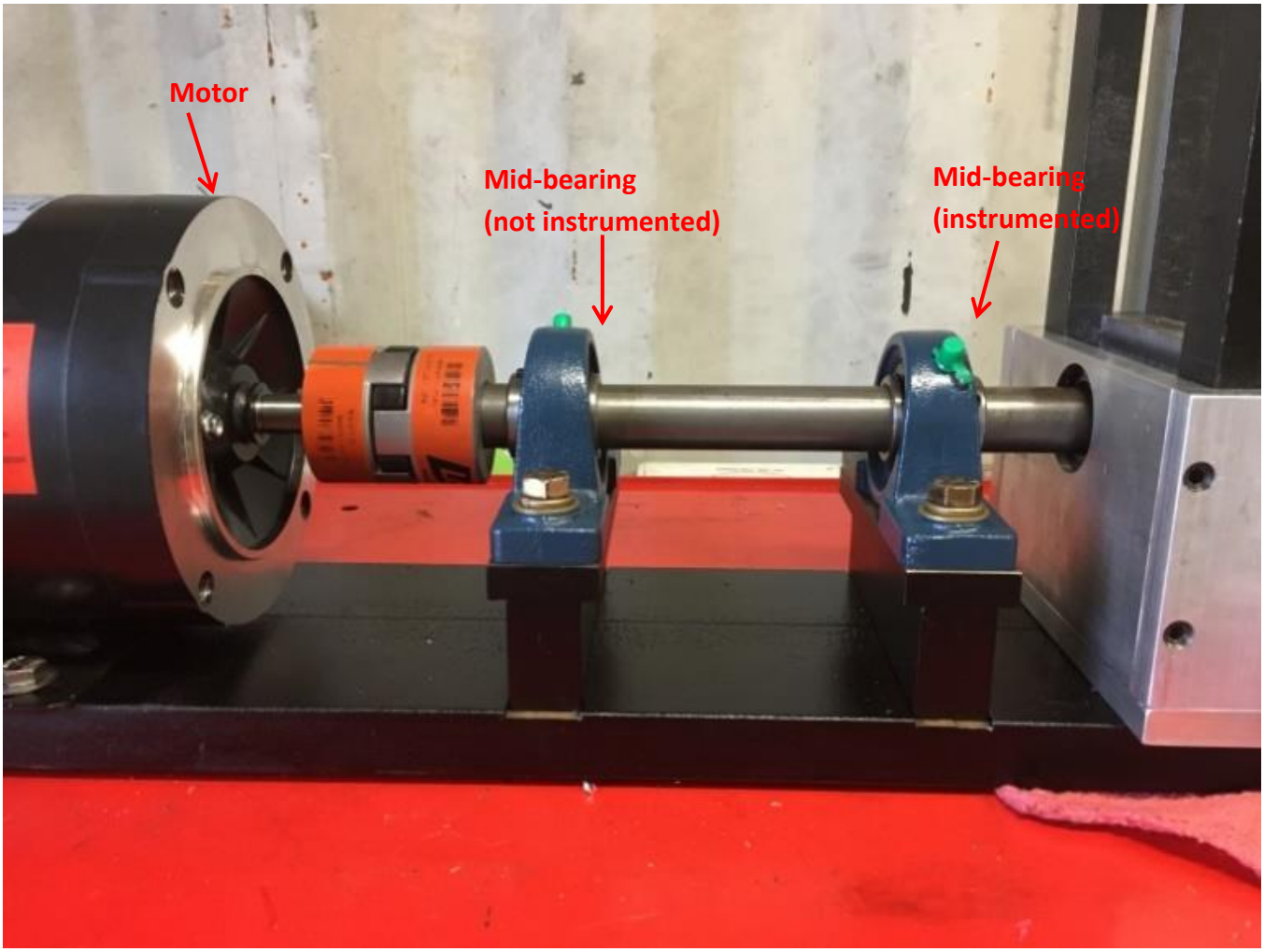

Figure 5: Close up side profile of test rig

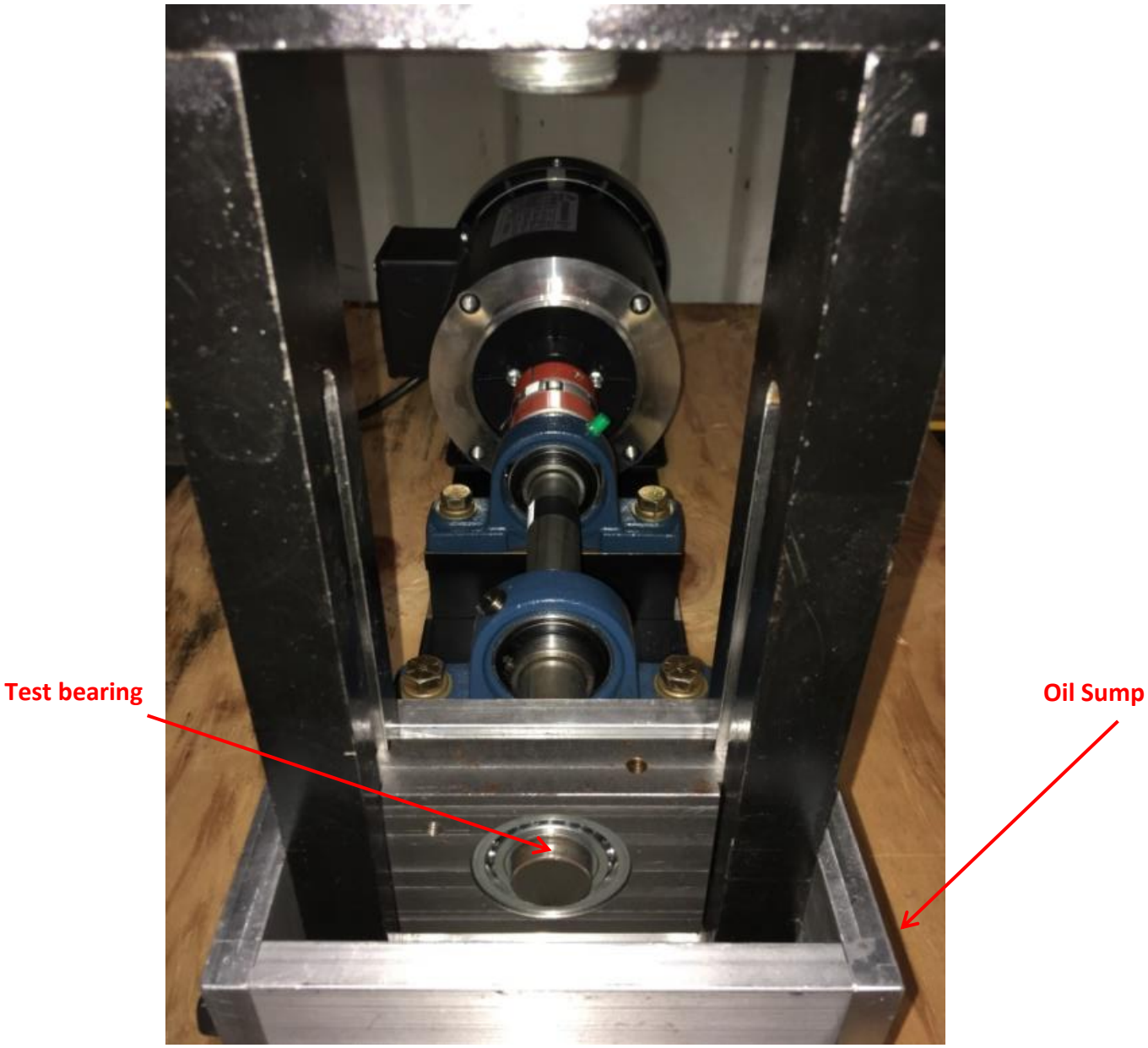

Figure 6: View along shaft (Load cell and hydraulic cylinder removed)

Figure 7 Bearing housing and shaft used for bearings with 2 in OD bearings

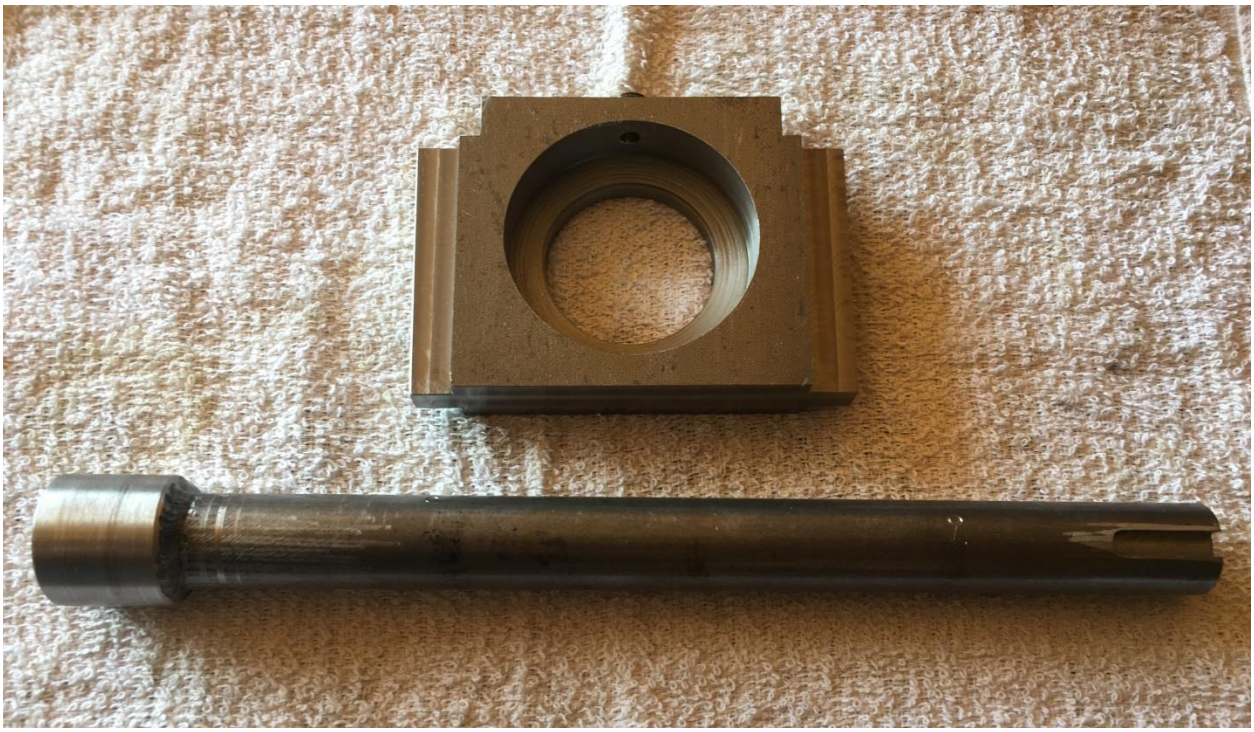

Figure 8: Bearing housing and shaft used for bearing with 72 mm OD bearings

Instrumentation and electronics Data

Piezoelectric load cell: PCM model 208C05

Strain gage load cell: Key Transducers model 1303-02A

Strain gage load cell signal conditioner: Key Transducers model 8120-11A

Accelerometers (test bearing and mid-bearing): IMI model 607A62/*

Thermocouple power supply: Phoenix Contact model CM62-PS

Data acquisition: National Instruments model BNC-2120 with National Instruments model USB-6251 interface

Piezo load cell signal conditioner: PCB Piezotronics model 482B05

VFD: Automation Direct model GS2-20P5

Tachometer: Neiko

Motor: Manufacturer: IronHorse model MTR2-P50-3BD36

Test bearing data

1” ID 2” OD standard bearing (Figure 9)

Manufacturer: Nice

Model: 1641DCTNTG18

As advertised: “Precision ground radial bearing…C0 internal clearance”

Dynamic load capacity: 2967 LBF

Race material: Nylon

Max RPM: 5000

Number of balls: 10

Figure 9: Image of small standard bearing

1” ID 2” OD deep groove bearing (Figure 10)

Manufacturer: Titan

Model: R16 2RS PRX BL

As packaged: “Ball - deep groove - inch”

Dynamic load capacity: 1850 LBF

Race material: metal

Max RPM: not provided

Number of balls: 10

Figure 10: Image of small deep groove bearing

1” ID 2” OD low quality bearing (Figure 11)

Manufacturer: General Bearing Corporation

Model: 23210-01

As packaged: “Value Collection” and “Unground full complement ball bearing”

Dynamic load capacity: 1384 LBF

Race material: no race

Max RPM: 2500

Number of balls: 19

Figure 11: Image of small low quality bearing

35mm ID 72mm OD standard bearing (Figure 12)

Manufacturer: ORS

Model: 6207-2RS-G93-C3

As advertised: “high precision” and “ABEC 5”

Dynamic load capacity: 5771

Race material: plastic

Max RPM: not provided

Number of balls: 9

Figure 12: Image of large standard bearing

35mm ID 72mm OD deep groove bearing (Figure 13)

Manufacturer: NTN

Model: 6207C4

As packaged: “Precision: Grade 0”

Dynamic load capacity: 25700 N

Race material: metal

Max RPM: 25700

Number of balls: 9

Figure 13: Image of large deep groove bearing

35mm ID 72mm OD low quality bearing (Figure 14)

Manufacturer: ZSKL

Model: 6207-2RS

As advertised: “ABEC 3” and “Premium ball bearing”

Dynamic load capacity: not provided

Race material: metal

Max RPM: not provided

Number of balls: 9

Figure 14: Image of large low quality bearing

Lubricant Data

Thin oil

Manufacturer: Mobil 1

Viscosity: 5W-20

As advertised: “Advanced full synthetic motor oil”

Thick oil

Manufacturer: Warren

Viscosity: 85W-140

As advertised: “Gear Oil” and “API service GL-5”

Chapter 4

Discussion

Tests were conducted at four speeds; 500, 1000, 1500, and 2000 rpm. Note that the motor produced insufficient torque at some low peeds at high loads; the motor stalled and was reported as such. Results for 1000 rpm and 2000 rpm were often used for comparison. Likewise, the bearings were tested as load was varied. Testing included four discrete loads with one being a no load condition. At the no load condition, the bearing was only subjected to the weight of the bearing itself and the weight of the bearing housing.

It was generally found that all bearings types, at all loads, all speeds, and with thin and thick oil had relatively similar vibrations signal. This was to be expected due to the fact that all bearing were new and defect free. As a result, the data analysis process had to be adjusted. Some analysis was abandoned due to not being sensitive enough to detect the minute differences between healthy bearings of various designs. Additional analysis and filtration was performed to reveal the minute details of a given bearing operating with a particular load, speed, and lubricant type.

Statistical Time Domain Methodology

A combination of Matlab and Excel were employed to process data and develop graphs. Mean, skewness, standard deviation, kurtosis, and crest factor were all calculated for the test bearing and piezoelectric load cell. A. Sharma used kurtosis, skewness, crest factor and standard deviation in his feature extraction and fault severity research and defined them as shown below [16].

Kurtosis: kurtosis is a statistical parameter that is used to describe the distribution of observable data around the mean. Kurtosis is defined as the degree to which a statistical frequency curve is peaked

$$Kurtosis = \left[\frac{n(n+1)}{(n-1)(n-2)(n-3)}\sum\left(\frac{x_i - \bar{x}}{s}\right)^4\right] - 3\frac{(n-1)^2}{(n-1)(n-2)}$$

A bearing with a low kurtosis is more desirable.

Skewness: skewness describes the degree of symmetry of distribution around its mean. Skewness can be negative or positive.

$$Skewness = \frac{n}{(n-1)(n-2)}\sum\left(\frac{x_i - \bar{x}}{s}\right)^3$$

Crest Factor: crest faction is the ratio of the peak value over RMS value for a given signal and indicates the shape of the waveform.

$$Crest\ Factor = \frac{maximum\ peak}{RMS}$$

Standard Deviation: standard deviation is a measure of the energy contained in a vibration signal.

$$Standard\ Deviation = \sqrt{\frac{n\sum x^2 - (\sum x)^2}{n(n-1)}}$$

Frequency Domain Methodology

A bearing vibration signal is composed of data a various frequencies strung together in sequence. A frequency domain analysis decomposes the vibration signal into its component frequencies. Portions of the signal with like frequencies are grouped together and summed. The vibration of the bearing is a form of kinetic energy and a frequency domain analysis illustrates the frequencies releasing more or less energy.

There are several analytical methods to convert time domain data into frequency domain data. The Fast Fourier Transform (FFT) is a popular method and used to generate data in this paper. The Burg method was also attempted. Ultimately, the Burg method, and the data it generated was abandoned due to poor data resolution.

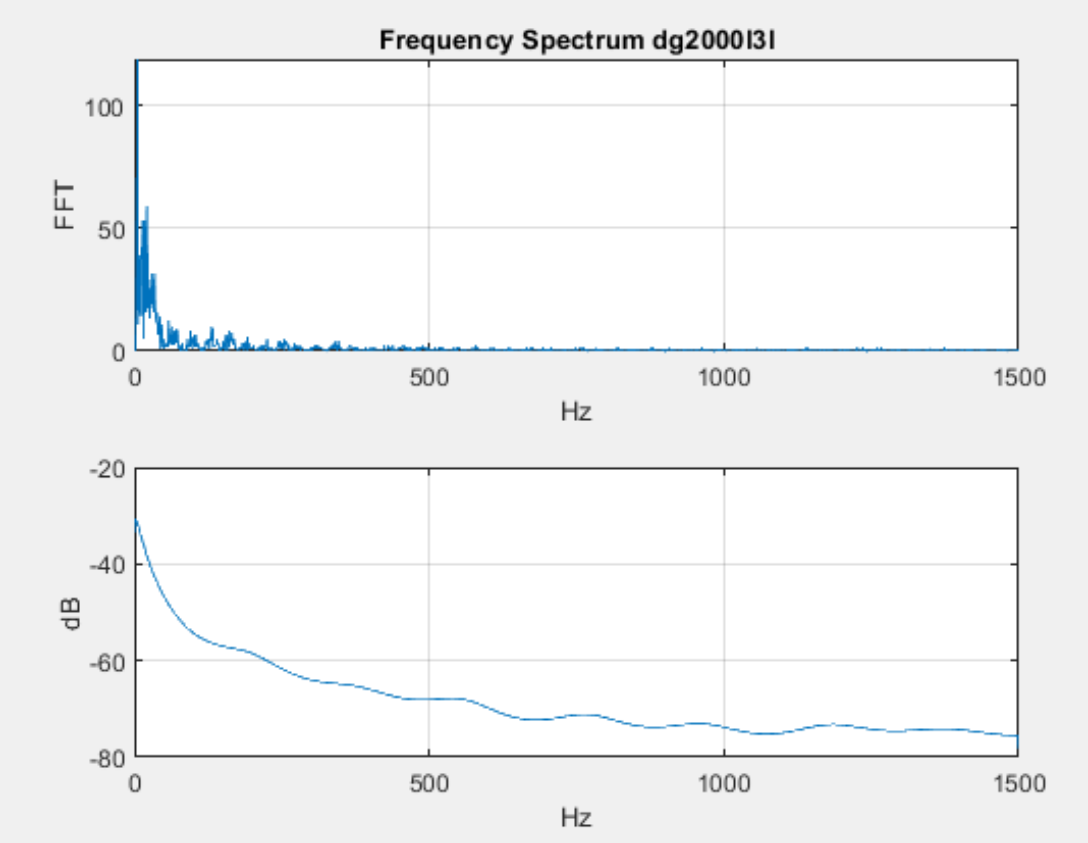

Figure 15: Example images produced by MATLAB of FFT (top) and Burg (bottom)

The superposition of one FFT graph over another FFT graph for bearings with similar vibration signals creates an image that is difficult to interpret. To make the data more easily interpreted, the FFT signal was divided into discrete segments and the averages of those segments are plotted. The size of the segments was selected as to not loose significant amounts of data when averaging.

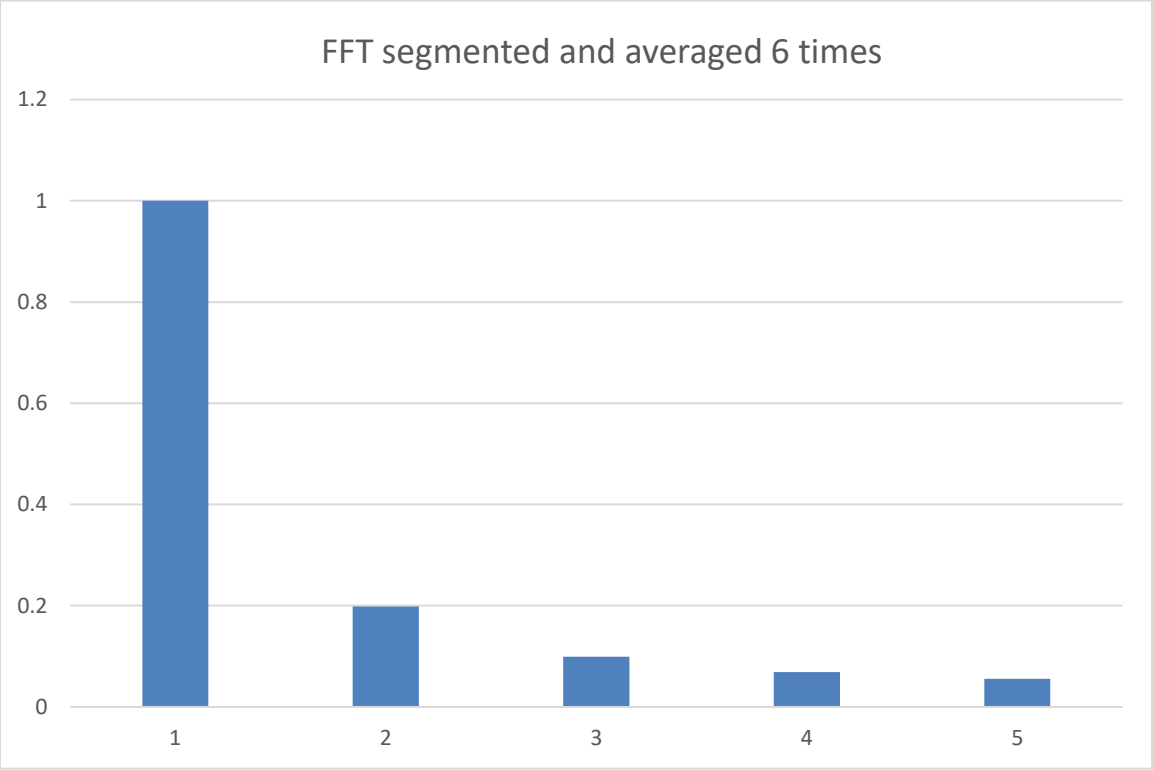

Figure 16: Sample images of FFT data segmented and averaged 6 times

The data processed to generate Figure 16 is the same data used to generate the FFT graph in Figure 15. Note the similarity in overall shape, parabolic decrease from left to right, but more easily compared as shown in Figure 17 below.

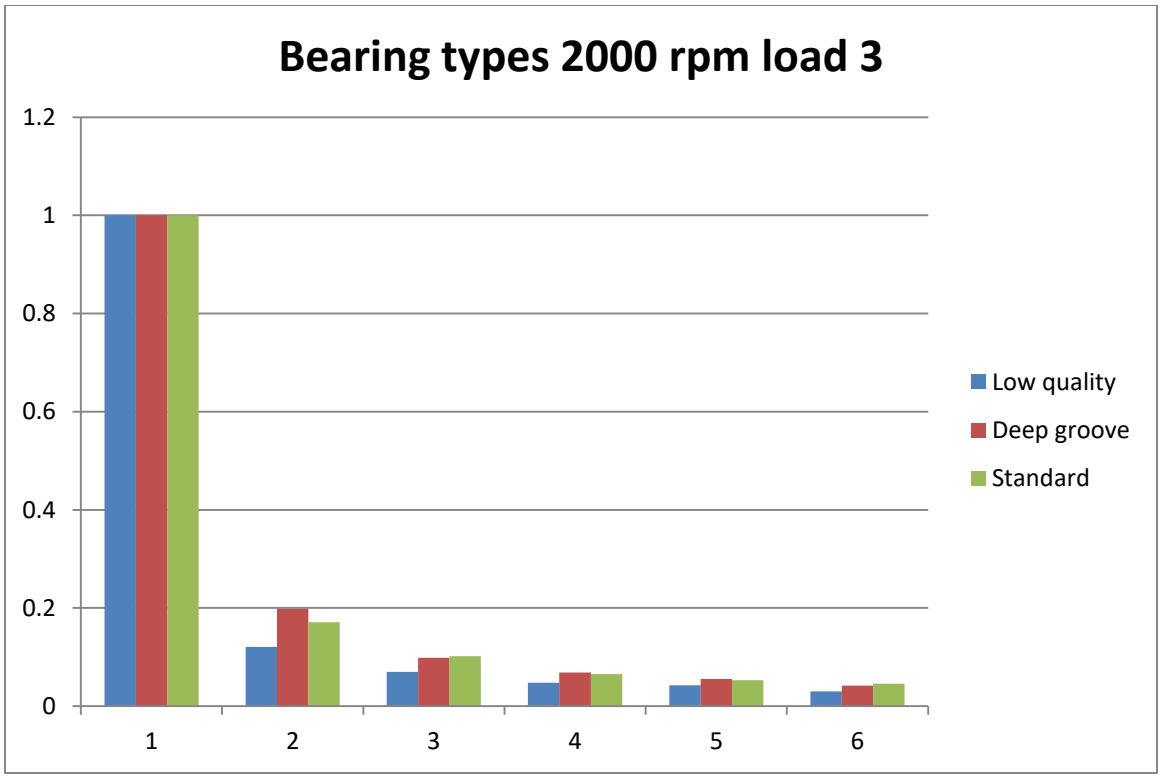

Figure 17: Sample images of multiple segmented and averaged FFT images plotted on same graph

Wavelet Analysis Methodology

The wavelet analysis was completed using Matlab's Continuous Waveform Transform function (CWT) employing the 'Mexican hat' wavelet form. An image of the Mexican hat waveform can be seen traced in black in Figure 18 below.

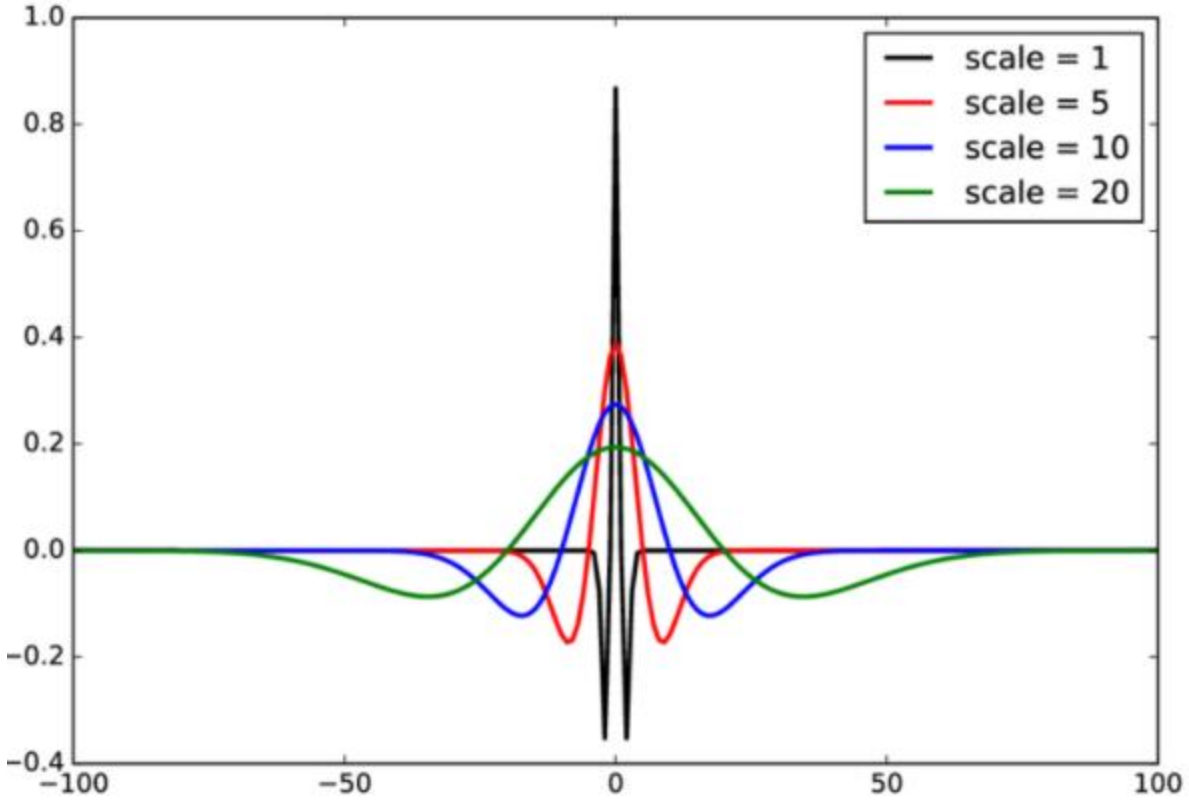

Figure 18: Various scales of the Mexican hat waveform (Image from CIELO-RGS: a catalogue of soft X-ray ionized emission lines by Junjie Mao)

Matlab's CWT function scales (dilated or contracted) the Mexican hat waveform along the horizontal axis; examples of Mexican hat waveform scales can be in blue, green and red lines in figure 18 above. For each scale, the CWT function will superimpose the scaled Mexican hat wave form over the vibration waveform data and analyze the difference/agreement. The difference/agreement is calculated by integration using the equation found below.

$$C(a,\mathrm{T}) = \int \frac{1}{\sqrt{a}} \Psi \frac{t-\mathrm{T}}{a} x(t)dt$$

Where Ψ (t) represents the Mexican hat waveform shifted in time by t and dilated or contracted by a and then correlating it with vibration waveform represented by x(t). The results of a

wavelet comparison can be shown visually in a scalogram. A sample scalogram is shown in Figure 19 below.

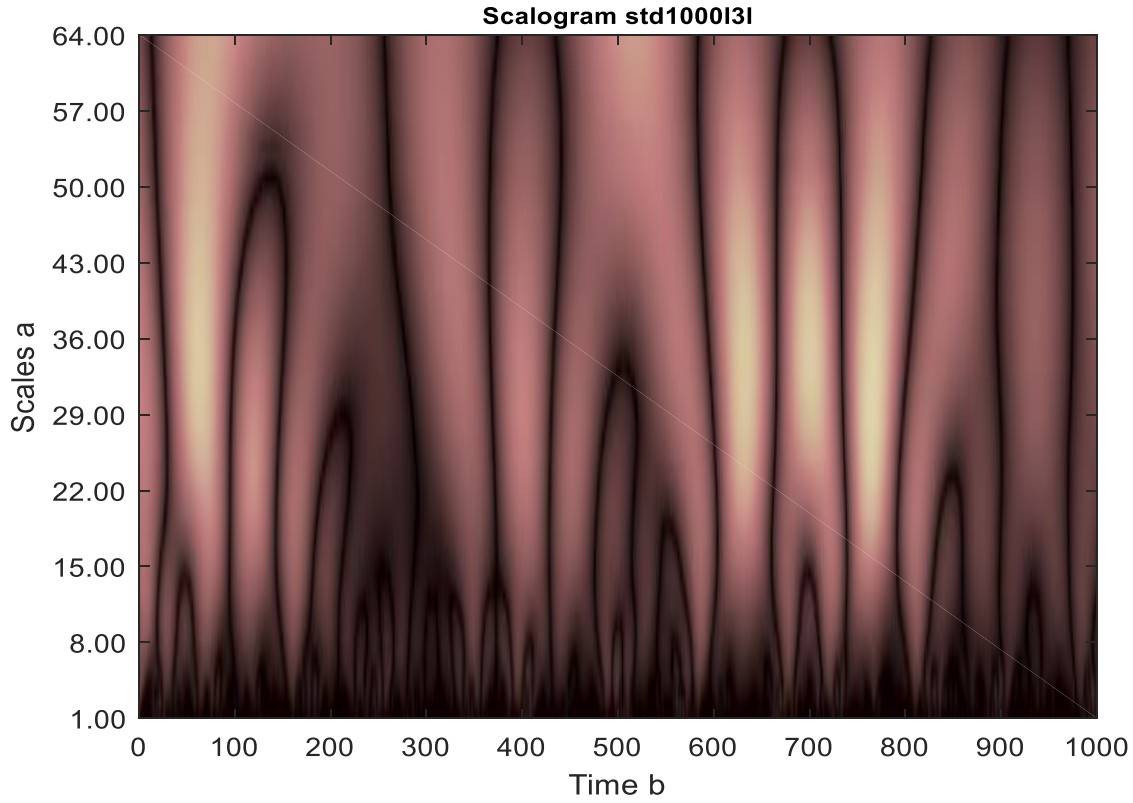

Figure 19: Sample scalogram

The vertical axis represents the dilation or contraction of the Mexican hat with large largest dilations at the top and the smallest contractions at the bottom. Bright areas represent strong agreement between the vibration signal and the Mexican hat signal for a particular scaling. Darker regions represent poor signal agreement. The horizon axis show the comparison of a scaled Mexican hat to 1000 vibration signals over time interval b. Scalograms are rarely used for a quantitative analysis. Note that approximations and the data at high scale values (top) of a scalogram represent low frequency data. Also, note that details and the data at low scale values (bottom) of a scalogram represent high frequency data.

The raw data was processed through a Savitzgy-Golay digital filter, Matlab function ‘sgolayfilt’. A pictorial representation of the Savitzgy-Golay filter is shown in Figure 20 below.

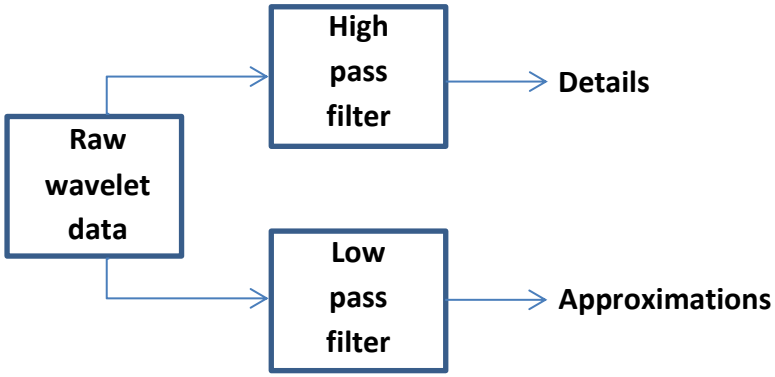

Figure 20: Savitzgy-Golay digital filter functional schematic

Following each pass through the Savitzgy-Golay filter the skewness and kurtosis was calculated. This process was repeated ten times for each signal. A sample of this process is shown below in Figure 21.

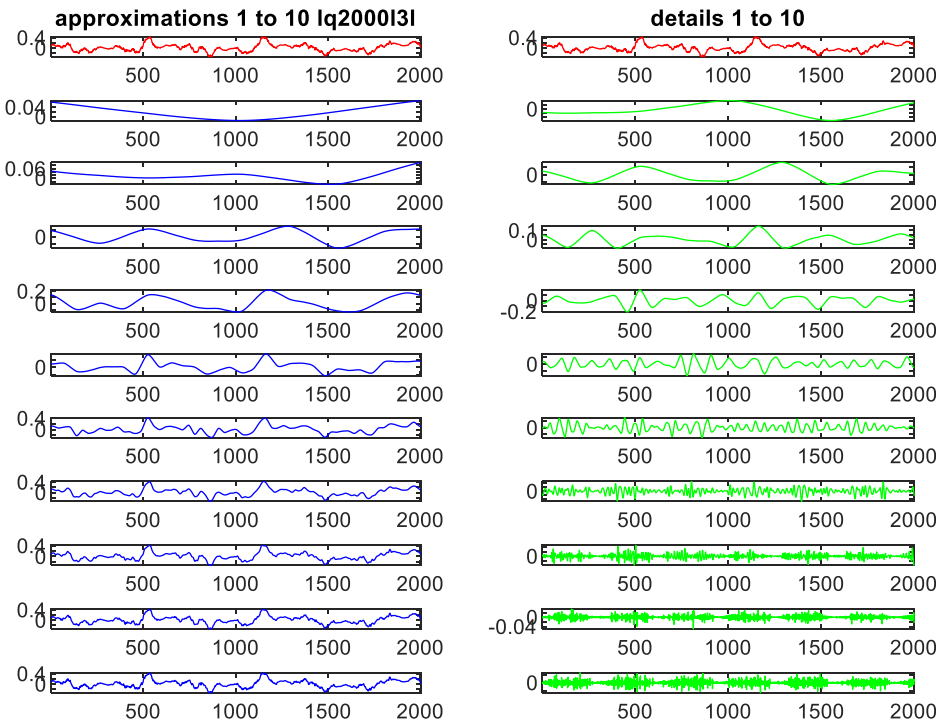

.

Figure 21: Sample progression of wavelet data through a Savitzgy-Golay filter

The red curve at the top represents original vibration signal with minimal filtering. The first pass through the Savitzgy-Golay filter is shown at the bottom, note approximations are on the left in blue and details are on the right in green. Also note the smoothing effect filtering has on the signal as it proceeds from the bottom to the top with each successive pass through the filtering process. Although each signal was filtered ten times, it's considered over filtered after the fifth pass through the filter as a significant amount of the original signal characteristics have been removed. The details represent the high frequency or 'low scale' data while the approximations represent the low frequency of 'high scale' data. The kurtosis and skewness was calculated after each pass through the filter.

Statistical Time Domain Analysis

The following conclusions were drawn from Figure 21 through Figures 38:

-Throughout the statistical time domain analysis, skewness and standard deviation never displayed any meaningful trends. In the few instances where a weak trend might be interpreted, they were treated as outlier in this paper.

Kurtosis:

-Larger bearings tend to have a lower kurtosis regardless of load or oil viscosity.

-Large bearings kurtosis was relatively unaffected by load for the loads tested.

-Small bearings experienced an increase in kurtosis as load increases. Speed had no significant impact on kurtosis.

-Bearing size had no significant impact on kurtosis.

-The standard and deep groove kurtosis showed no dependency on size.

-Larger bearing kurtosis performance did not show a dependency on quality; the small low quality hearing had a higher kurtosis than the other bearing types.

-Exceptions to the above trends were noted.

Crest factor:

-Larger bearing tend to have a lower crest factor regardless of load or oil viscosity.

-Small bearing experienced an increase in crest factor as load increases.

-Speed had no significant impact on crest factor.

-Bearing size had no significant impact on crest factor.

-The standard and deep groove crest factor showed no dependency on size.

-Larger bearing crest factor performance did not show a dependency on quality; the small low quality hearing had a higher crest factor than the other bearing types.

-Exceptions to the above trends were noted.

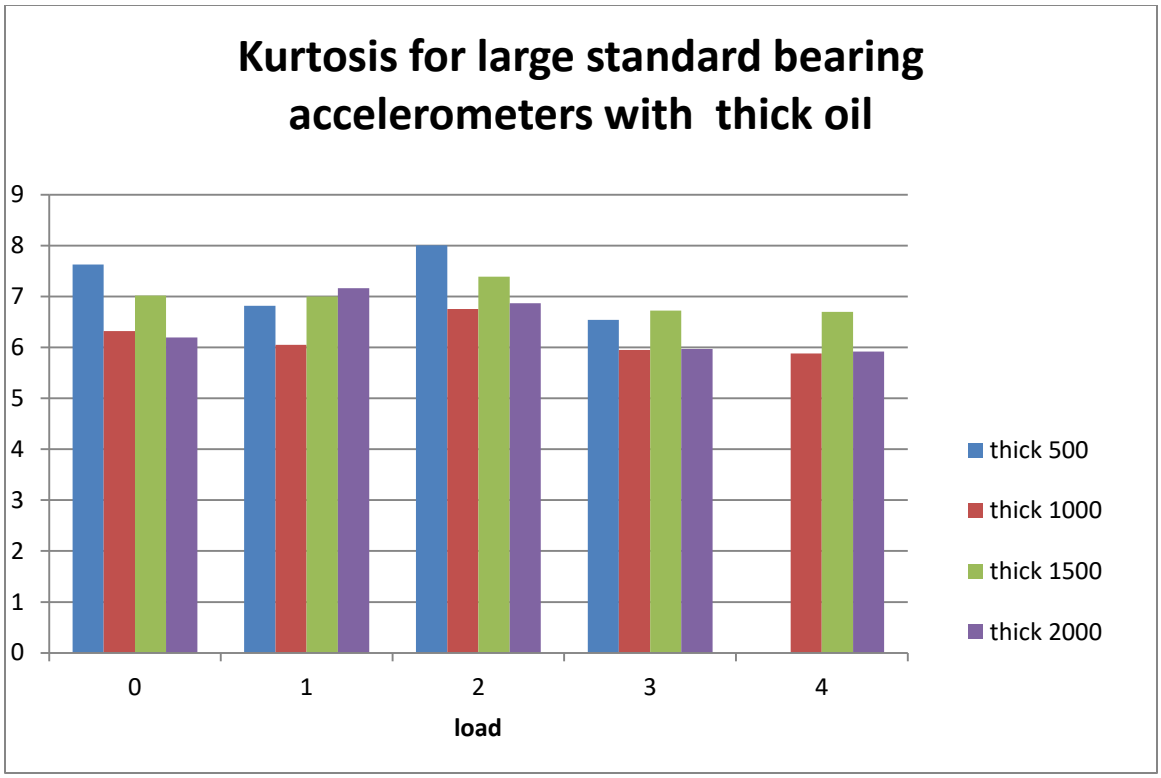

Figure 21: Kurtosis for large standard bearing accelerometers with thick oil

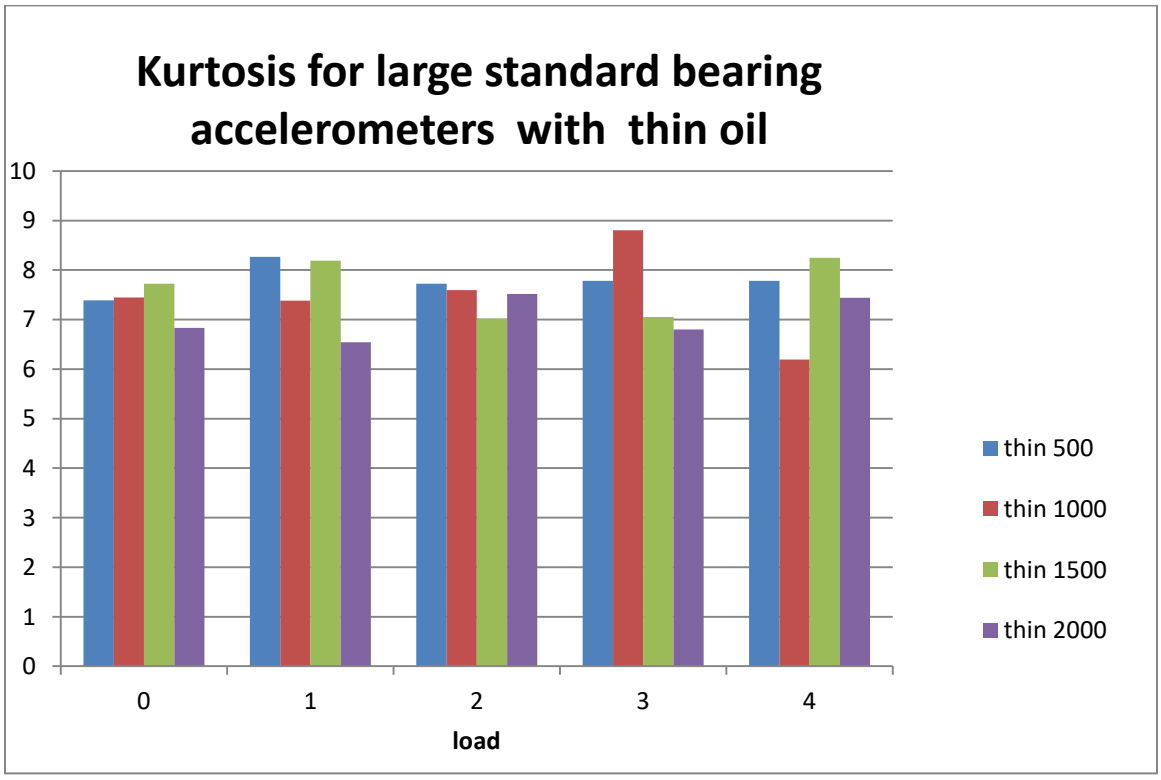

Figure 22: Kurtosis for large standard bearing accelerometers with thick oil

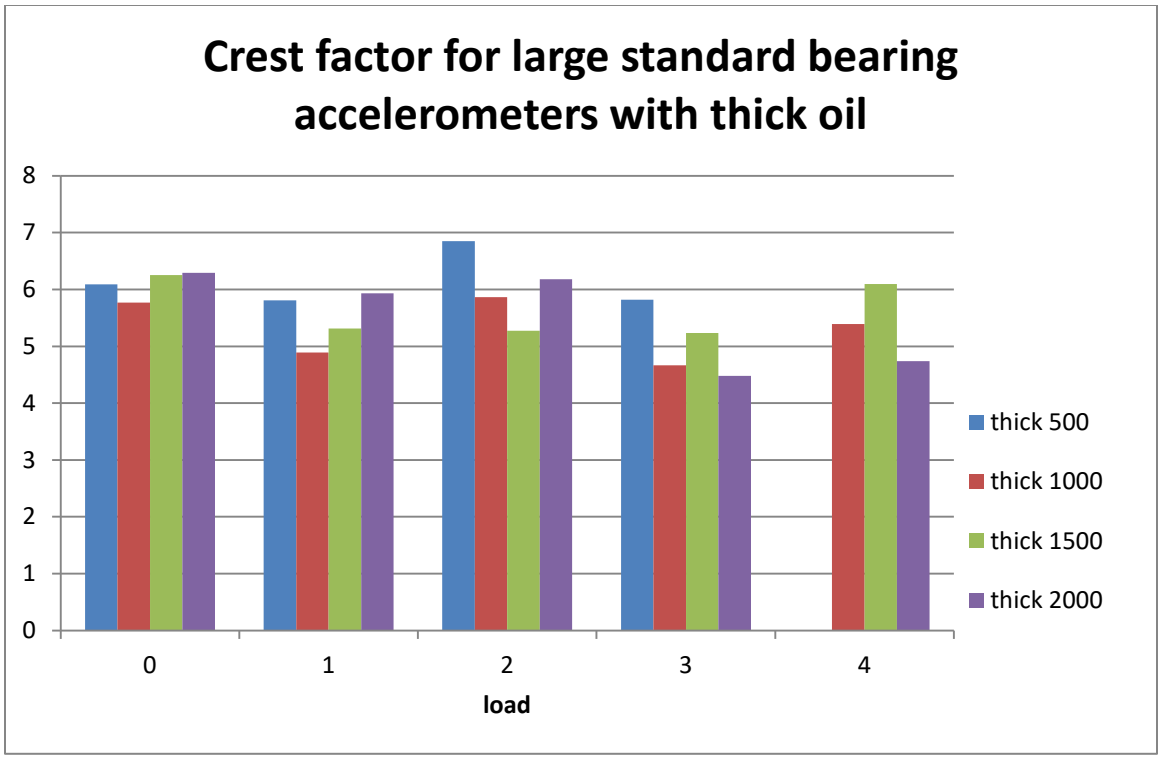

Figure 23: Crest factor for large standard bearing accelerometers with thick oil

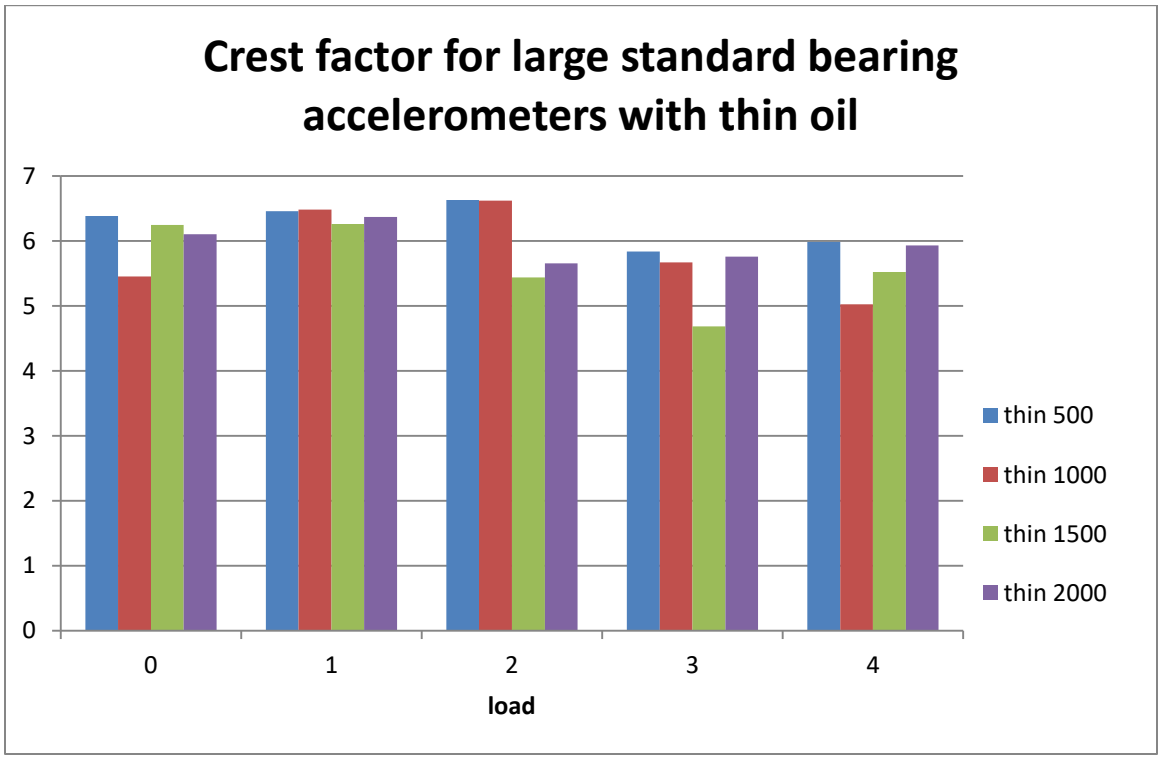

Figure 24: Crest factor for large standard bearing accelerometers with thin oil

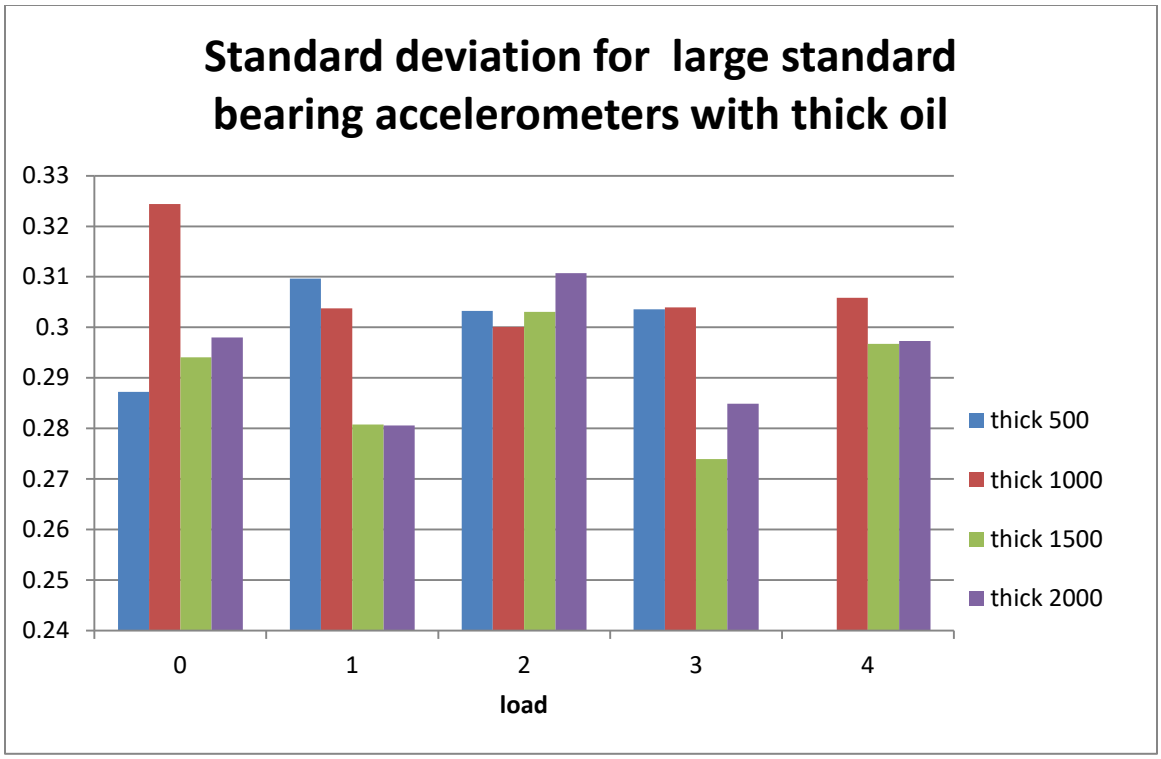

Figure 25: Standard deviation for large standard bearing accelerometers with thick oil

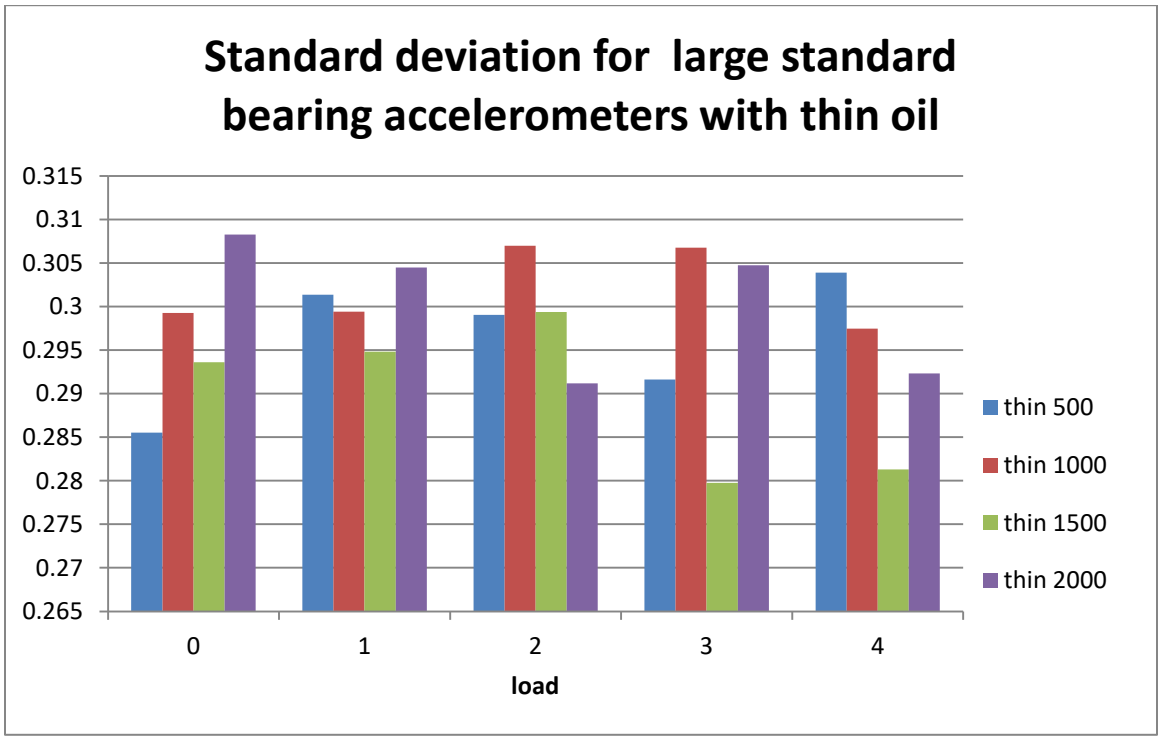

Figure 26: Standard deviation for large standard bearing accelerometers with thin oil

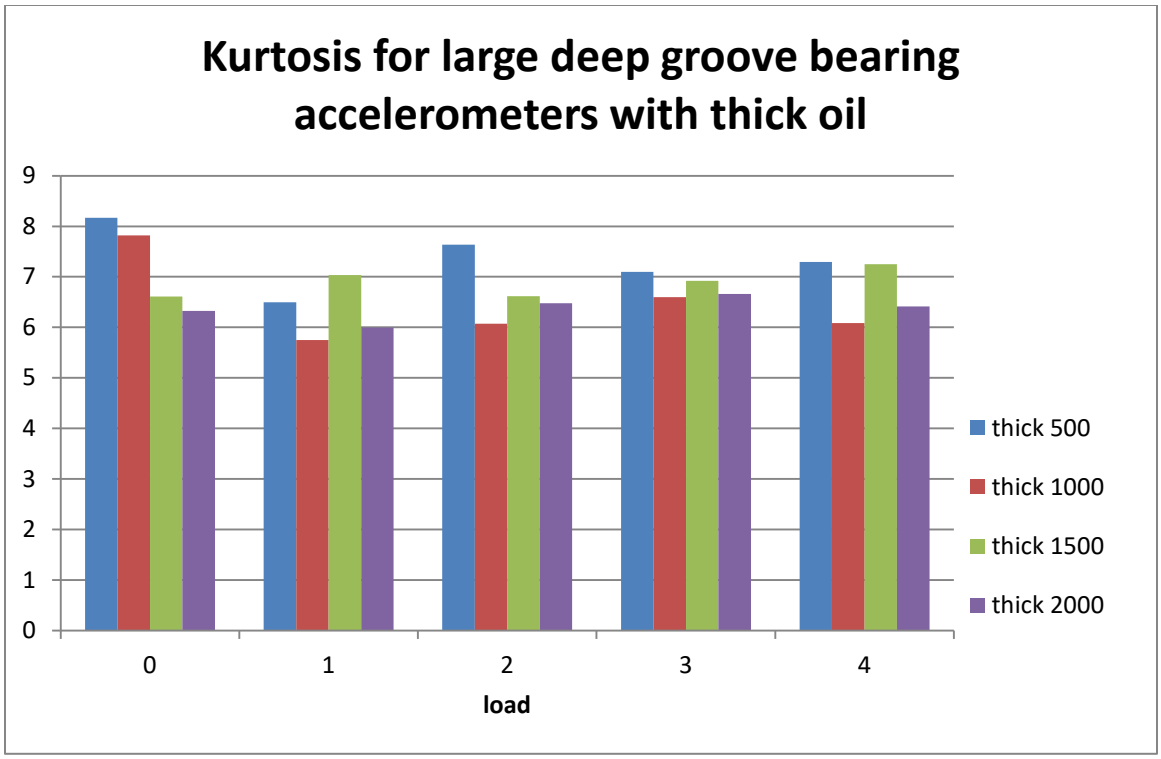

Figure A-27: Kurtosis for large deep groove bearing accelerometers with thick oil

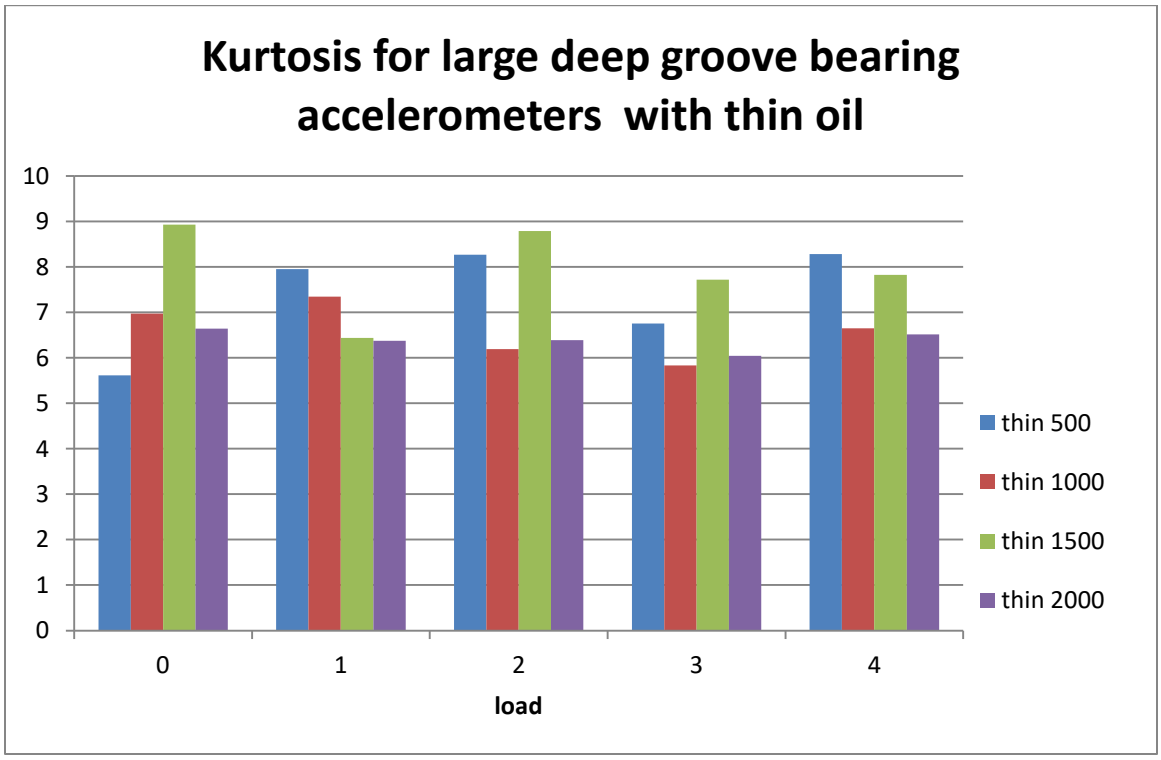

Figure 28: Kurtosis for large deep groove bearing accelerometers with thin oil

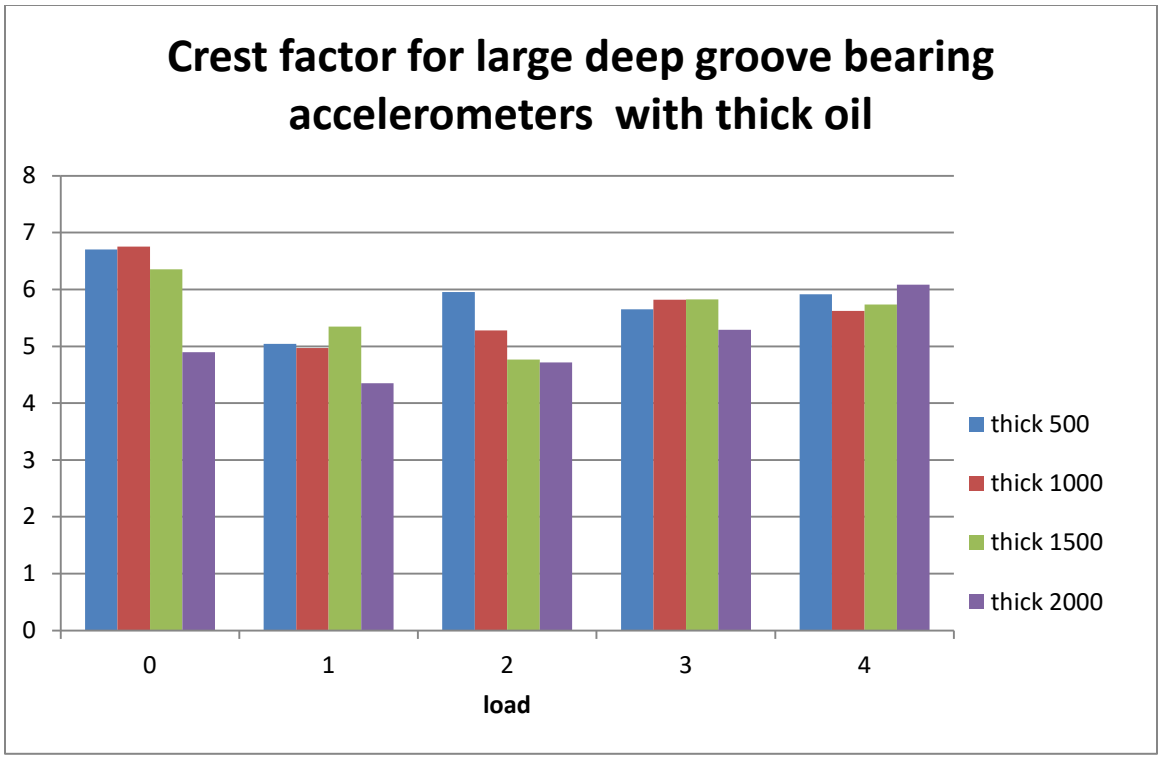

Figure 29: Crest factor for large deep groove bearing accelerometers with thick oil

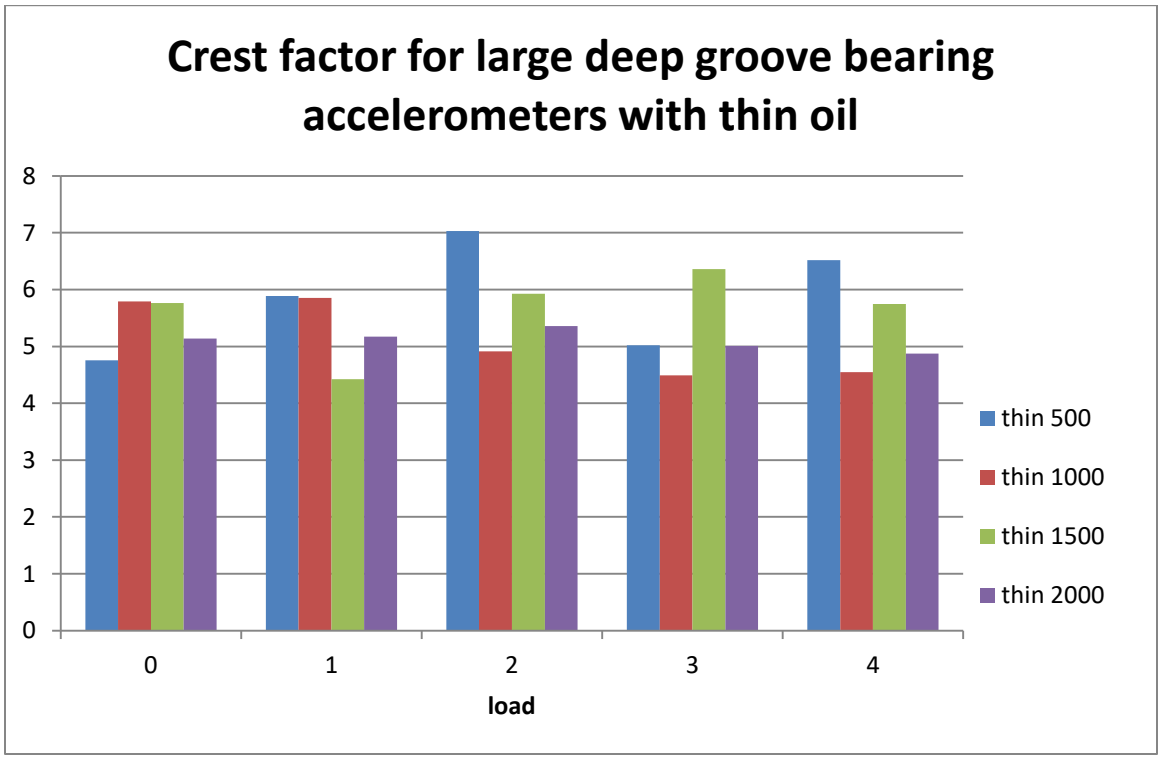

Figure 30: Crest factor for large deep groove bearing accelerometers with thin oil

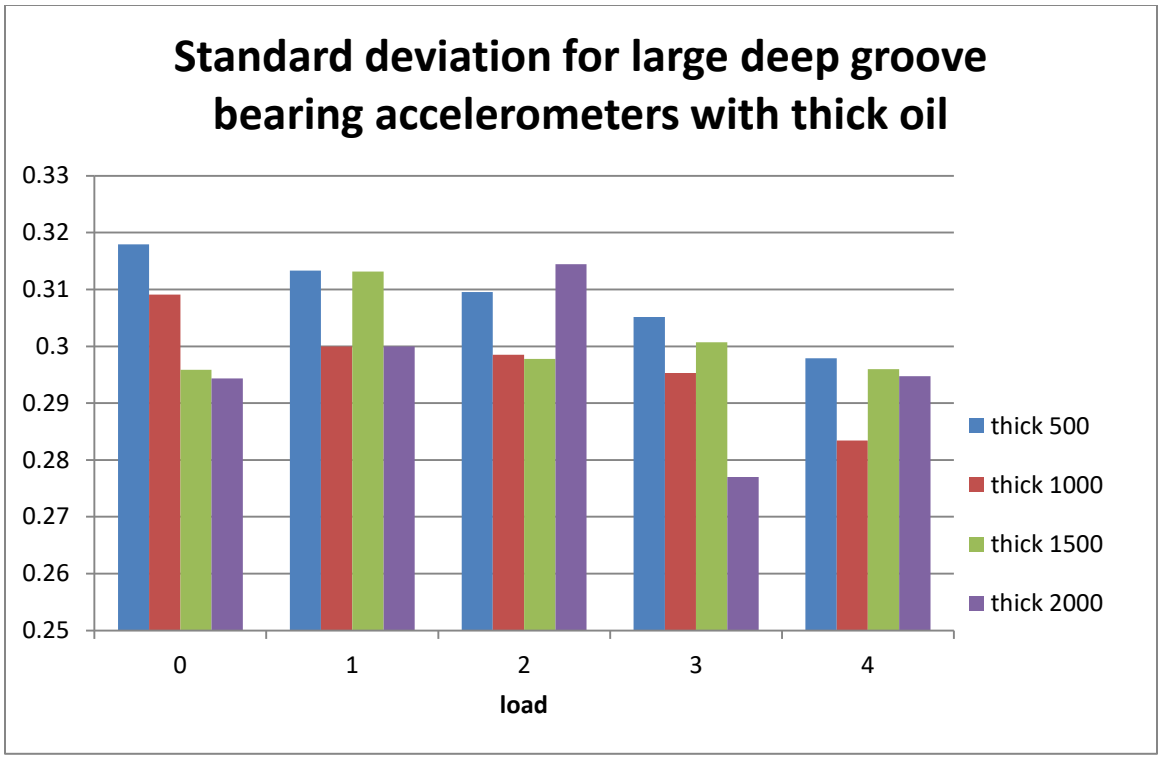

Figure 31: Standard deviation for large deep groove bearing accelerometers with thick oil

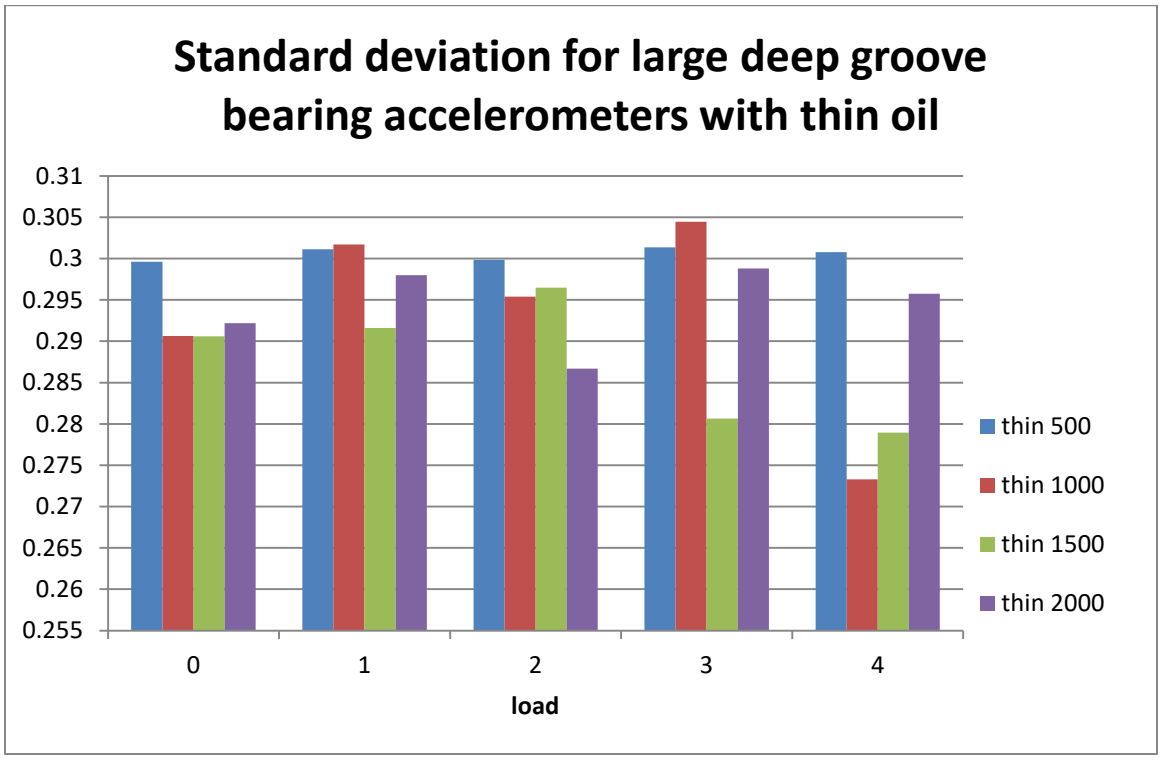

Figure 32: Standard deviation for large deep groove bearing accelerometers with thin oil

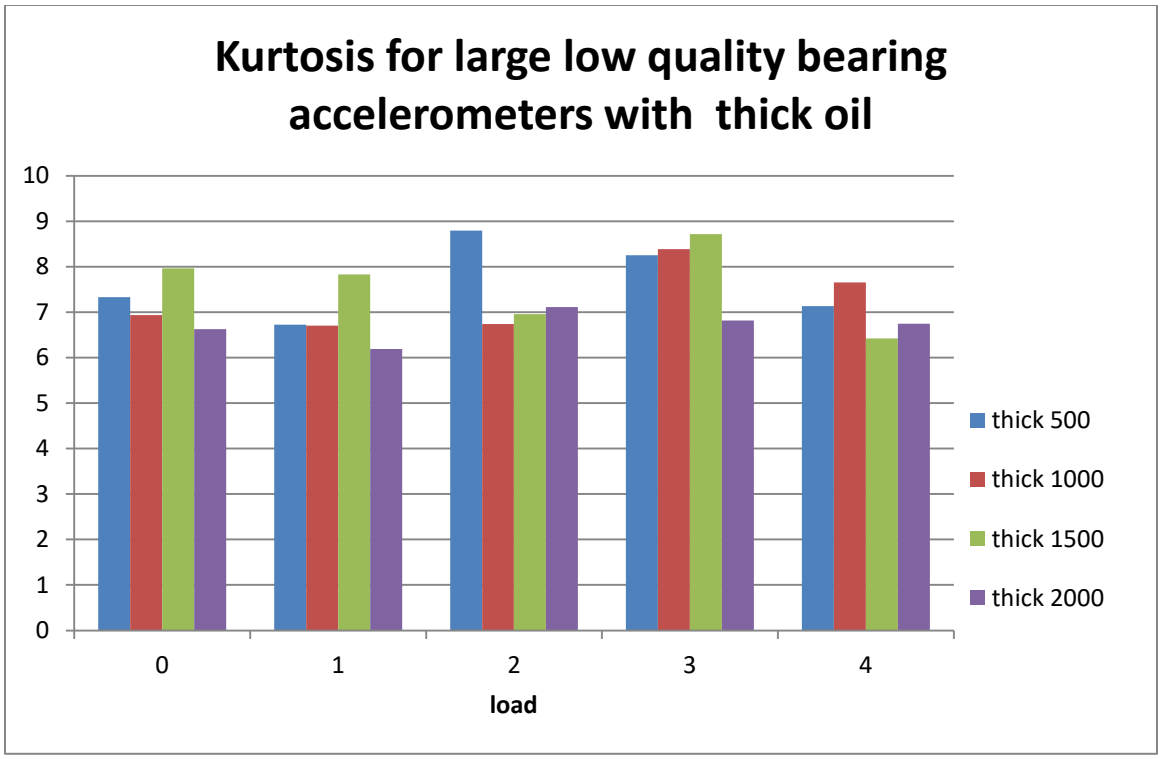

Figure 33: Kurtosis for large low quality bearing accelerometers with thick oil

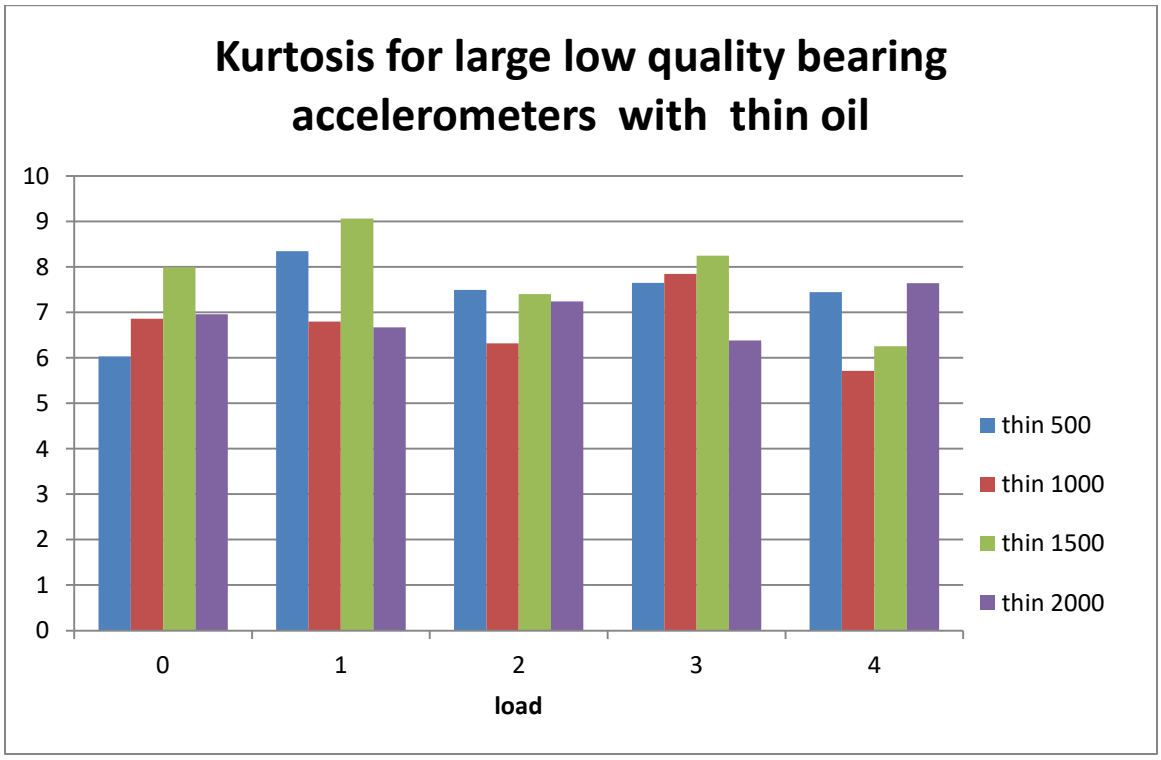

Figure 34: Kurtosis for large low quality bearing accelerometers with thin oil

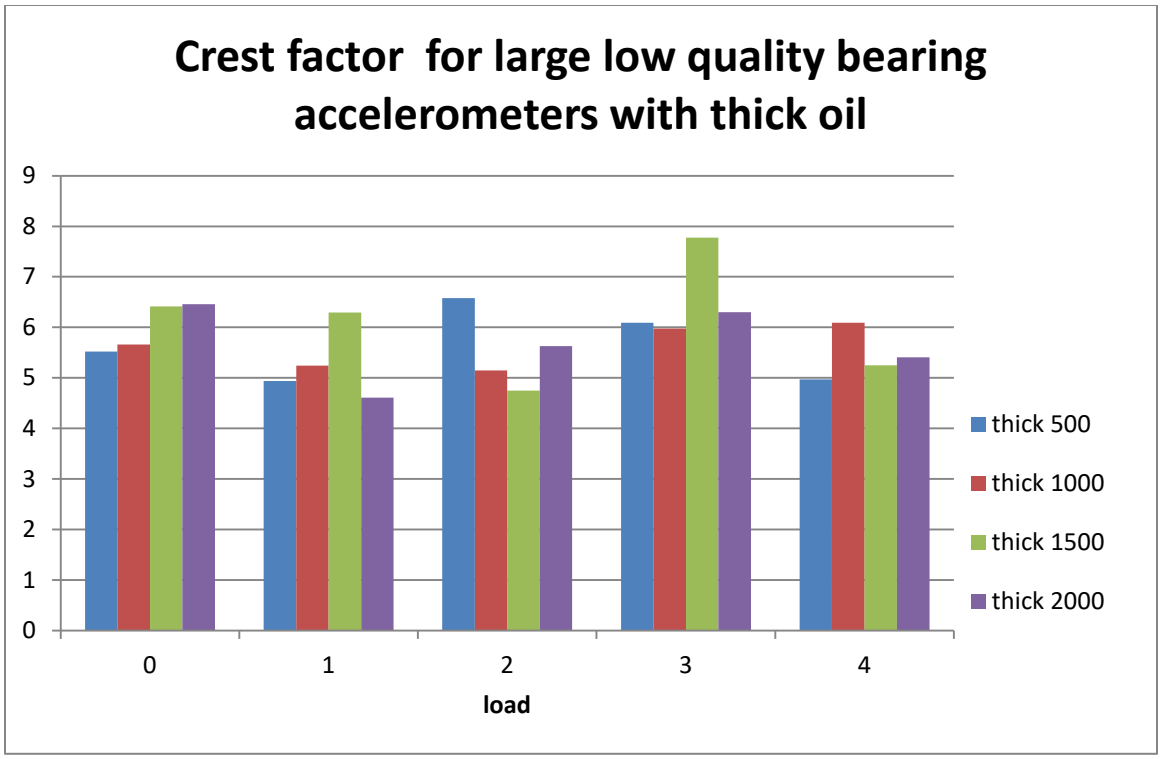

Figure 35: Crest factor for large low quality bearing accelerometers with thick oil

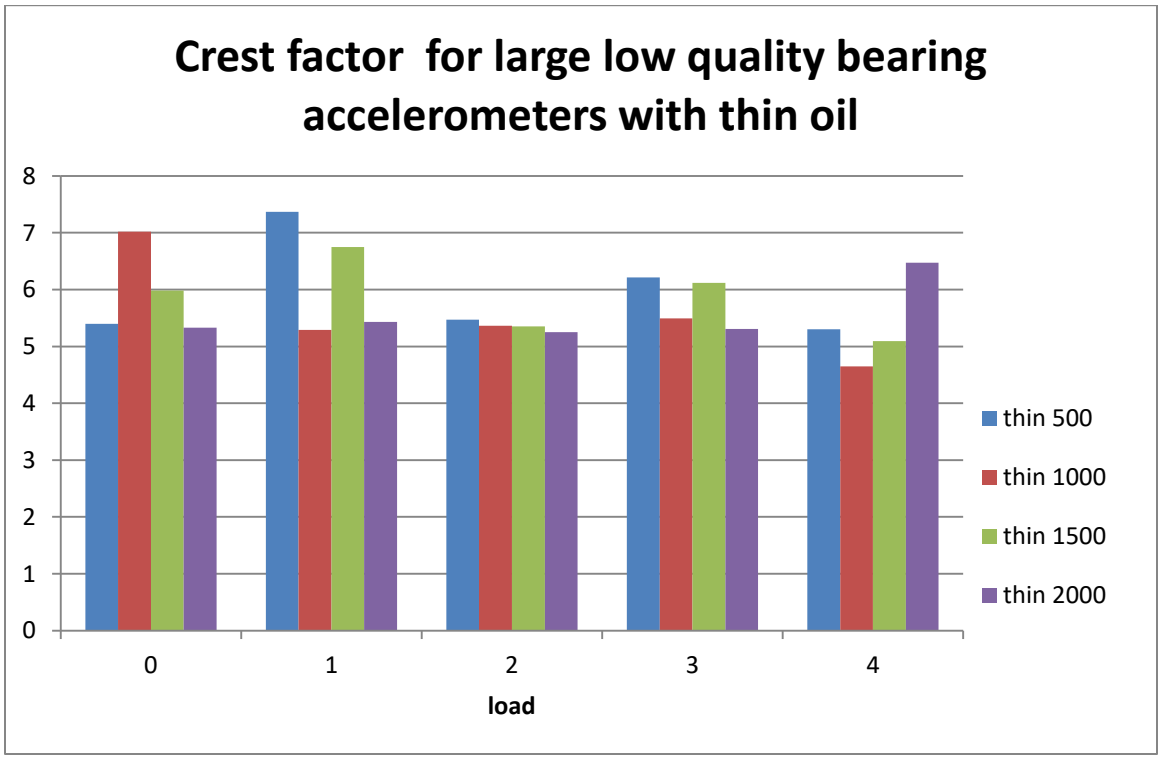

Figure 36: Crest factor for large low quality bearing accelerometers with thin oil

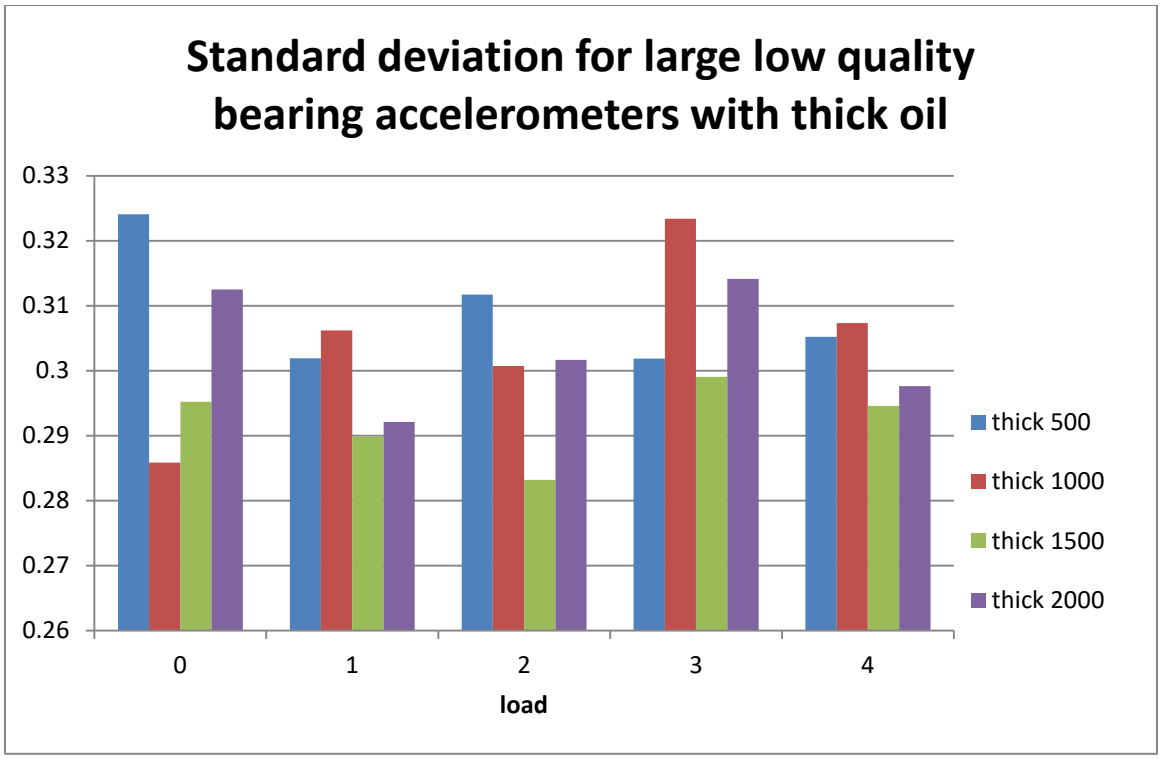

Figure 37: Standard deviation for large low quality bearing accelerometers with thick oil

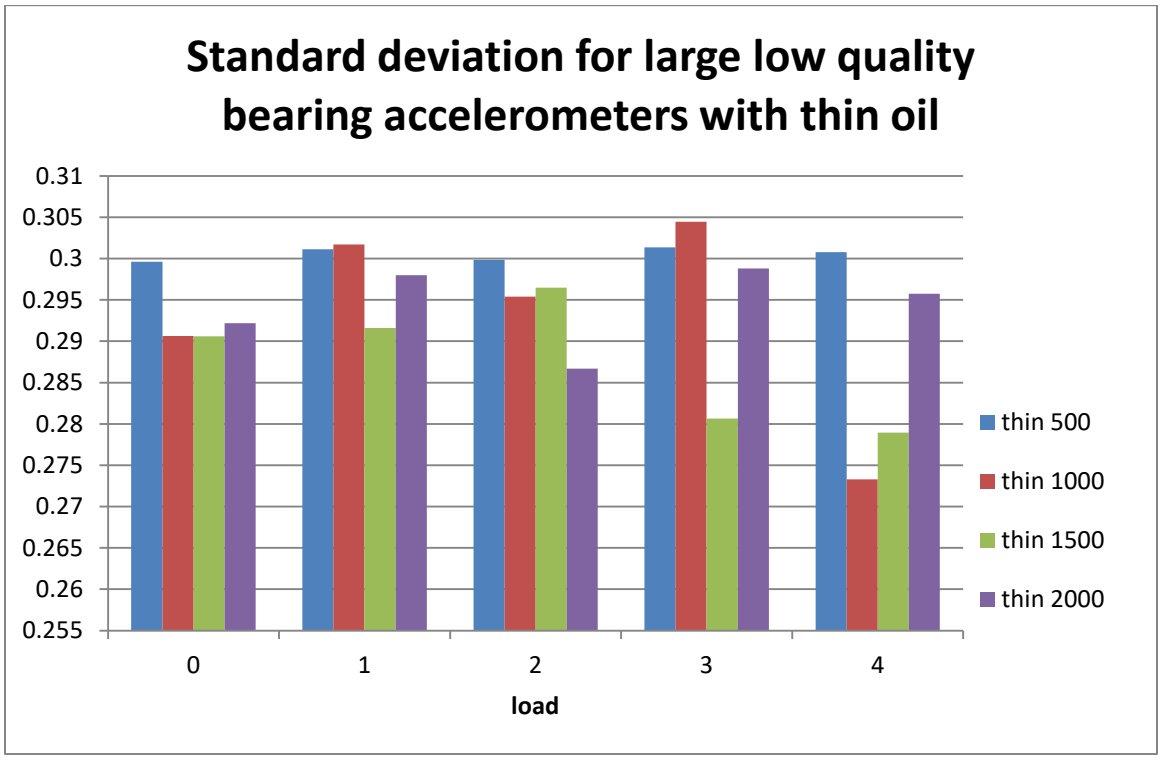

Figure 38: Standard deviation for large low quality bearing accelerometers with thin oil

Frequency Domain Analysis

The following conclusions were drawn from Figure 39 through Figures 46:

-The standard, deep groove, and low quality bearings all had similar FFT signals at 1000 rpm with no load applied.

-When a load is applied at 1000 rpm, FFT values increase strongest for the deep groove bearing and weakest for the standard bearing

-No trends are observable for the bearings at 2000 rpm in an unloaded condition.

-When loaded at 2000 rpm, the low quality bearing consistently has the weakest signal with the deep groove bearing having the strongest signal.

-For the low quality bearing, the FFT signal increases with load at 1000 rpm but decreases with load at 2000 rpm. This unexplainable behavior of the low quality bearing was found again when the FFT signal increased with speed at no load but decreased with speed when loaded.

-The deep groove bearing had the FFT signal consistently increase with load at 1000 rpm and 2000 rpm, with some outliers.

-The standard bearing saw the FFT signal consistently increase with load at 1000 rpm and 2000 rpm with no outliers.

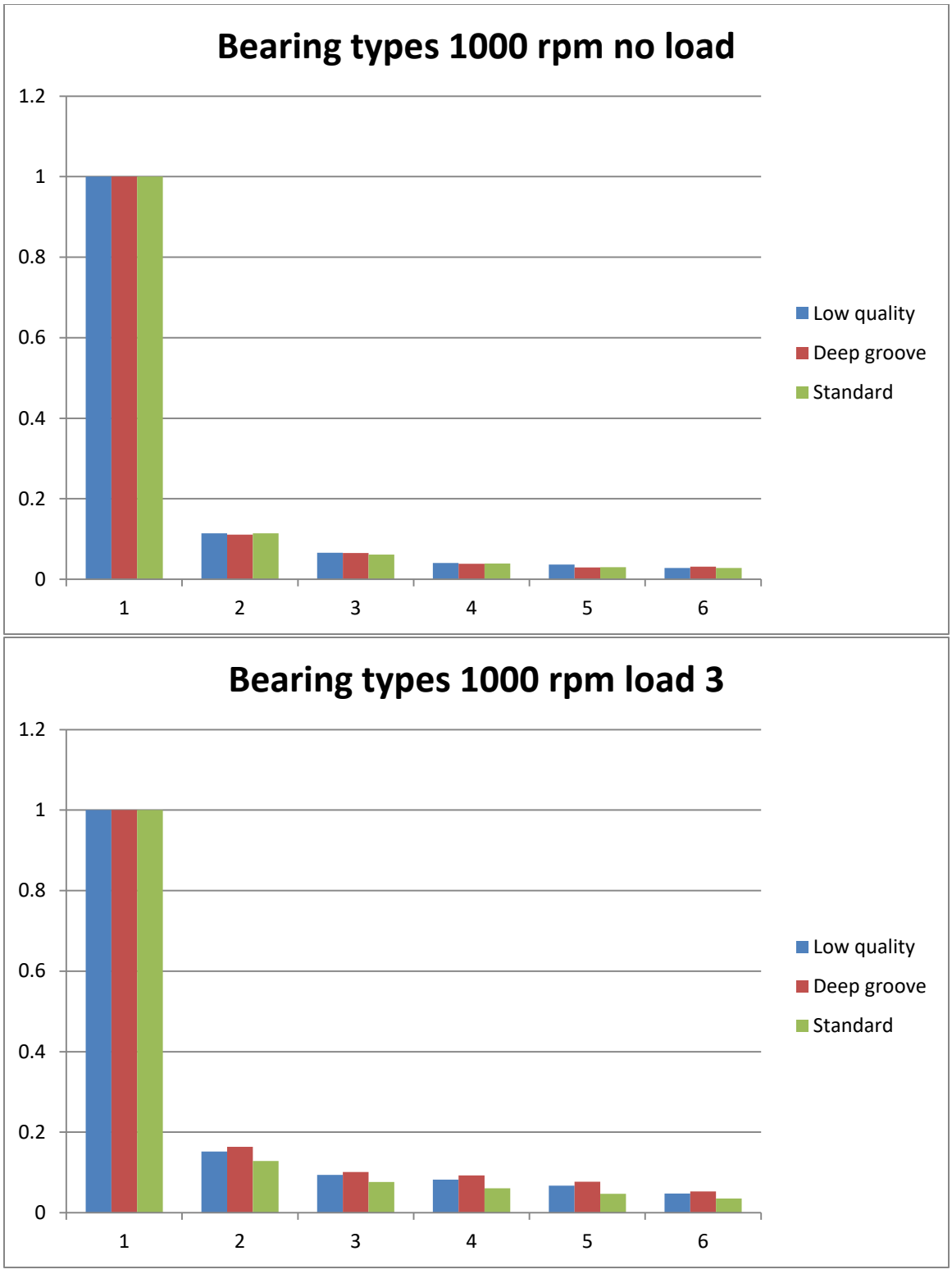

Figure 39: FFT of bearings at 1000 rpm at load 3

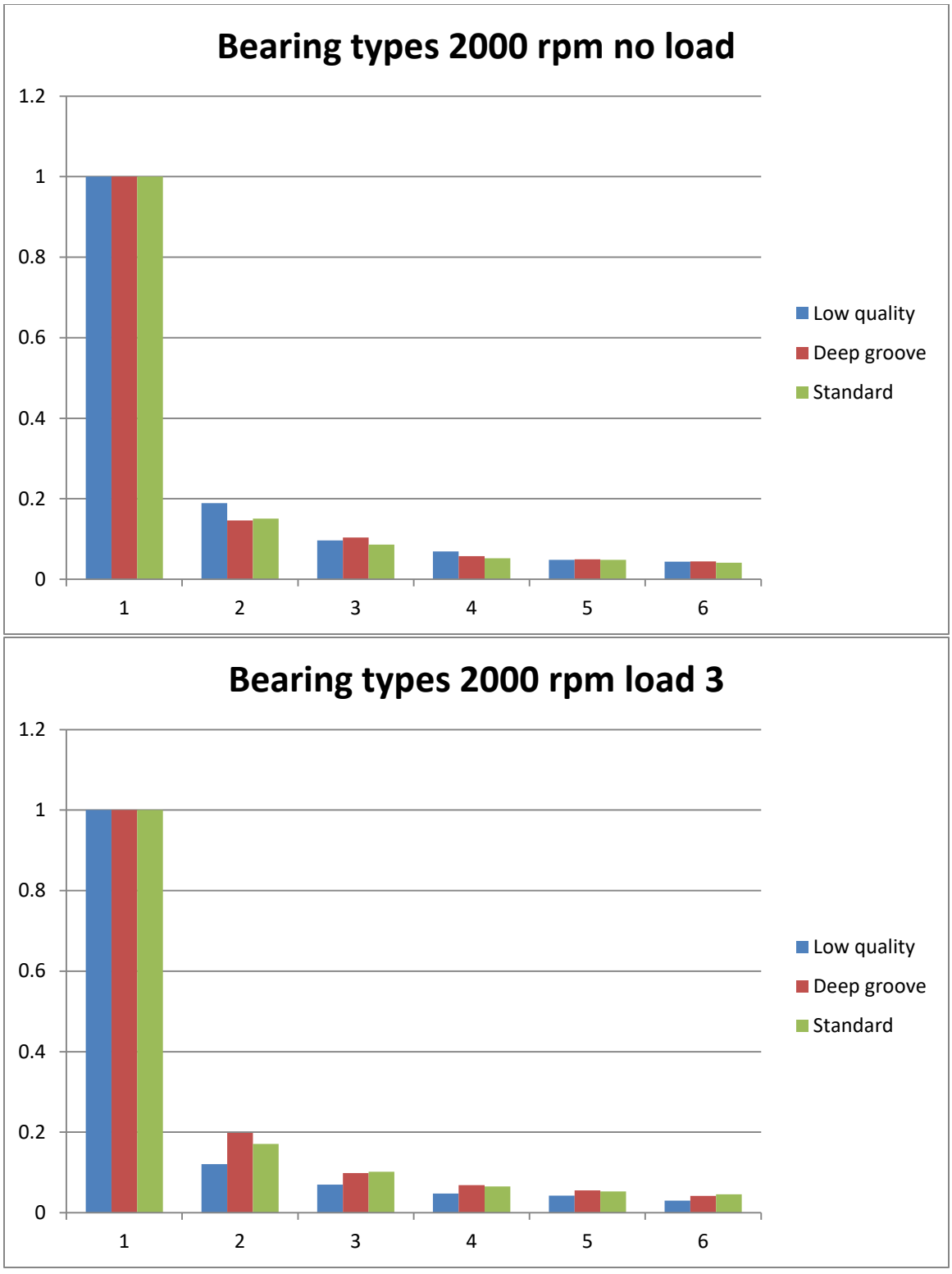

Figure 40: FFT of bearings at 2000 rpm at no load

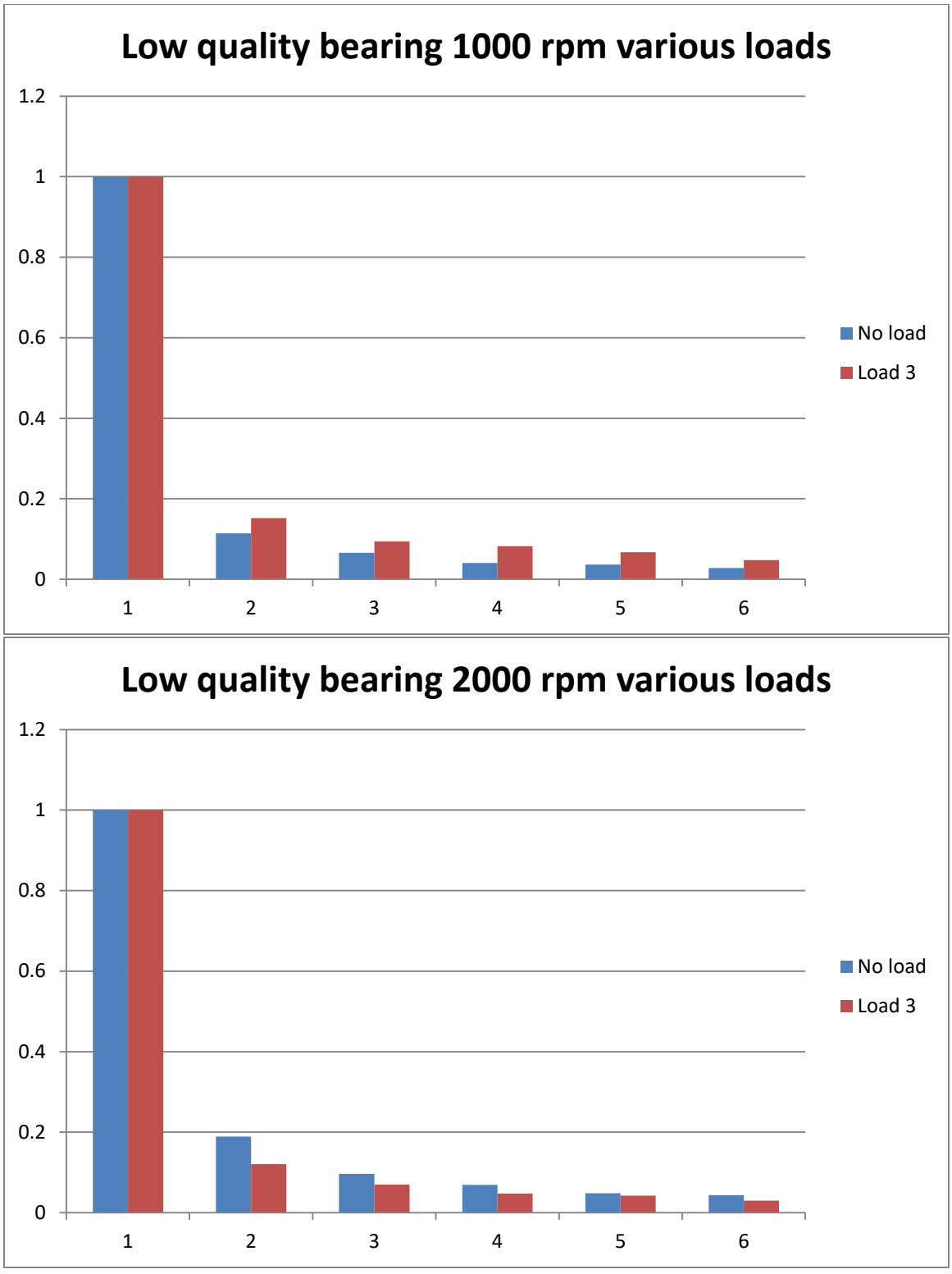

Figure 41: FFT of low quality bearings with speed varied

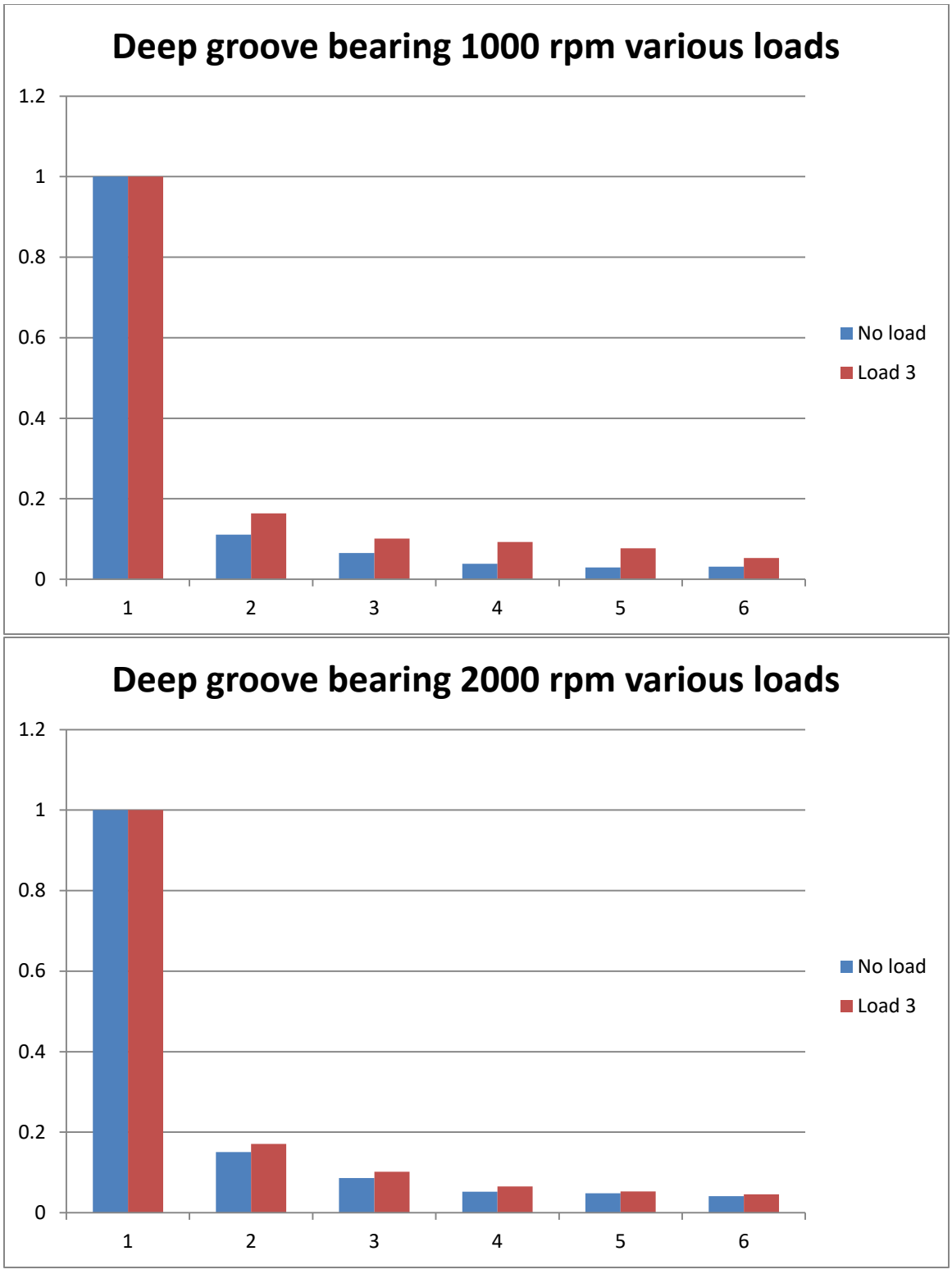

Figure 42: FFT of deep groove bearings with speed varied

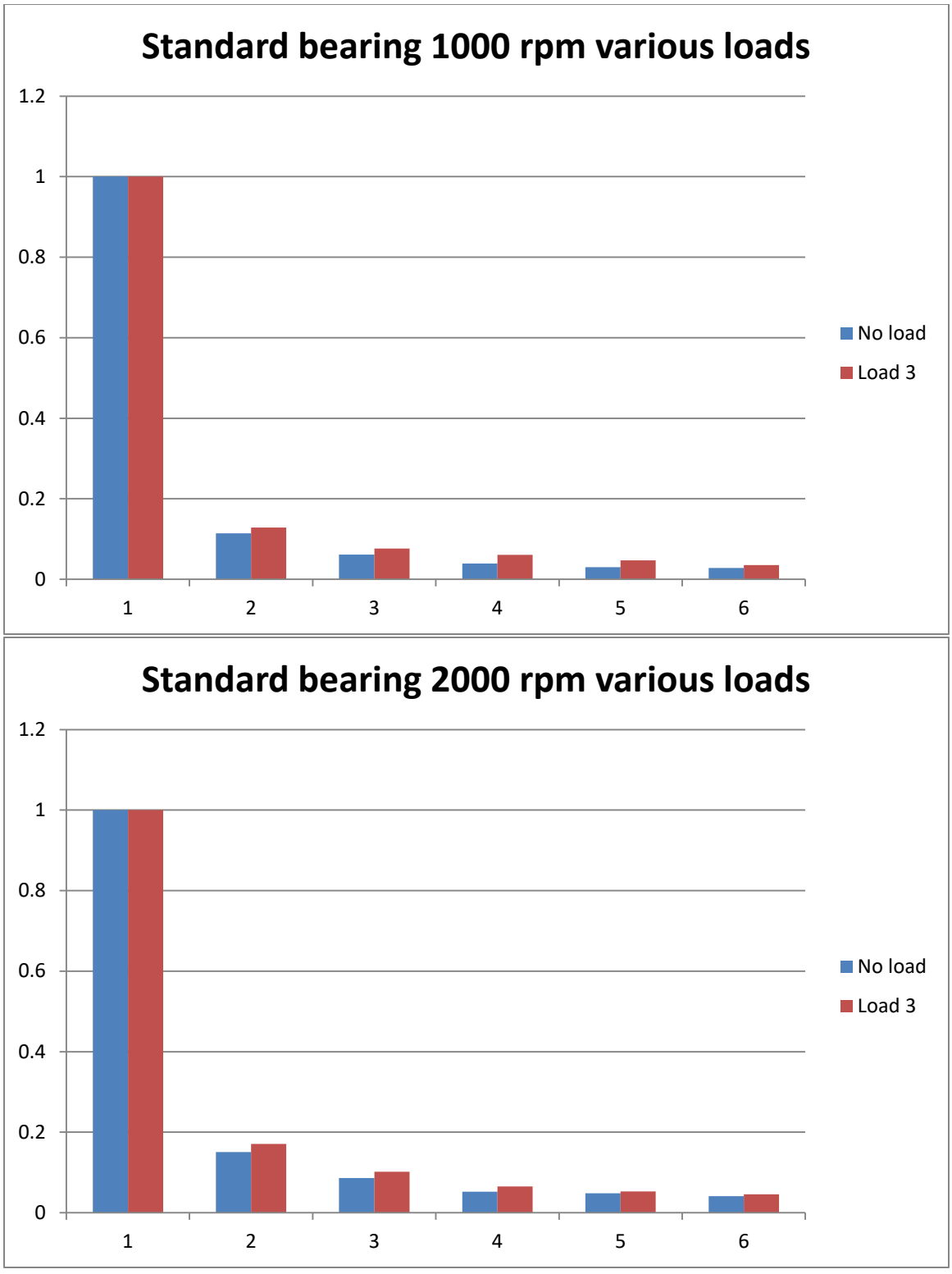

Figure 43: FFT of standard bearings with speed varied

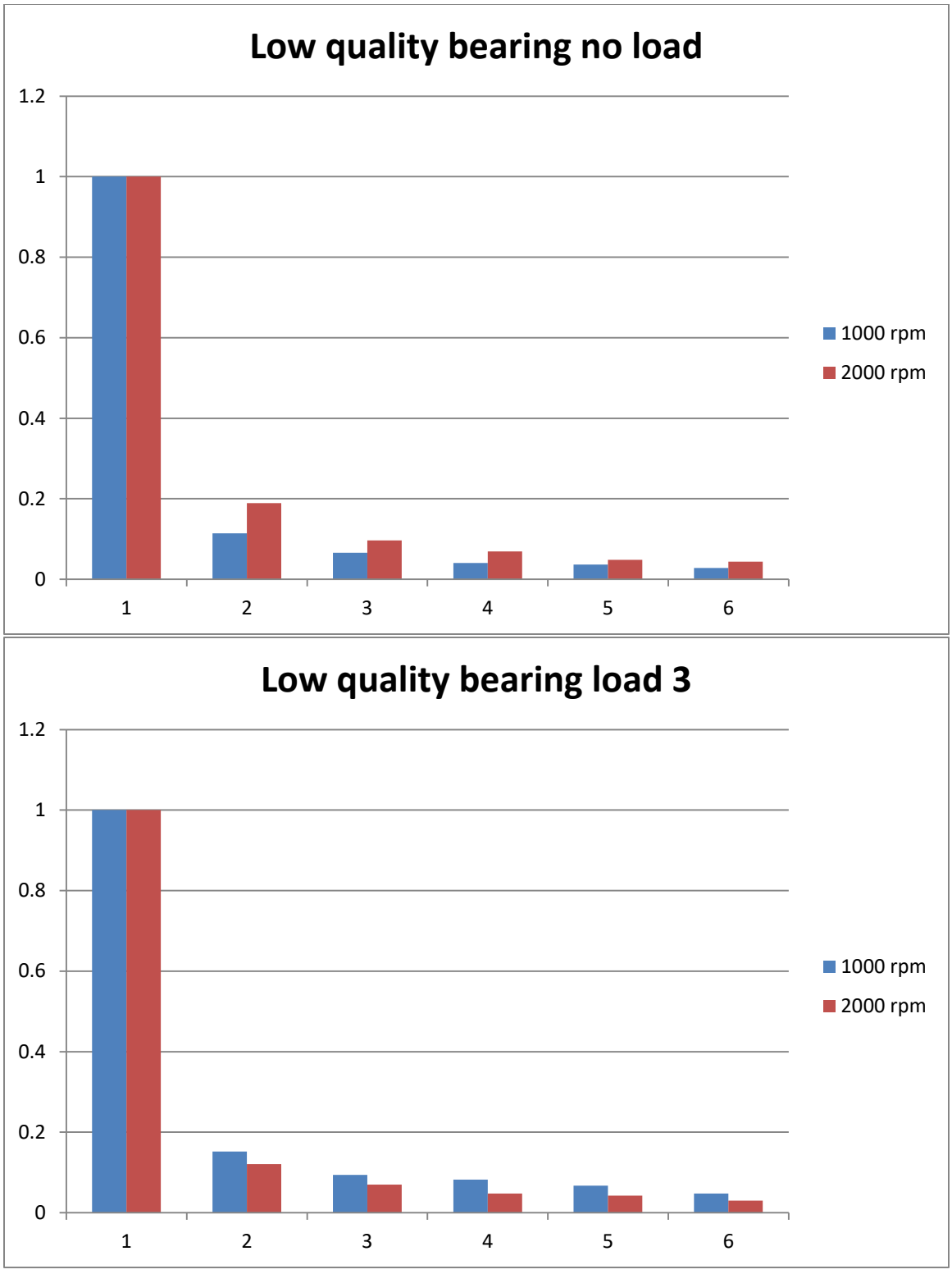

Figure 44: FFT of low quality bearings with load varied

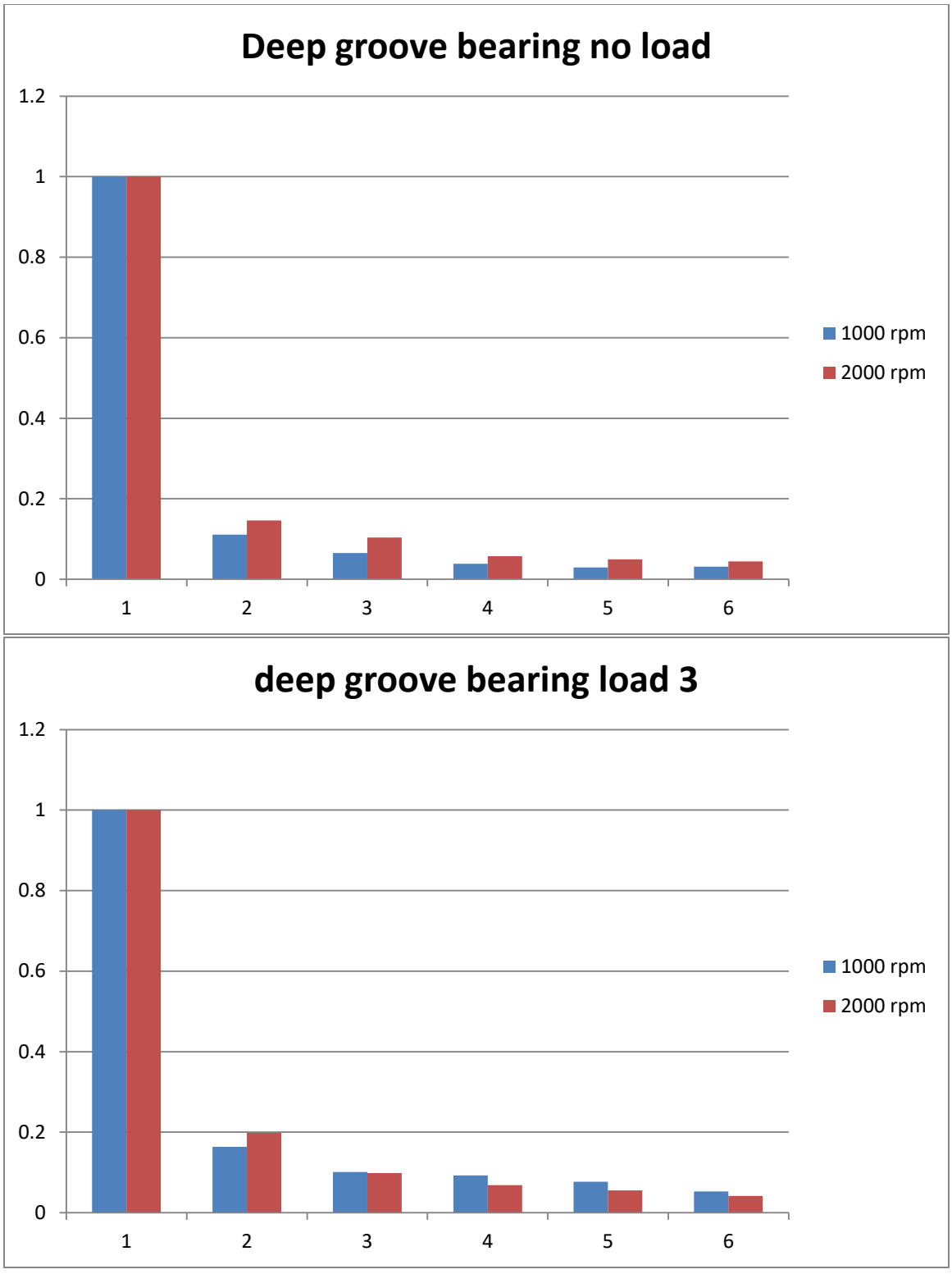

Figure 45: FFT of deep groove bearings with load varied

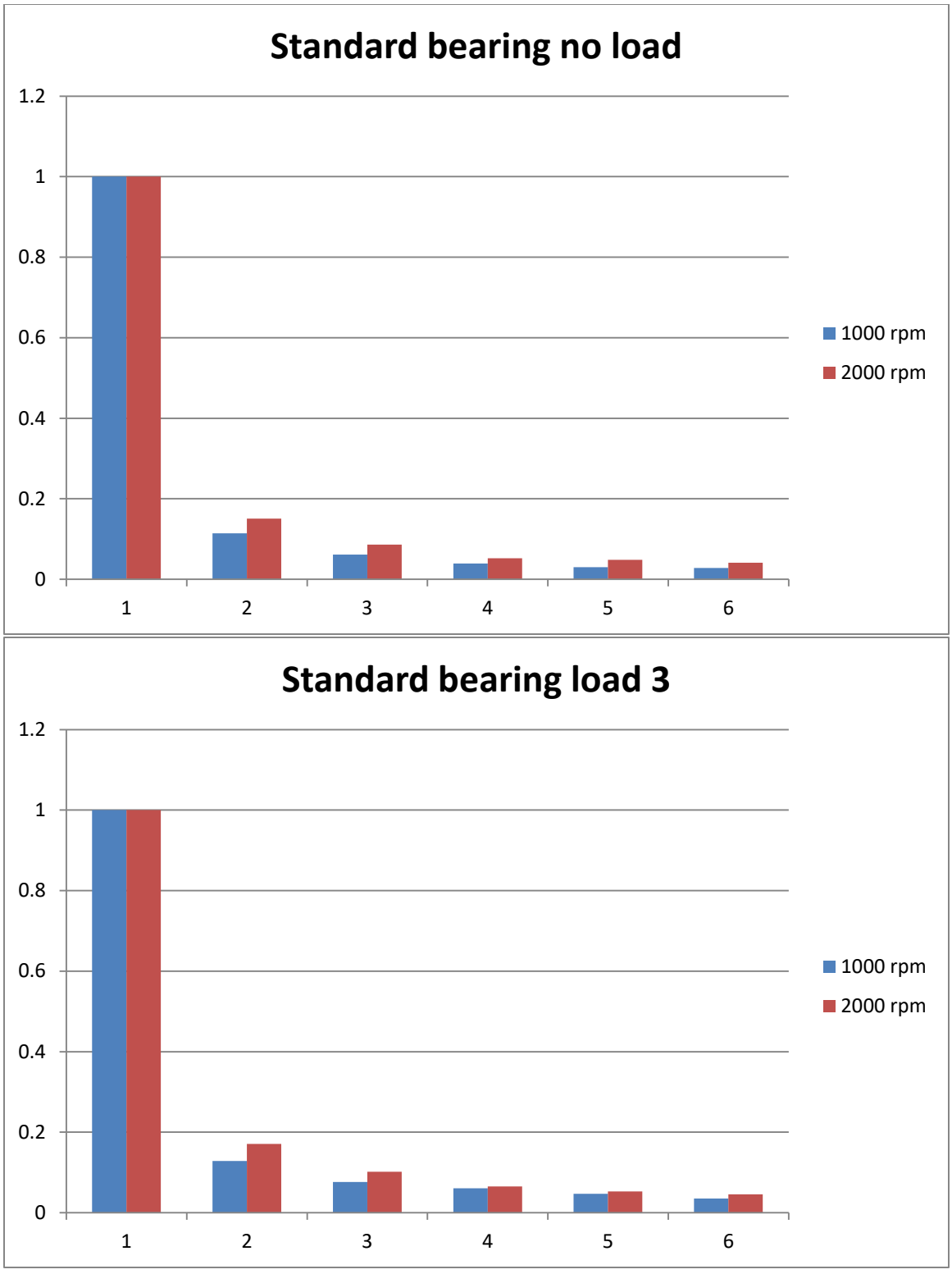

Figure 46: FFT of standard bearings with load varied

Wavelet Analysis

Select scalograms have been provided for visual comparison in Figure 47 through Figure 51.

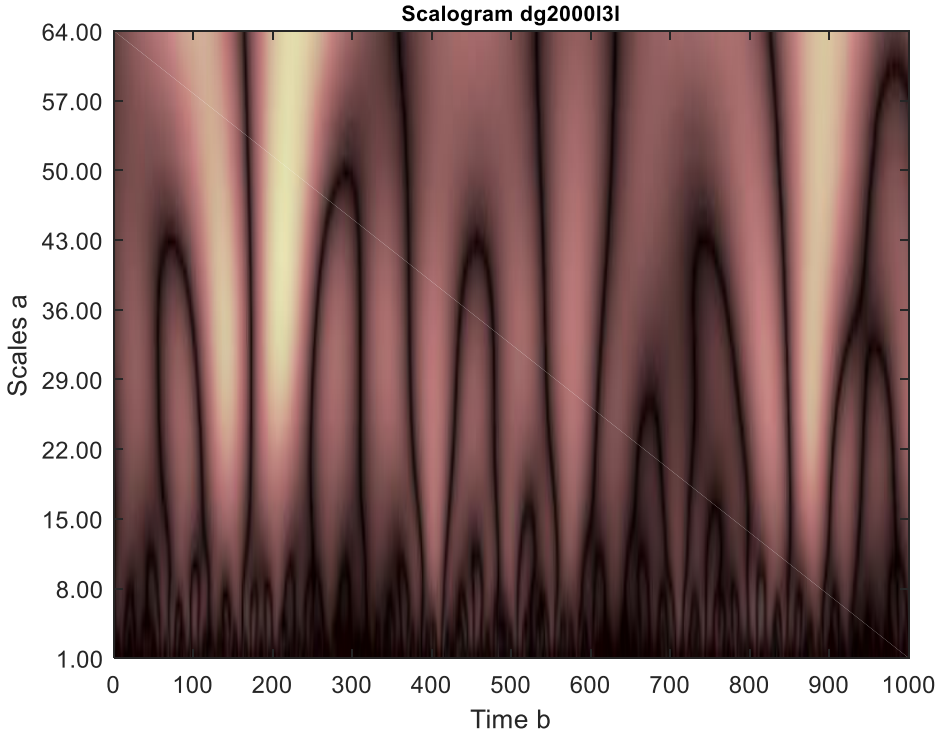

Figure 47: Large deep groove bearing scalogram at 2000 rpm, load 3 in light oil

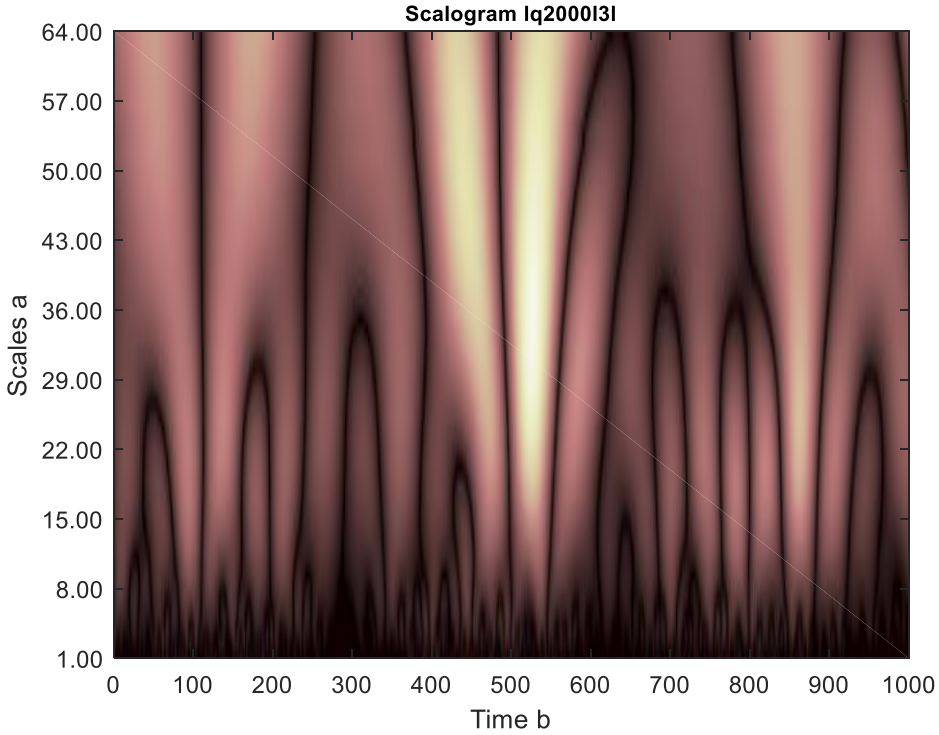

Figure 48: Large low quality bearing scalogram at 2000 rpm, load 3 in light oil

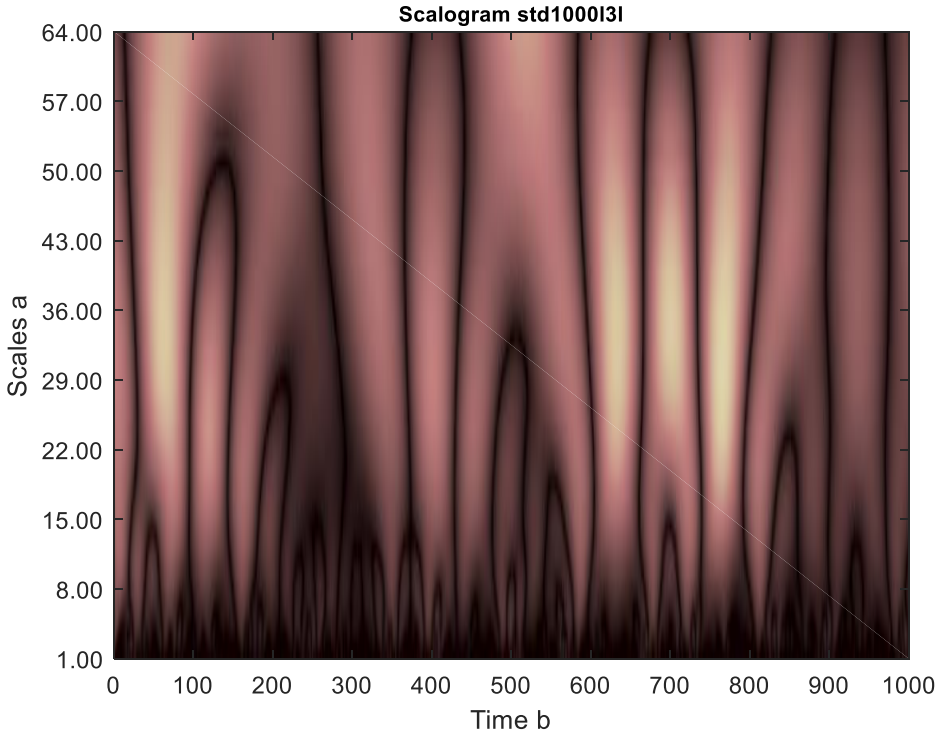

Figure 49: Large standard bearing scalogram at 1000 rpm, load 3 in light oil

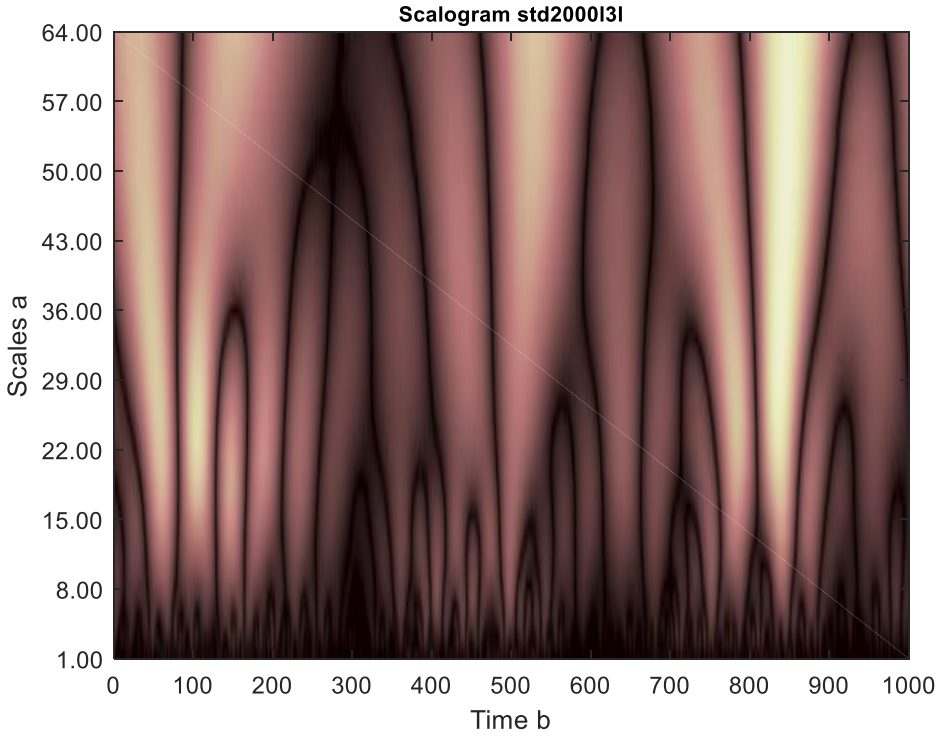

Figure 50: Large standard bearing scalogram at 2000 rpm, load 3 in light oil

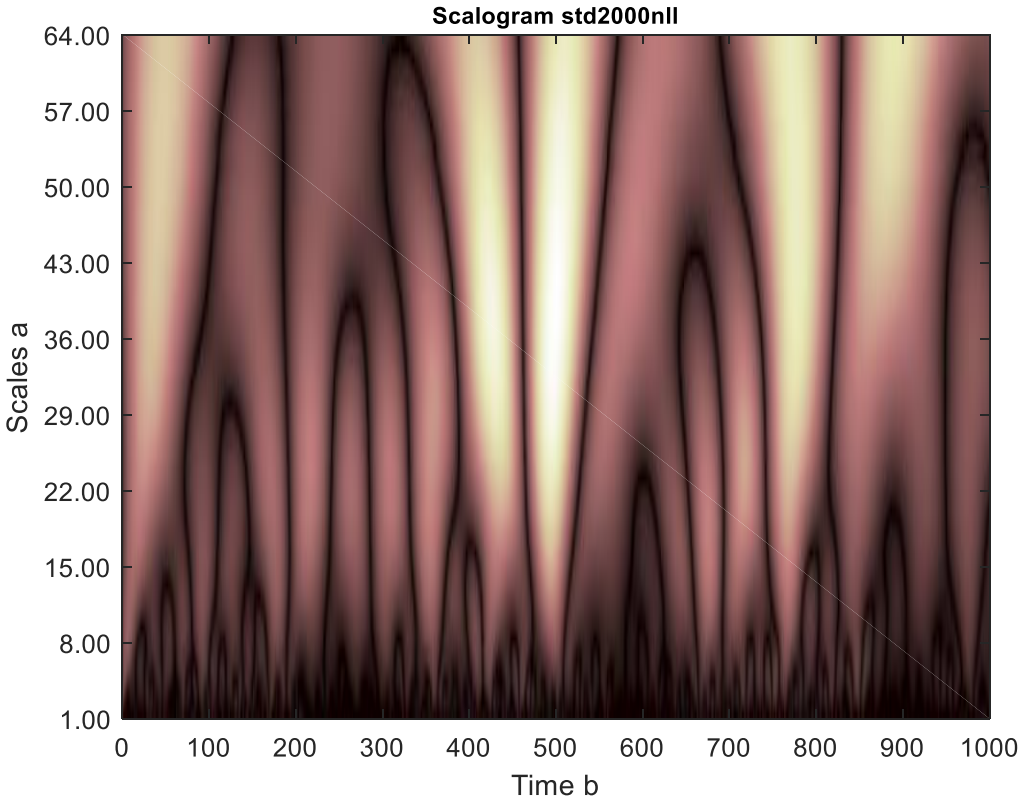

Figure 51: Large standard bearing scalogram at 2000 rpm, no load in light oil

The results of the filtered details and approximations are shown in Figure 52 through Figure 58. Graphs of the kurtosis for approximations and details can be found in Figure 59 through 62. Graphs of the skewness for details and approximations can be found in figure shown in Figure 63 through Figure 78. Select graphs of crest factor can be found in Figure 79 through Figure 82.

Kurtosis:

Approximations:

Figure 59 and Figure 69 examine how kurtosis of the approximations varies with changes in load in heavy oil. Here a strong trend emerges showing that kurtosis increases with increased load. This held true for all bearing types regardless of speed when tested in heavy oil. The standard bearing kurtosis approximations are shown in Figure 61 and show the two curves being very similar. An examination shows the higher load to have a slightly kurtosis. No trend was noticed when tested under identical circumstances except with lighter oil, see Figure 69 and Figure 71. Here, of the six graphs presented in Figure 69 and Figure 71, two had kurtosis remain essentially unchanged with increased load (low quality and deep groove bearings at 2000 rpm), two had kurtosis increase (standard bearing at 2000 rpm and low quality bearing at 1000 rpm), and two had kurtosis decrease with increased load (deep groove and standard bearing at 1000 rpm).

Figure 65 and Figure 67 examine how kurtosis of the approximations varies with changes in load in heavy oil. Here a strong trend emerges showing that kurtosis increases with increased speed. This was found to be true with all bearing types when unloaded and loaded in

heavy oil. When the same test was conducted in light oil, a similar trend was noticed. When the bearing was loaded, kurtosis always increased with increased speed as shown in Figure 77. Some exceptions are noted in Figure 75 when the standard and low quality bearing showed a decreasing kurtosis with increased speed.

Details:

Kurtosis of the details tends to be more erratic when compared to the kurtosis of the approximations as seen in Figures 60, 62, 70, and 72. Also, observed trends tend to be weaker with little to no consistency when oil type and load are changed. Figure 60 and Figure 70 are completely erratic and no trends are considered. Figure 62 shows kurtosis details consistently higher at higher loads at 1000 rpm in heavy oil. Figure 72 shows kurtosis being consistently higher at higher loads in light oil.

Skewness:

Approximations:

Skewness of the approximations was found to increase as load to increase with increasing load when the bearing were lubricated with heavy oil as can be seen in Figure 63 and Figure 64. It is can be seen in Figure 64 that the low quality bearing approximation skewness increase was minimal with increasing load. Also in Figure 64 it can be seen that the standard bearing approximation skewness was an outlier and decreased slightly with increased load. Figure 73 and Figure 74 show the approximation skewness of the bearing lubricated in light oil. The trends here were found to be speed dependent. At 1000 rpm it was found that approximation skewness generally increased with the standard bearing being the exception,

see Figure 74. For bearing operating at 2000 rpm the opposite trend was true, approximation skewness decreased with increased load for all bearings, see Figure 73.

Skewness approximations were found to increase as speed was increased as shown in Figures 66, 68, 76, and 78. Note that the skewness approximation was minimal for the low quality bearing as shown in Figure 78. This was true for all bearings in light or heavy oil with the deep groove bearing being the exception when lubricated by heavy oil, see Figure 66 and Figure 68.

Details:

No trends were observed.

Crest Factor:

Approximations:

Crest factor approximations can be seen in Figures 79 and 84 and showed a weak trend with lower speeds tending to have lower values. The low quality bearing was consistent in this sense in light oil. The deep groove bearing crest factor approximations were not sensitive to speed at no load conditions but proved to be an exception with crest factor decreasing with increasing speed in light oil. The standard bearing showed mixed results with trend lines for various speeds sometimes crossing. Figure 81 through Figure 84 compare the bearings in different oils. No trends can be seen with lines often crossing as speed and load are changed.

Details:

Graphs of crest factor details can be found in Figure 85 and Figure 86. The graphs of various speeds and load often cross and no trends can be inferred.

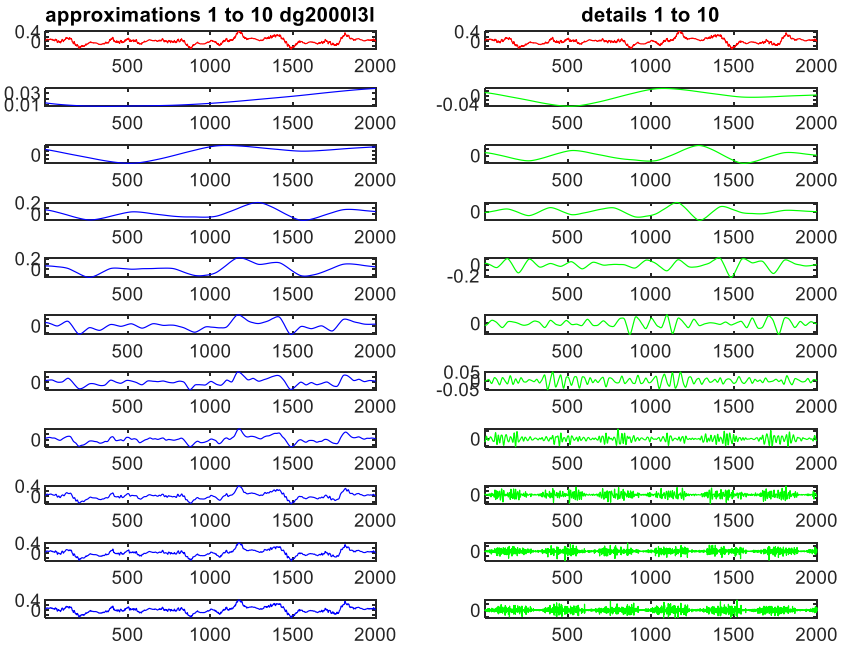

Figure 52: Details and approximations for large deep groove bearing at 2000 rpm, load 3 in light oil

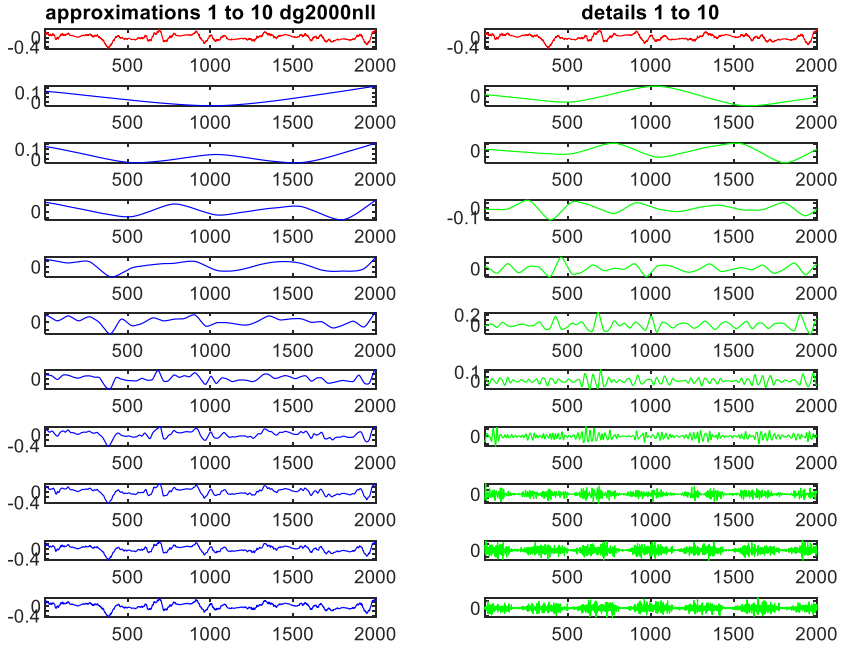

Figure 53: Details and approximations for large deep groove bearing at 2000 rpm, no load in light oil

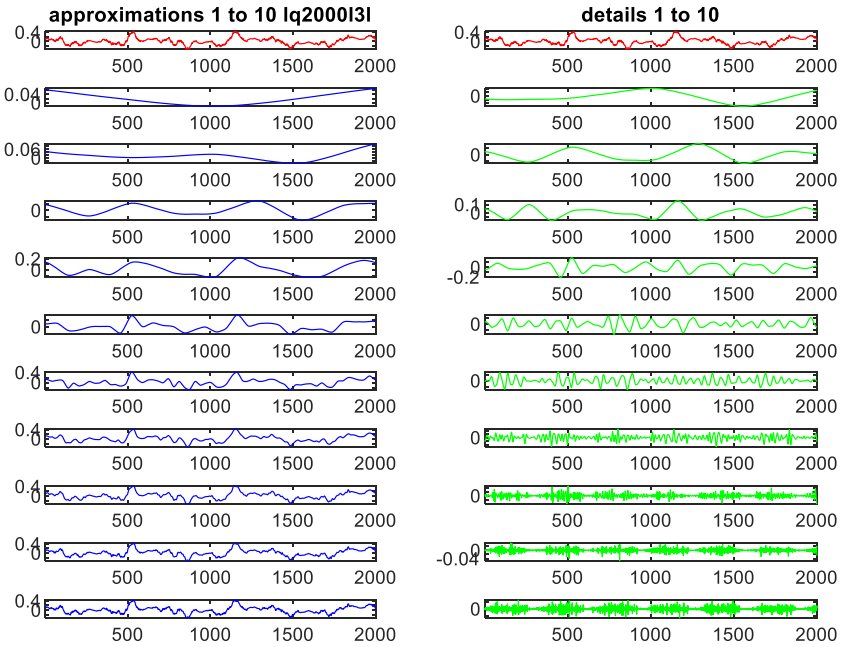

Figure 54: Details and approximations for large deep groove bearing at 2000 rpm, load 3 in light oil

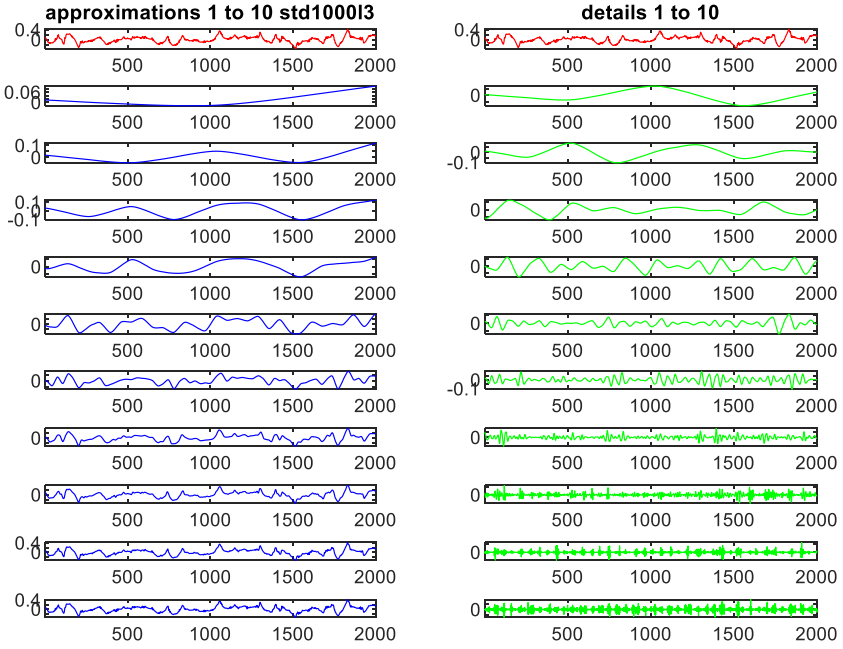

Figure 55: Details and approximations for large standard bearing at 2000 rpm, load 3 in light oil

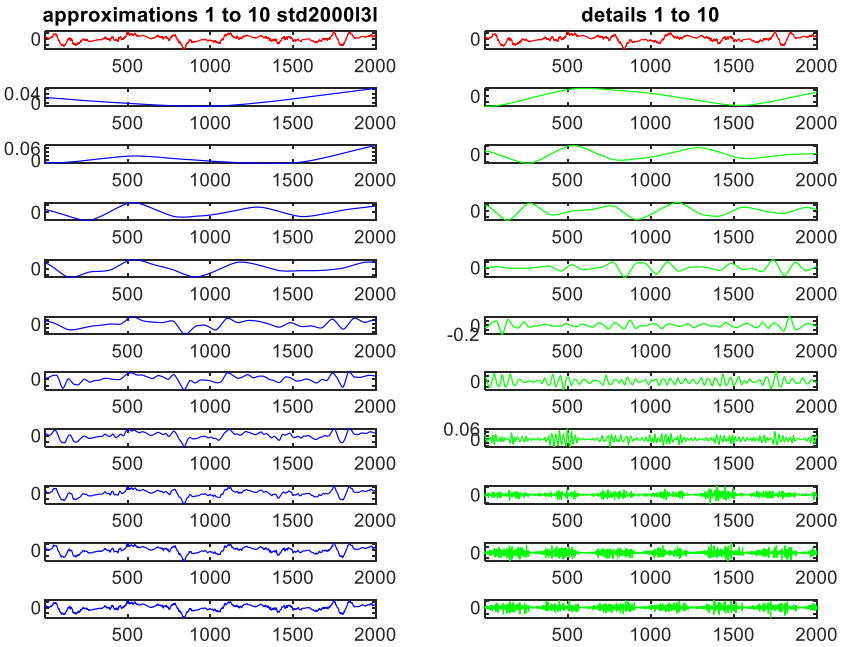

Figure 56: Details and approximations for large standard bearing at 2000 rpm, load 3 in light oil

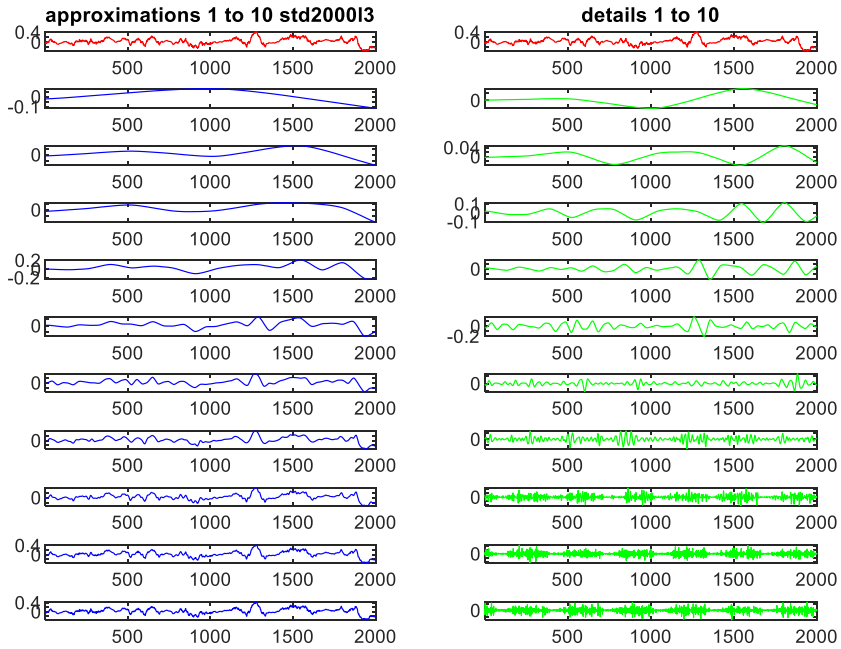

Figure 57: Details and approximations for large standard bearing at 2000 rpm, load 3 in light oil

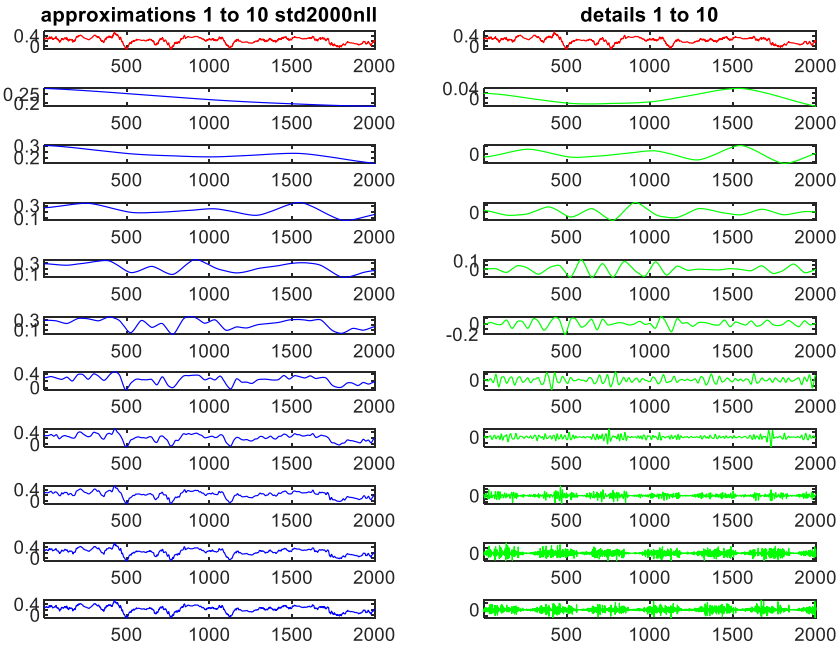

Figure 58: Details and approximations for standard bearing at 2000 rpm, no load in light oil

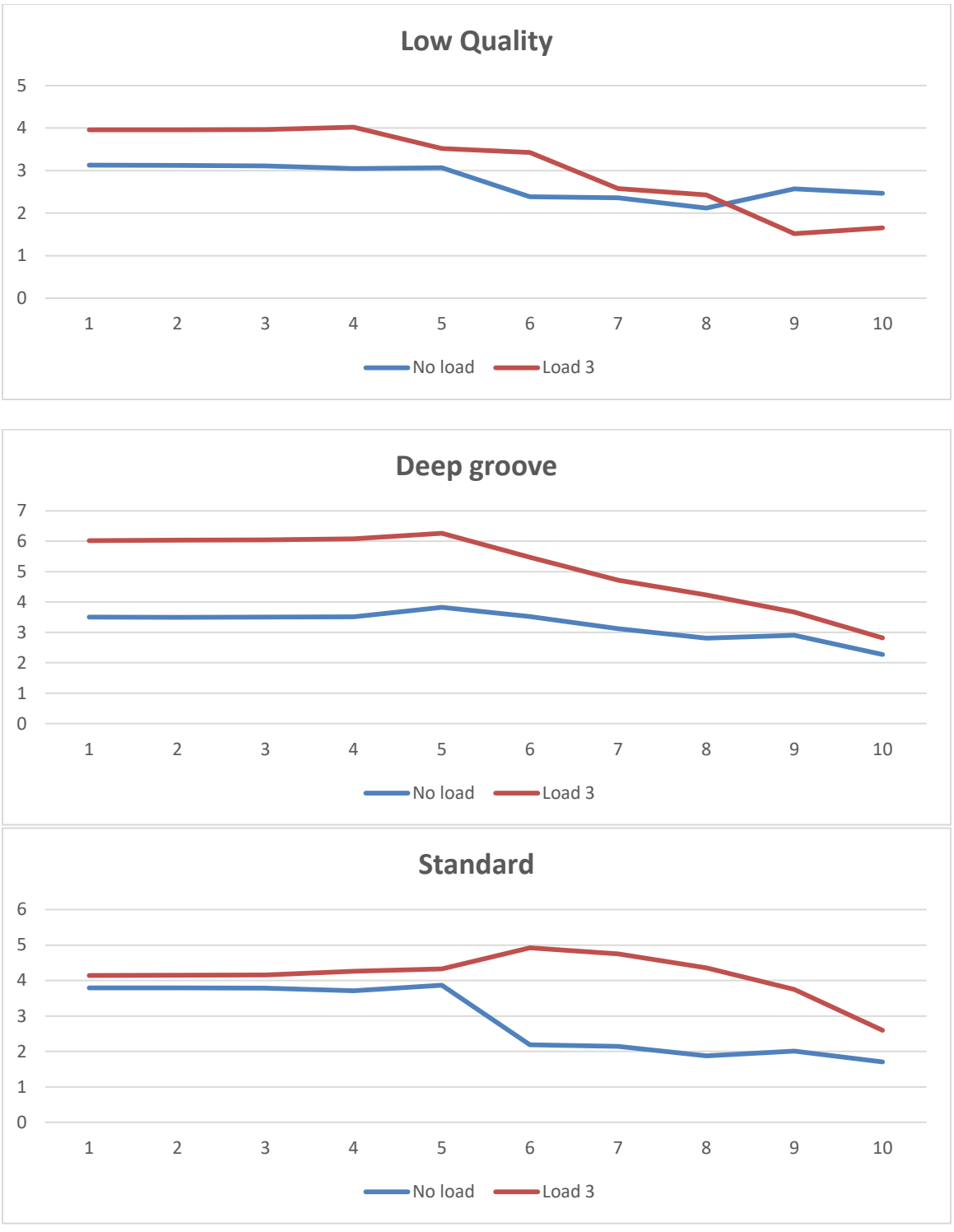

Figure 59: Large bearing kurtosis approximations at 2000 RPM in heavy oil

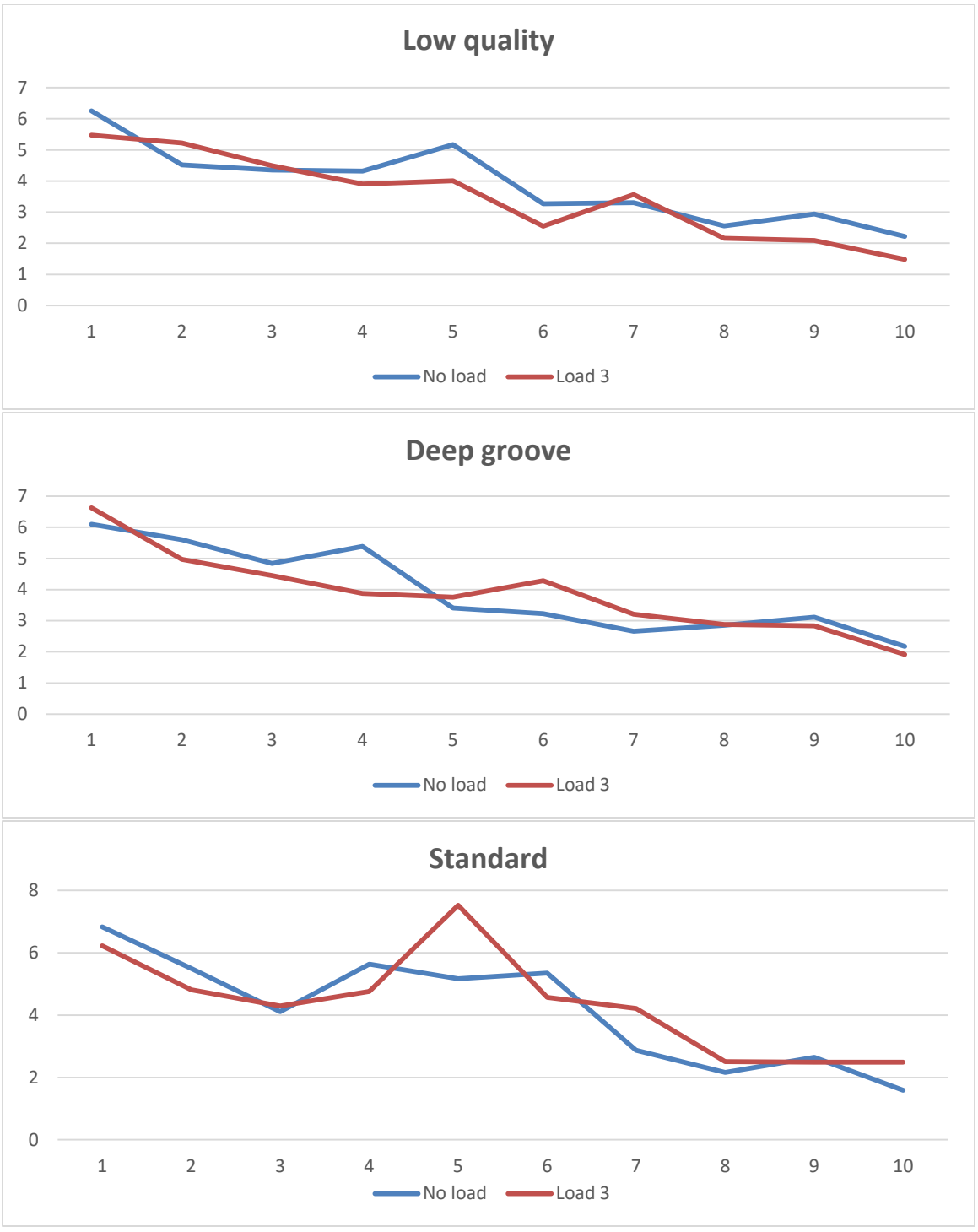

Figure 60: Large bearing kurtosis details at 2000 RPM in heavy oil

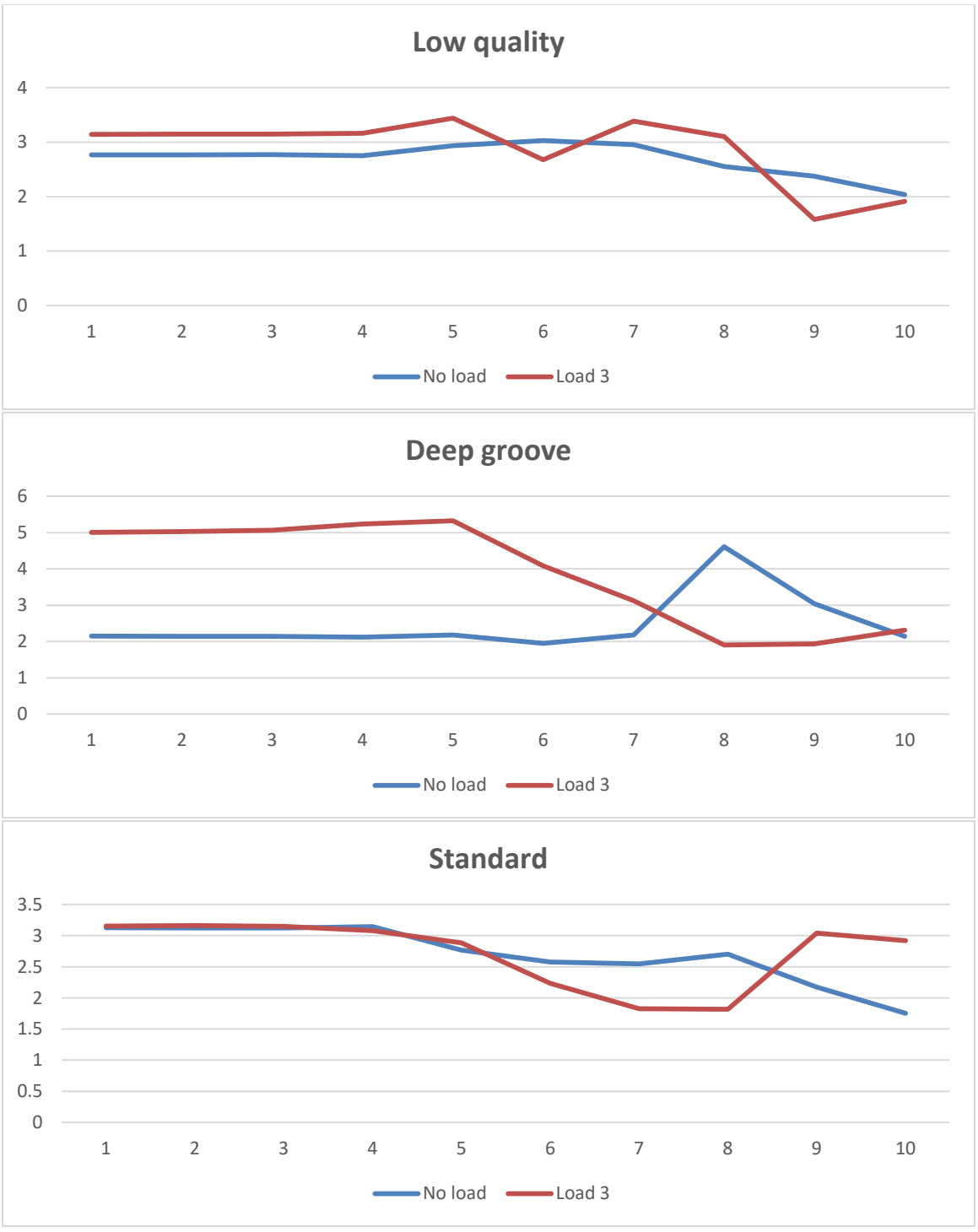

Figure 61: Large bearing kurtosis approximations at 1000 RPM in heavy oil

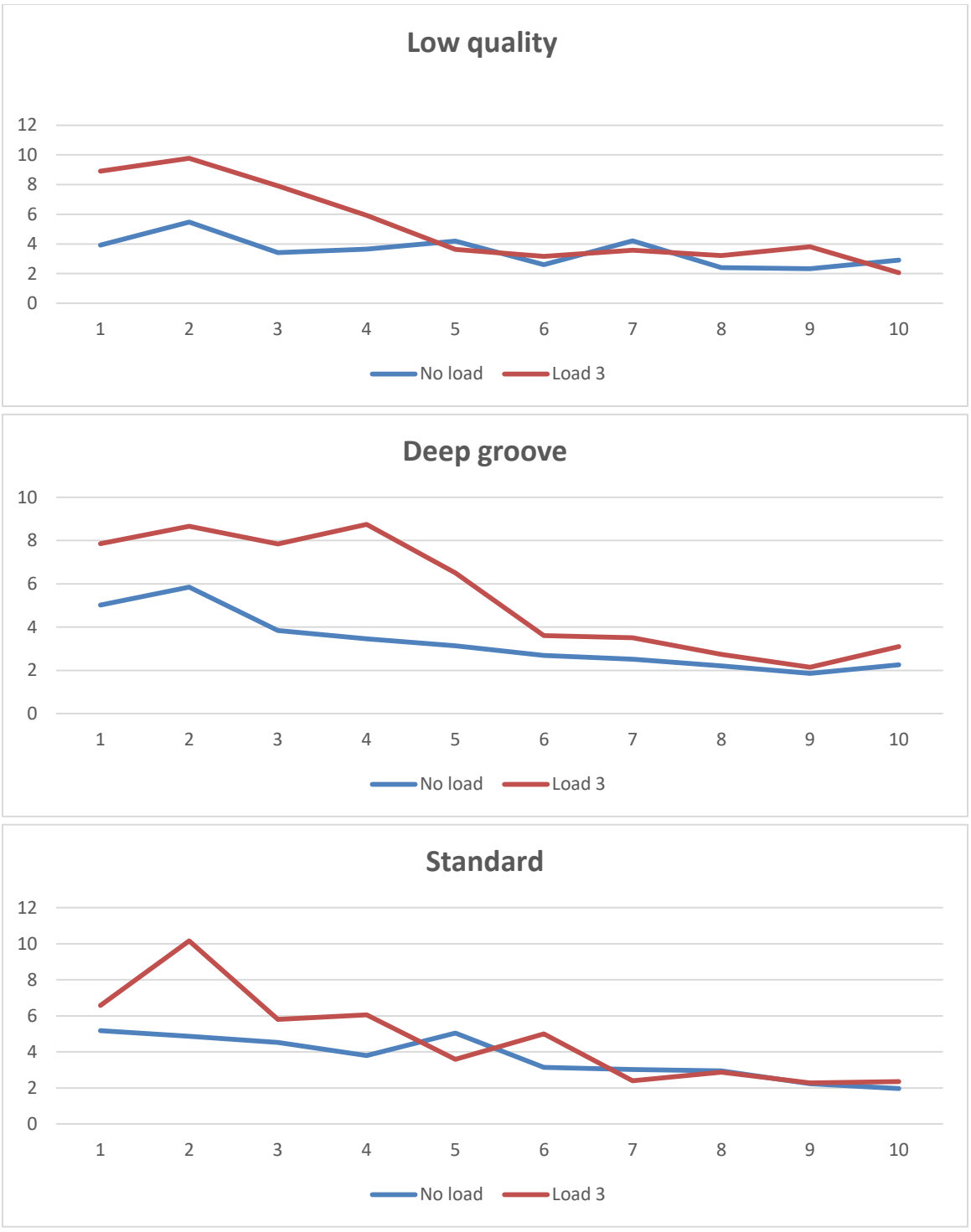

Figure 62: Large bearing kurtosis details at 1000 RPM in heavy oil

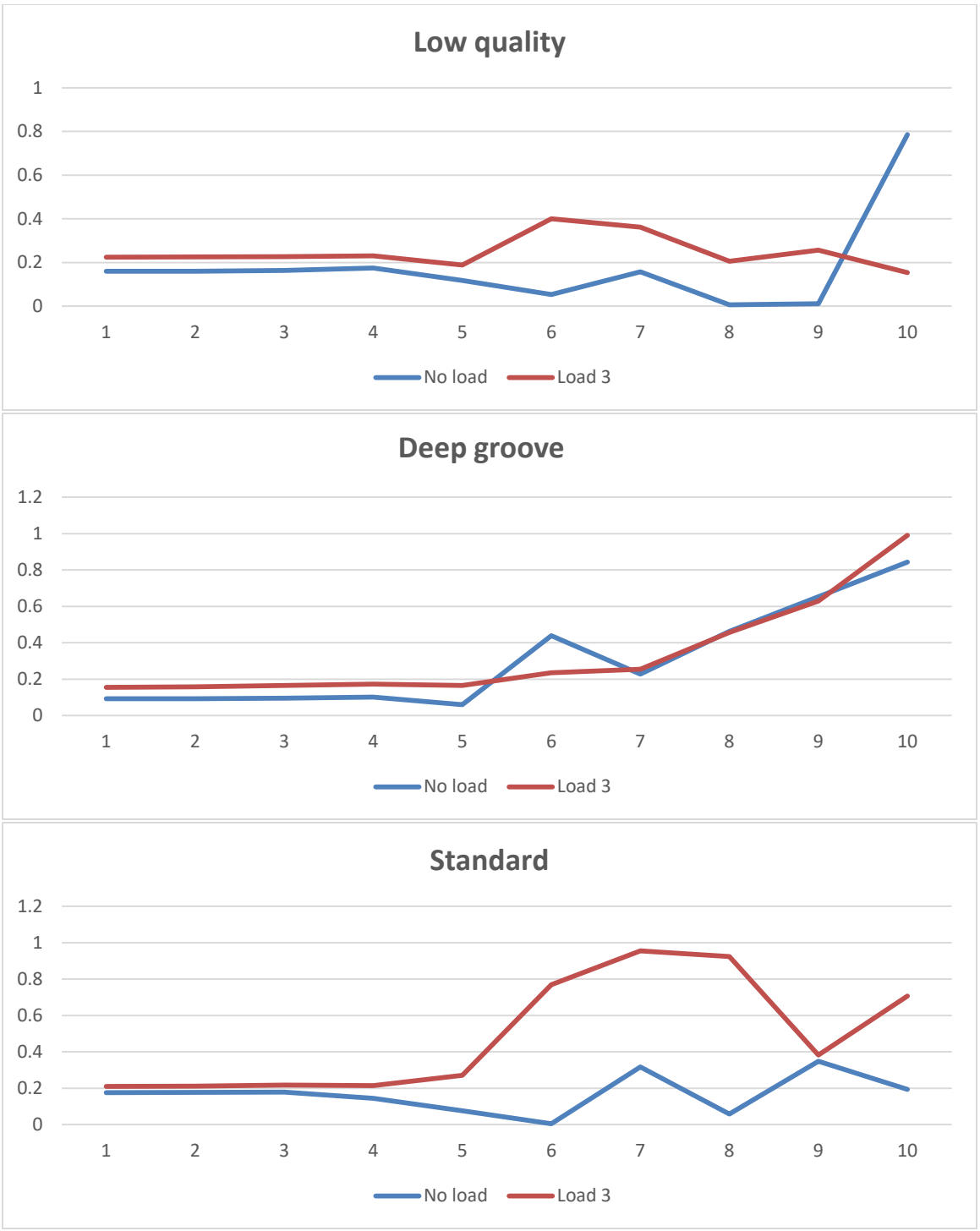

Figure 63: Large bearing skewness approximations at 2000 RPM in heavy oil

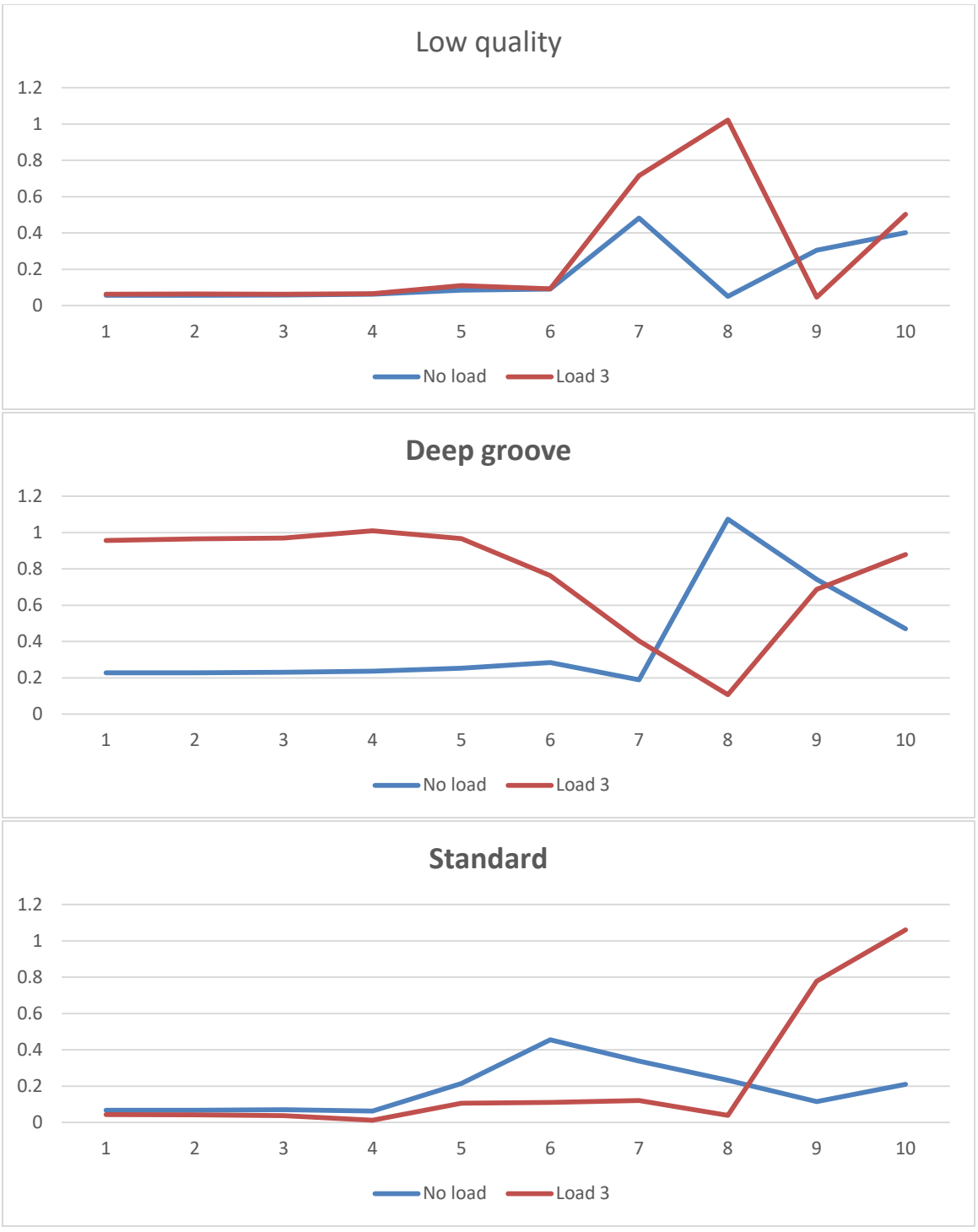

Figure 64: Large bearing skewness approximations at 1000 RPM in heavy oil

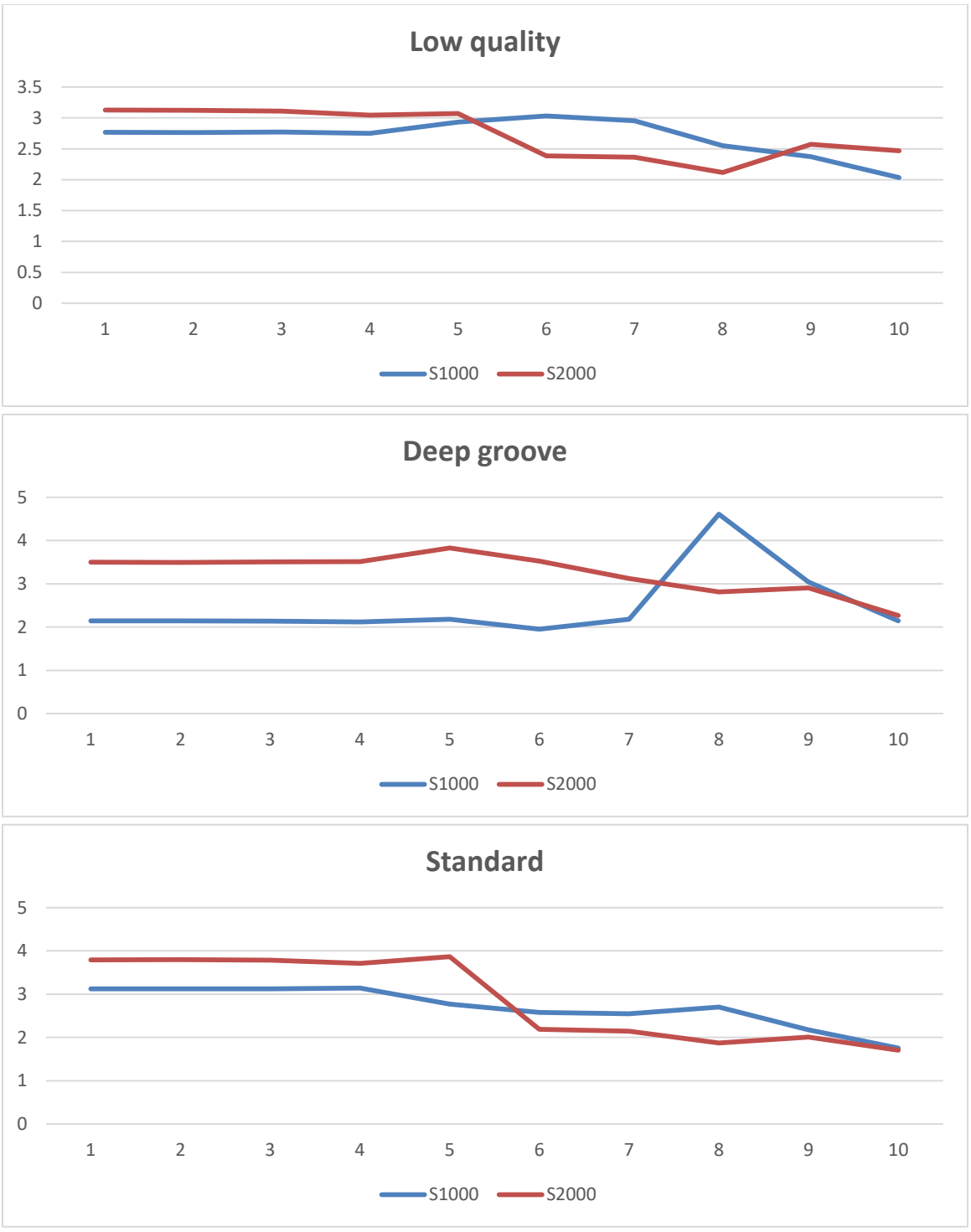

Figure 65: Large bearing no load kurtosis approximations in heavy oil

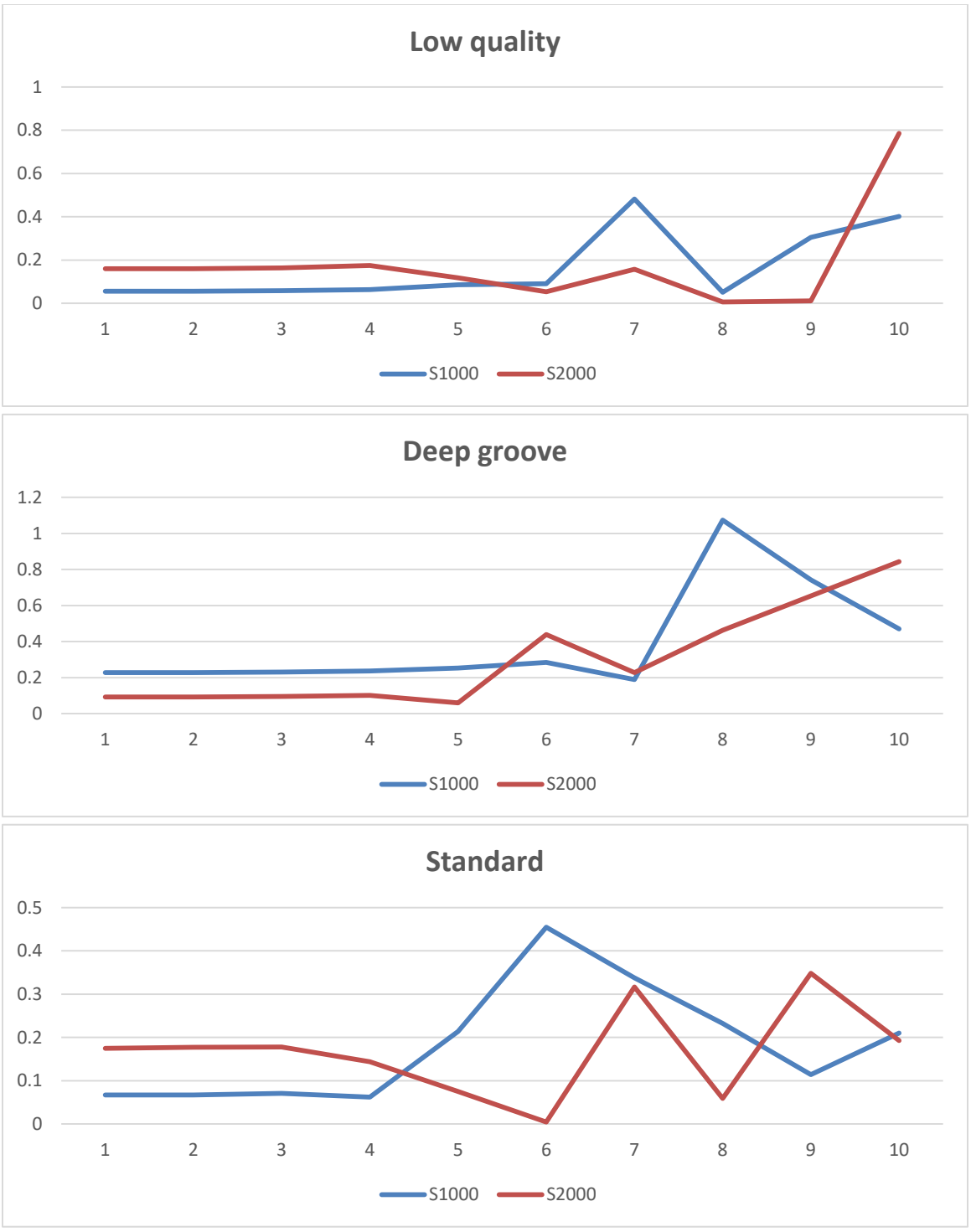

Figure 66: Large bearing no load skewness approximations in heavy oil

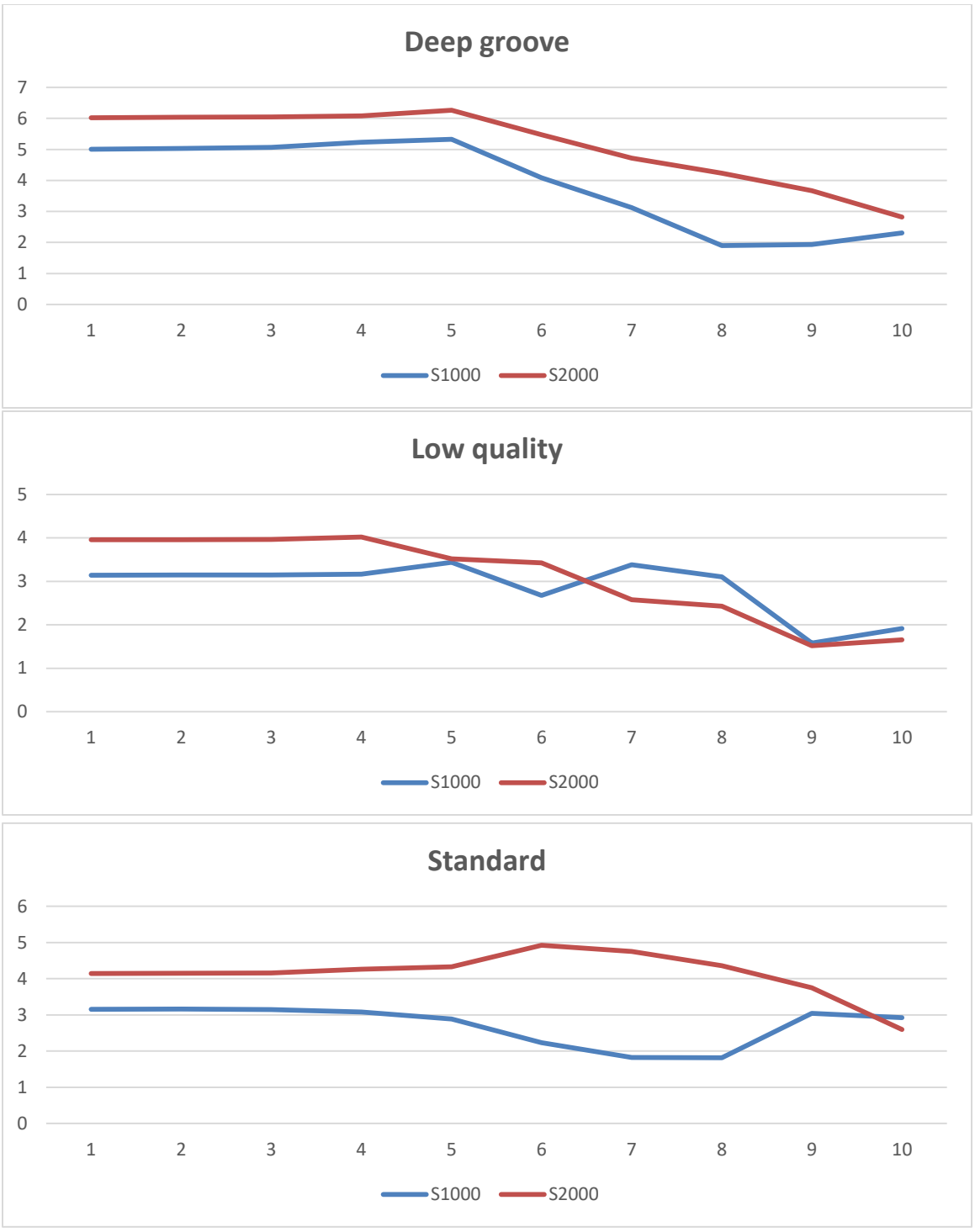

Figure 67: Large bearing at load three kurtosis approximations in heavy oil

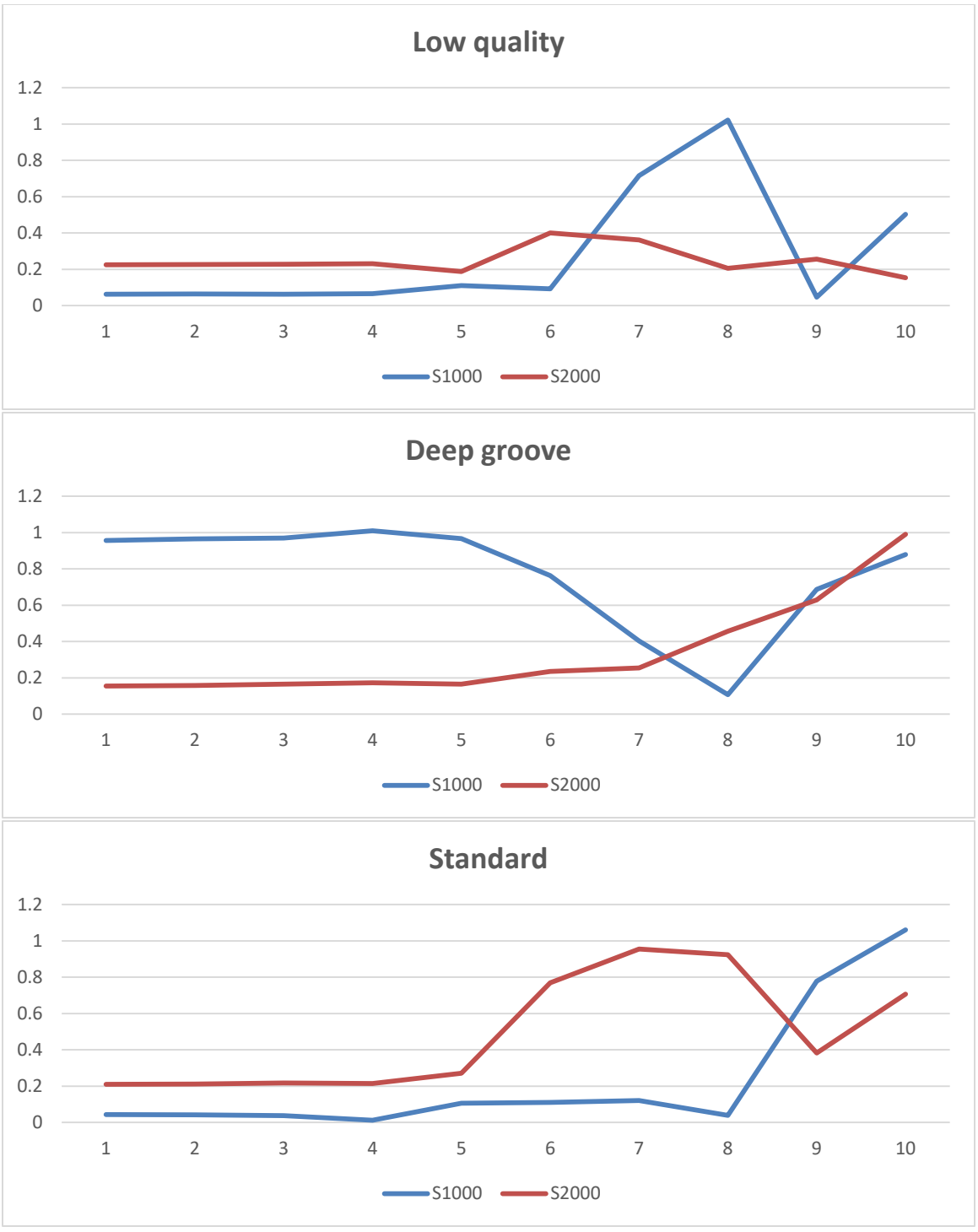

Figure 68: Large bearing at load three skewness approximations in heavy oil

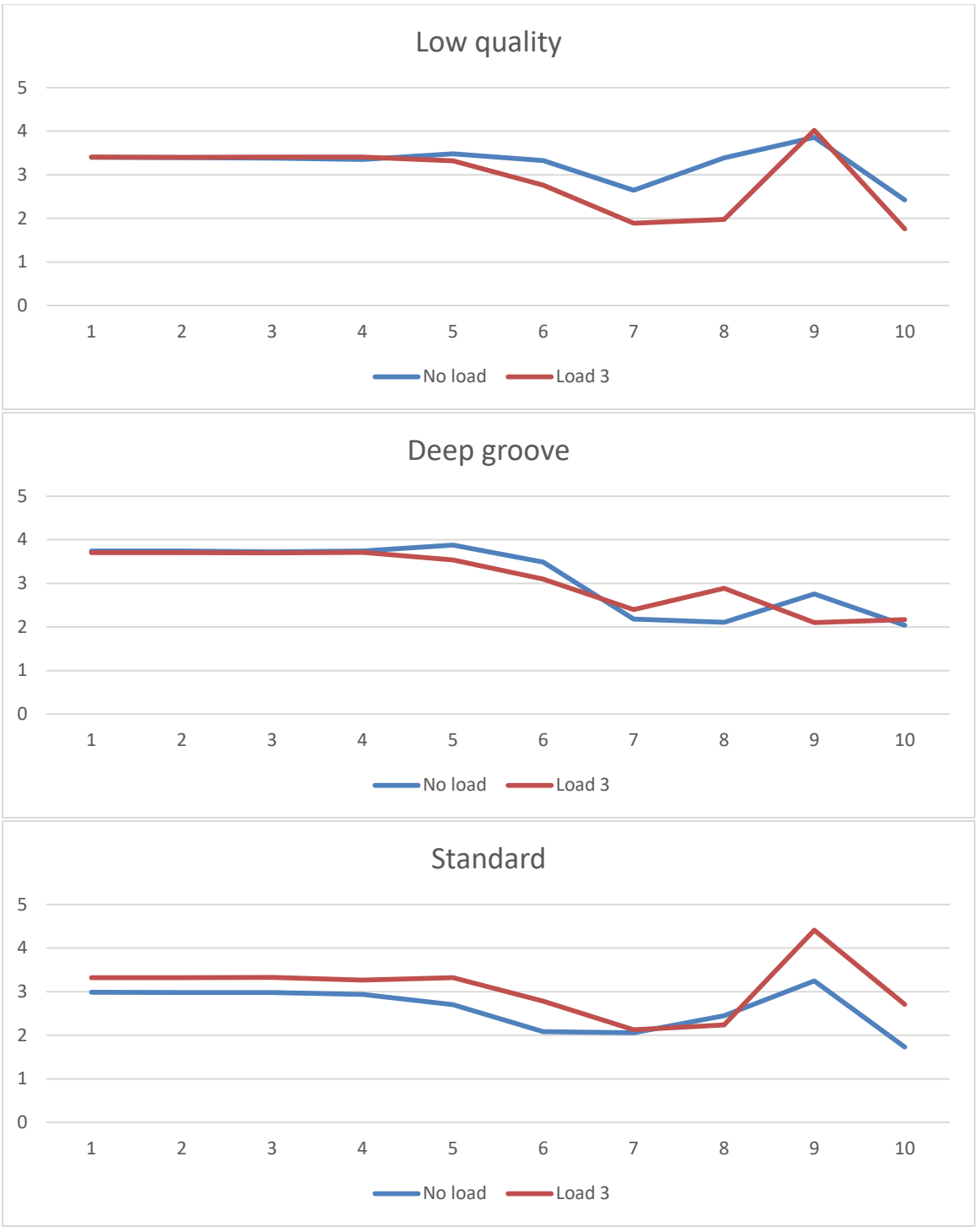

Figure 69: Large bearing kurtosis approximations at 2000 RPM in light oil

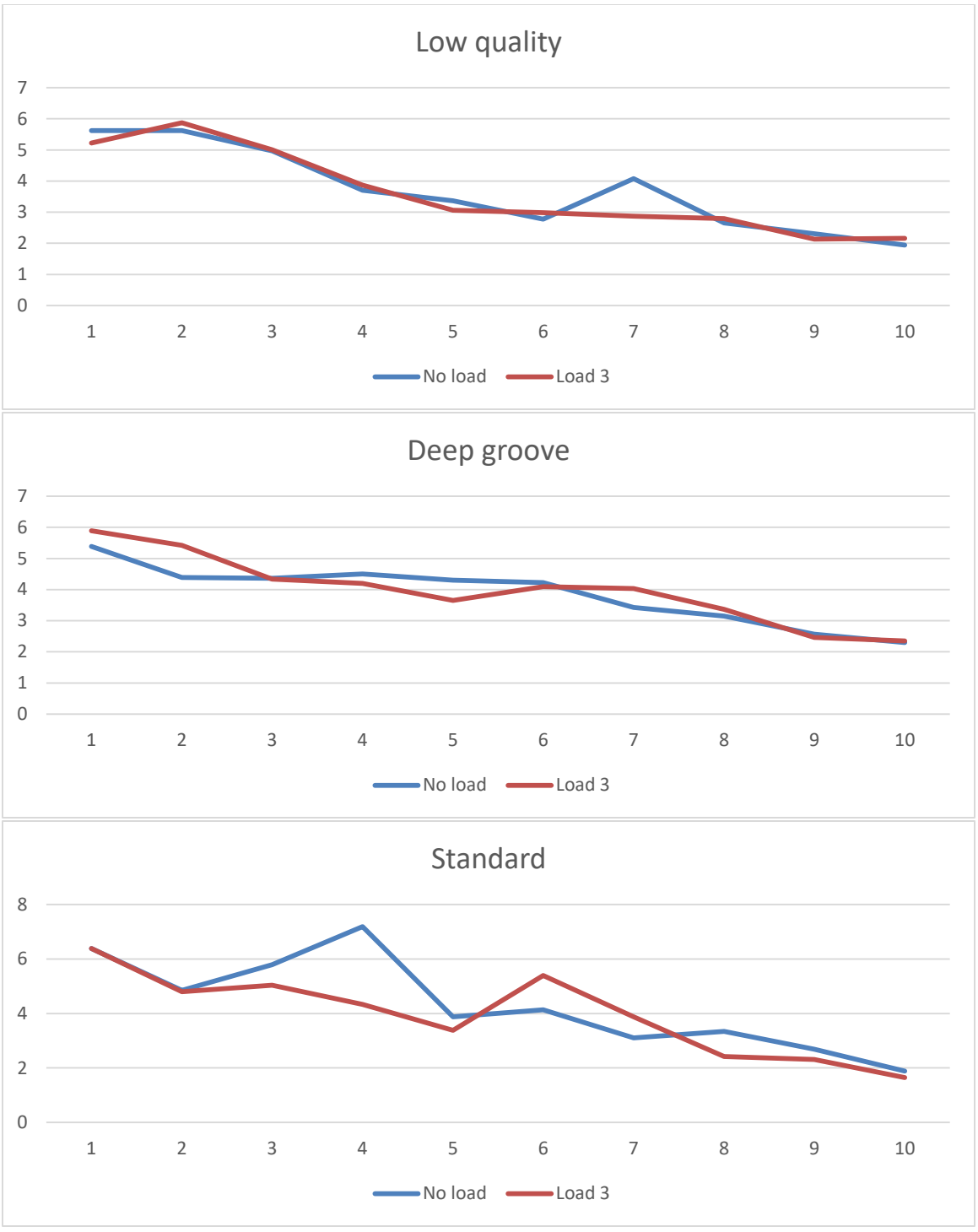

Figure 70: Large bearing kurtosis details at 2000 RPM in light oil

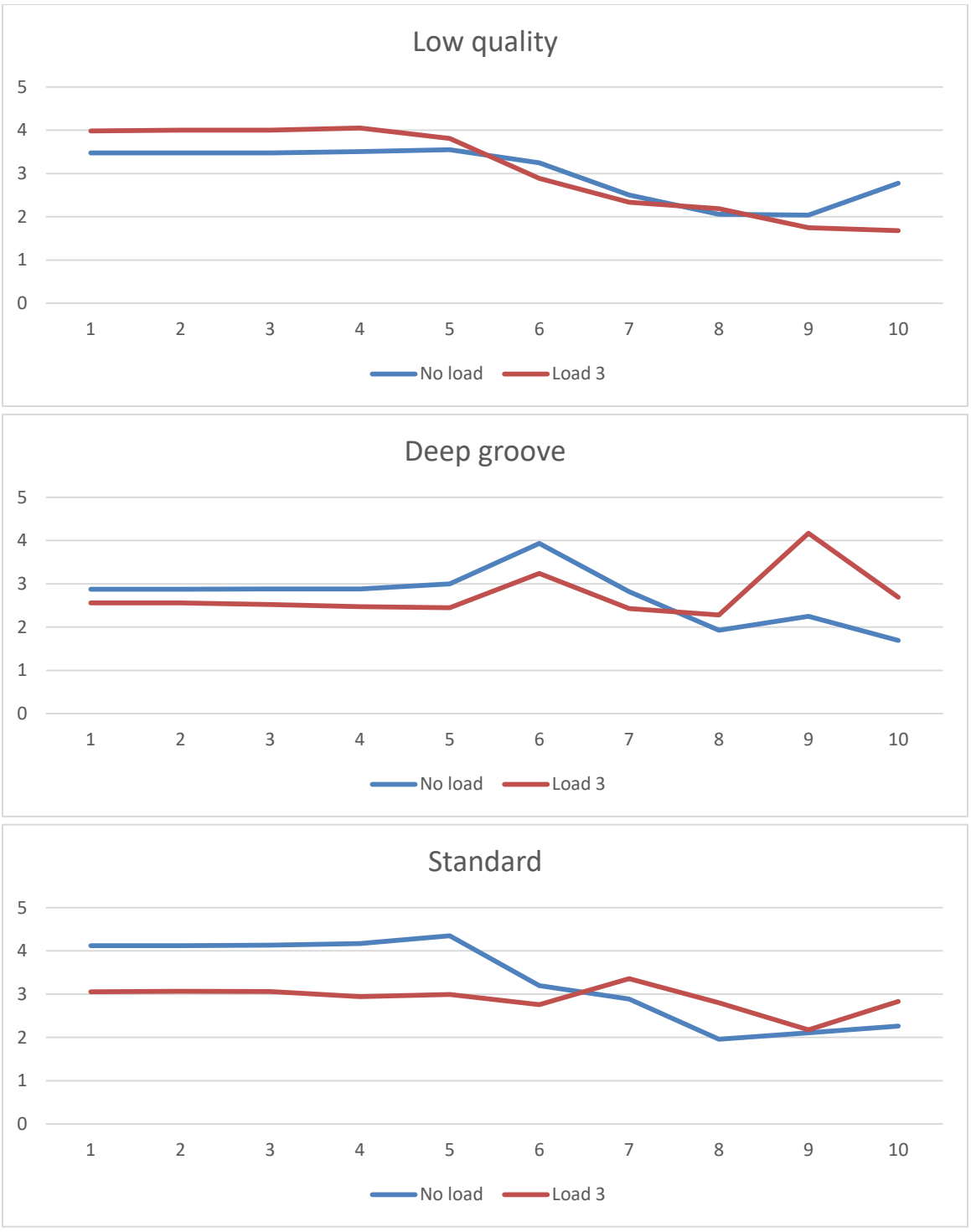

Figure 71: Large bearing kurtosis approximations at 1000 RPM in light oil

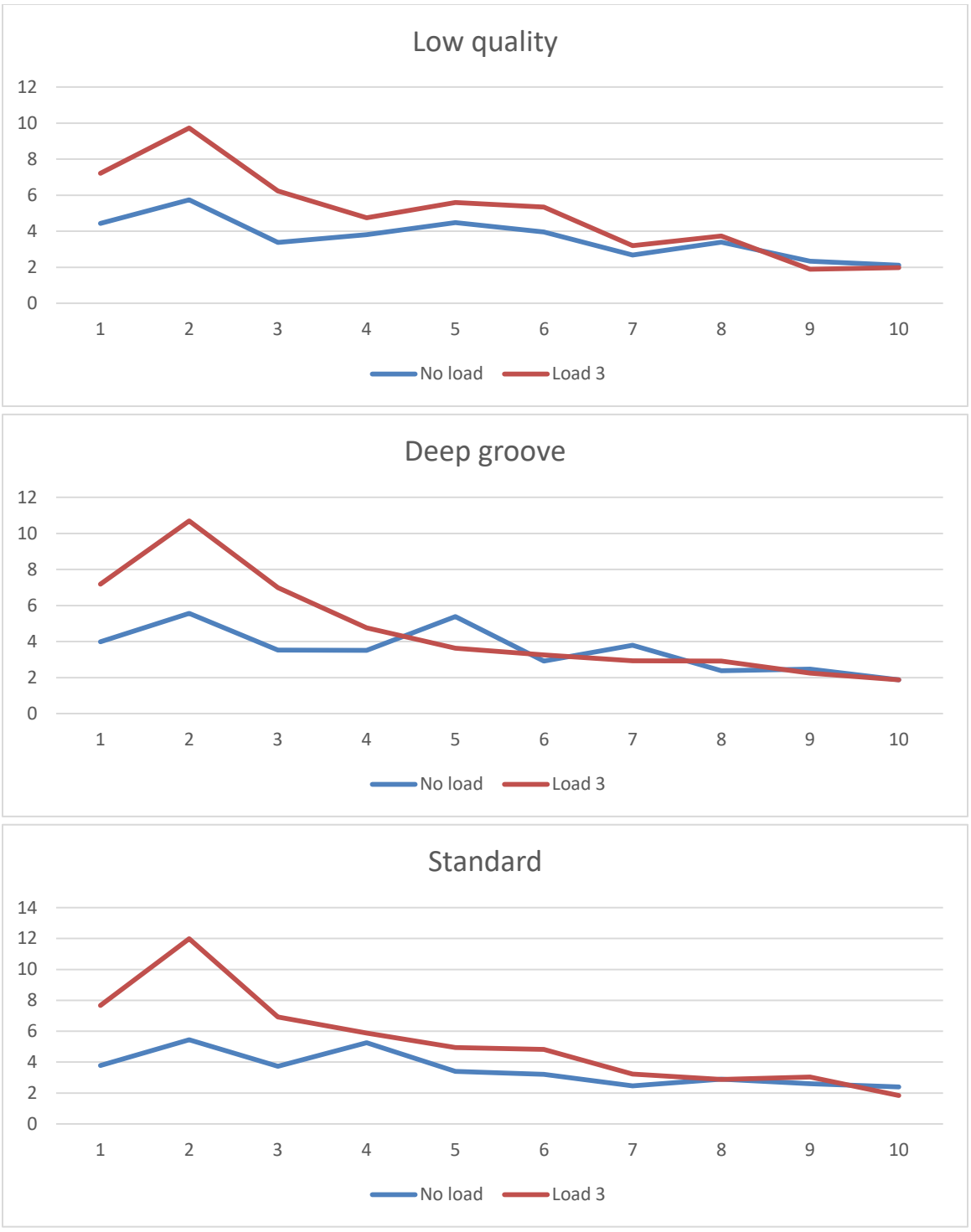

Figure 72: Large bearing kurtosis details at 1000 RPM in light oil

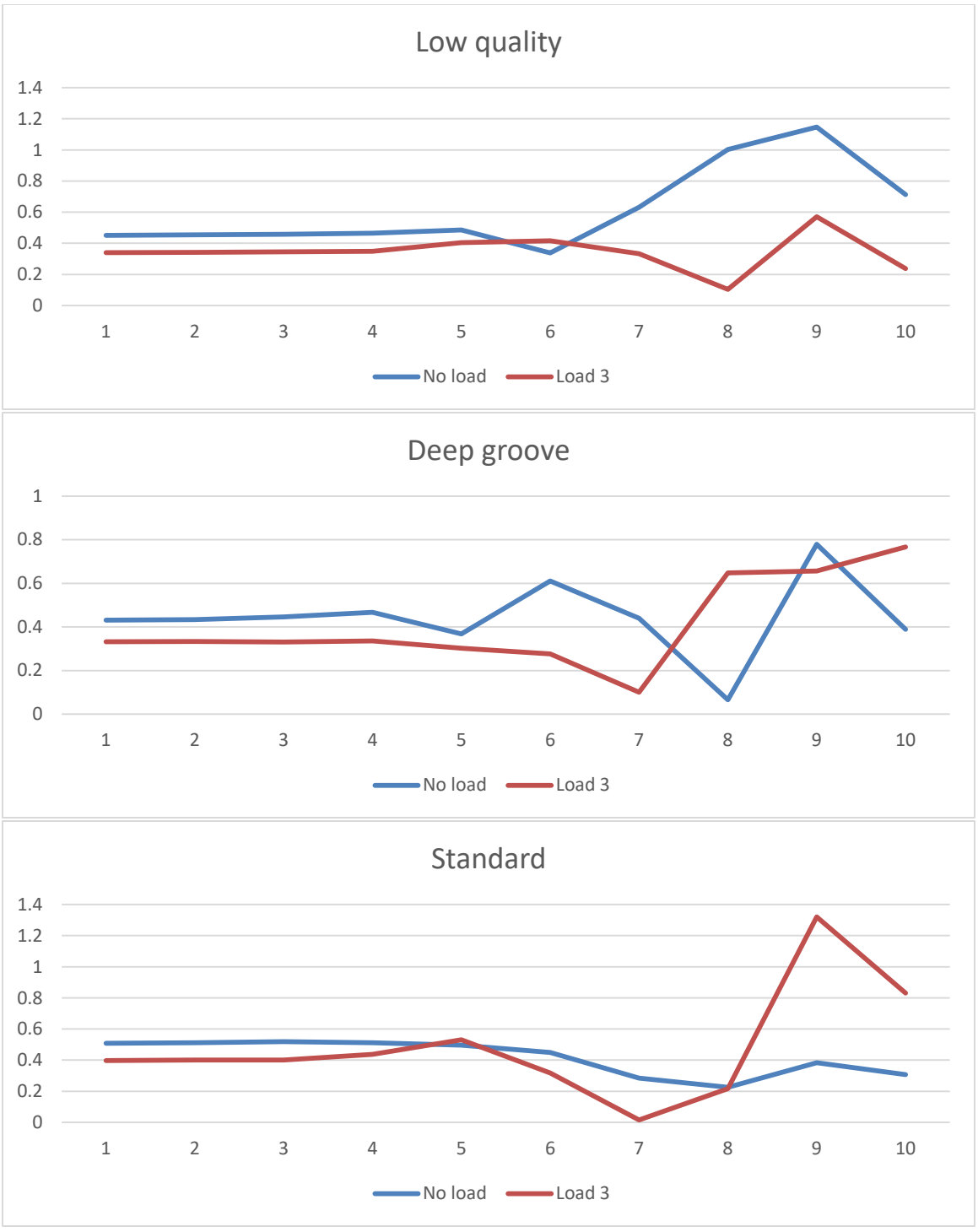

Figure 73: Large bearing skewness approximations at 2000 RPM in light oil

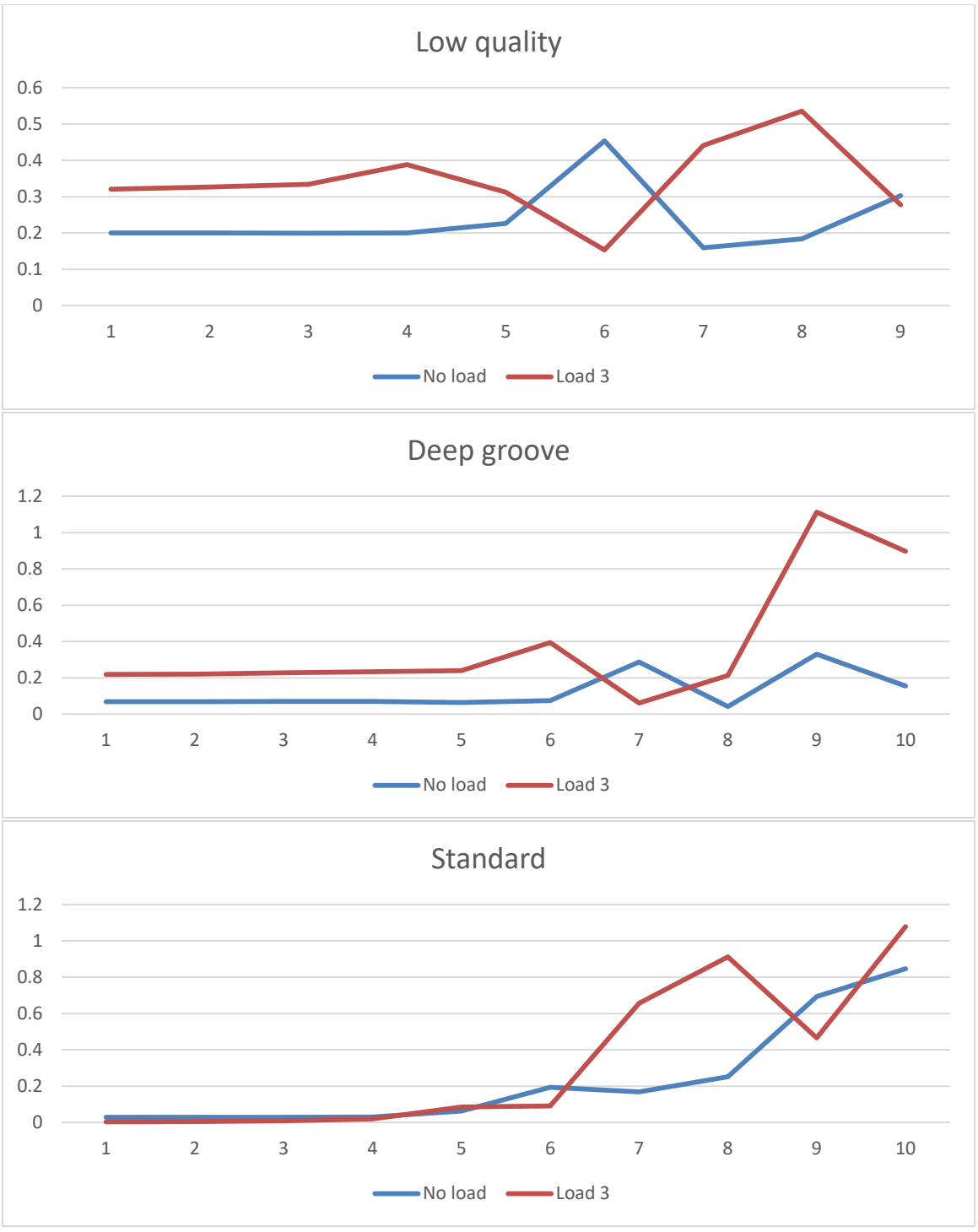

Figure 74: Large bearing skewness approximations at 1000 RPM in light oil

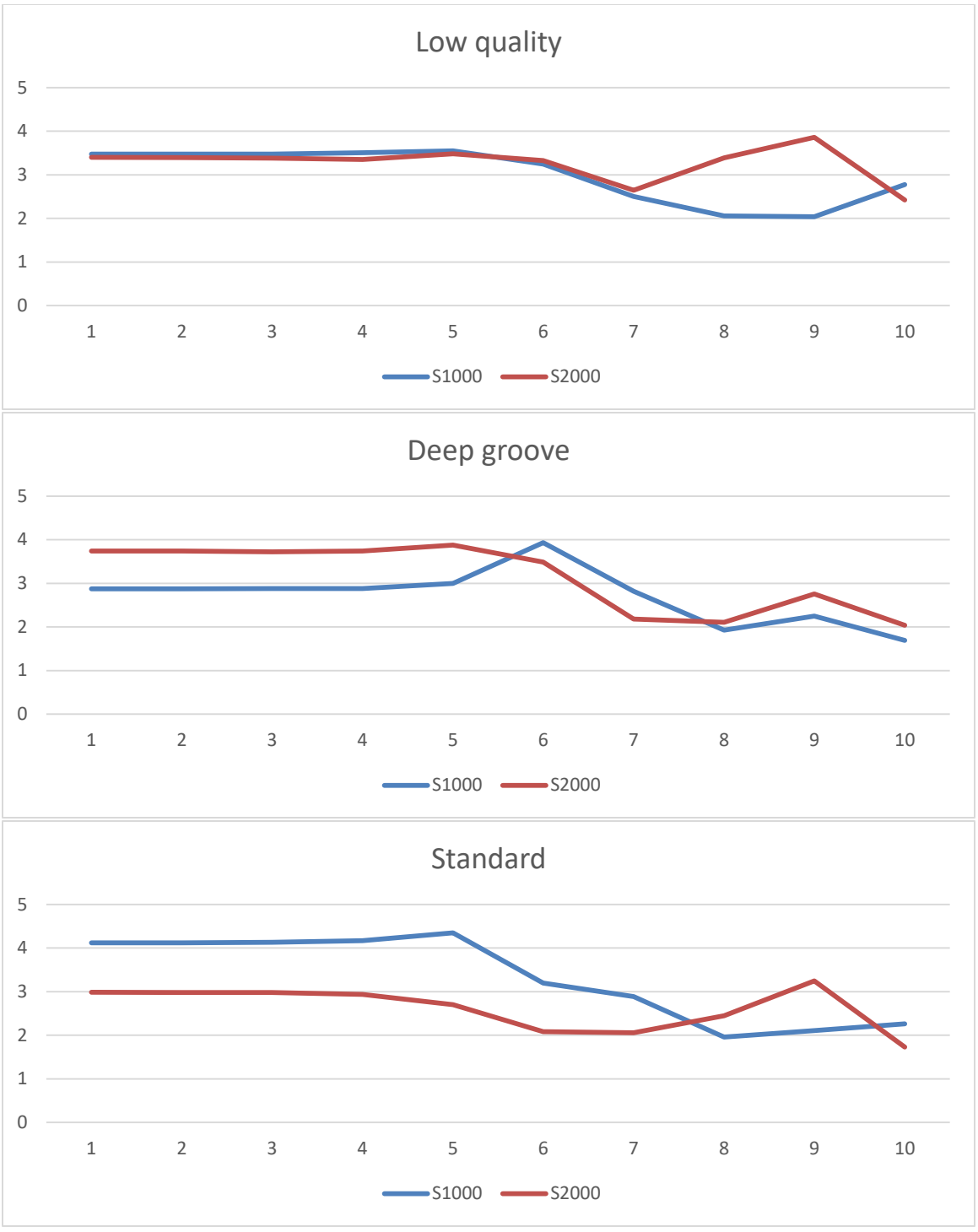

Figure 75: Large bearing no load kurtosis approximations in light oil

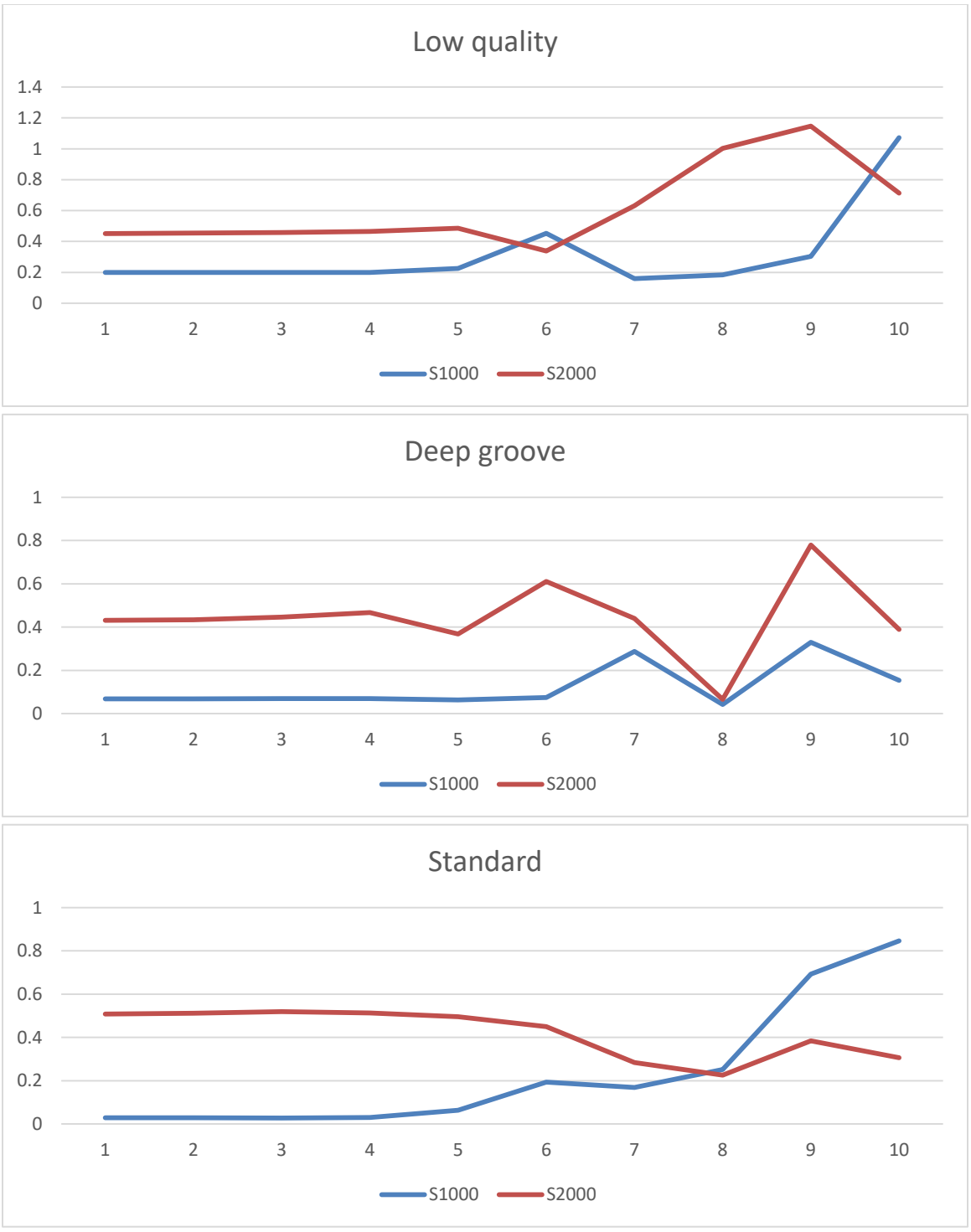

Figure 76: Large bearing no load skewness approximations in light oil

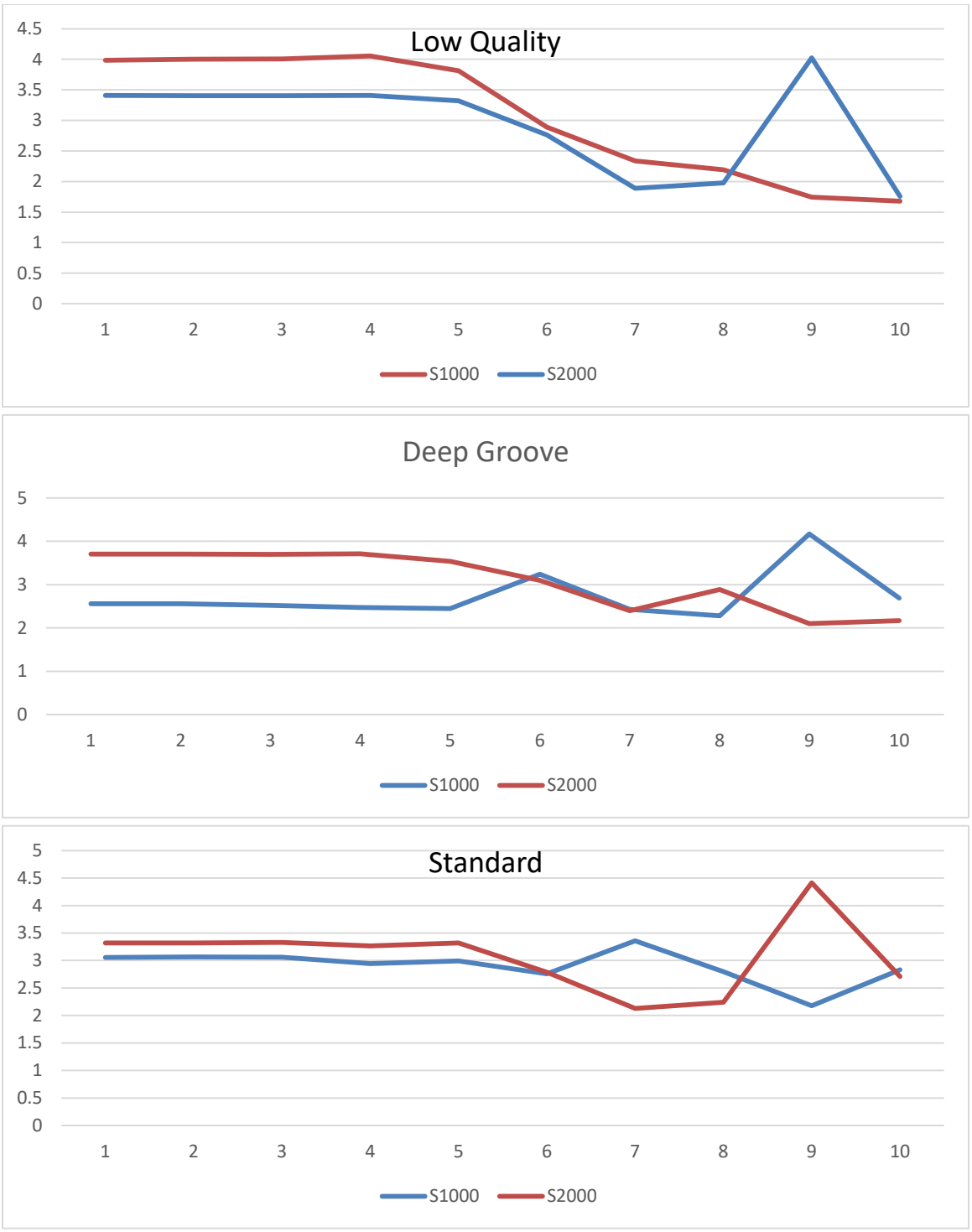

Figure 77: Large bearing at load three kurtosis approximations in light oil

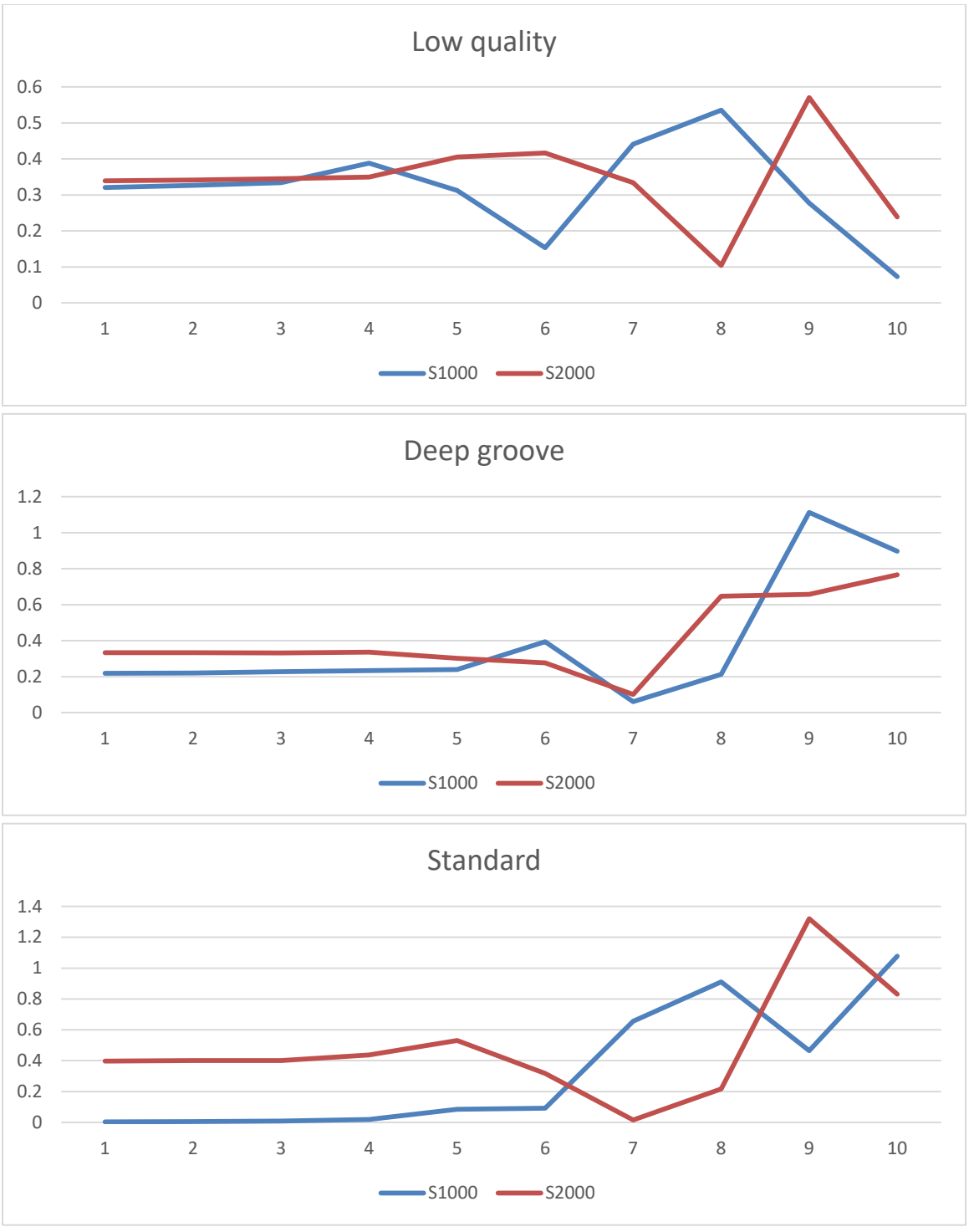

Figure 78: Large bearing at load three skewness approximations in light oil

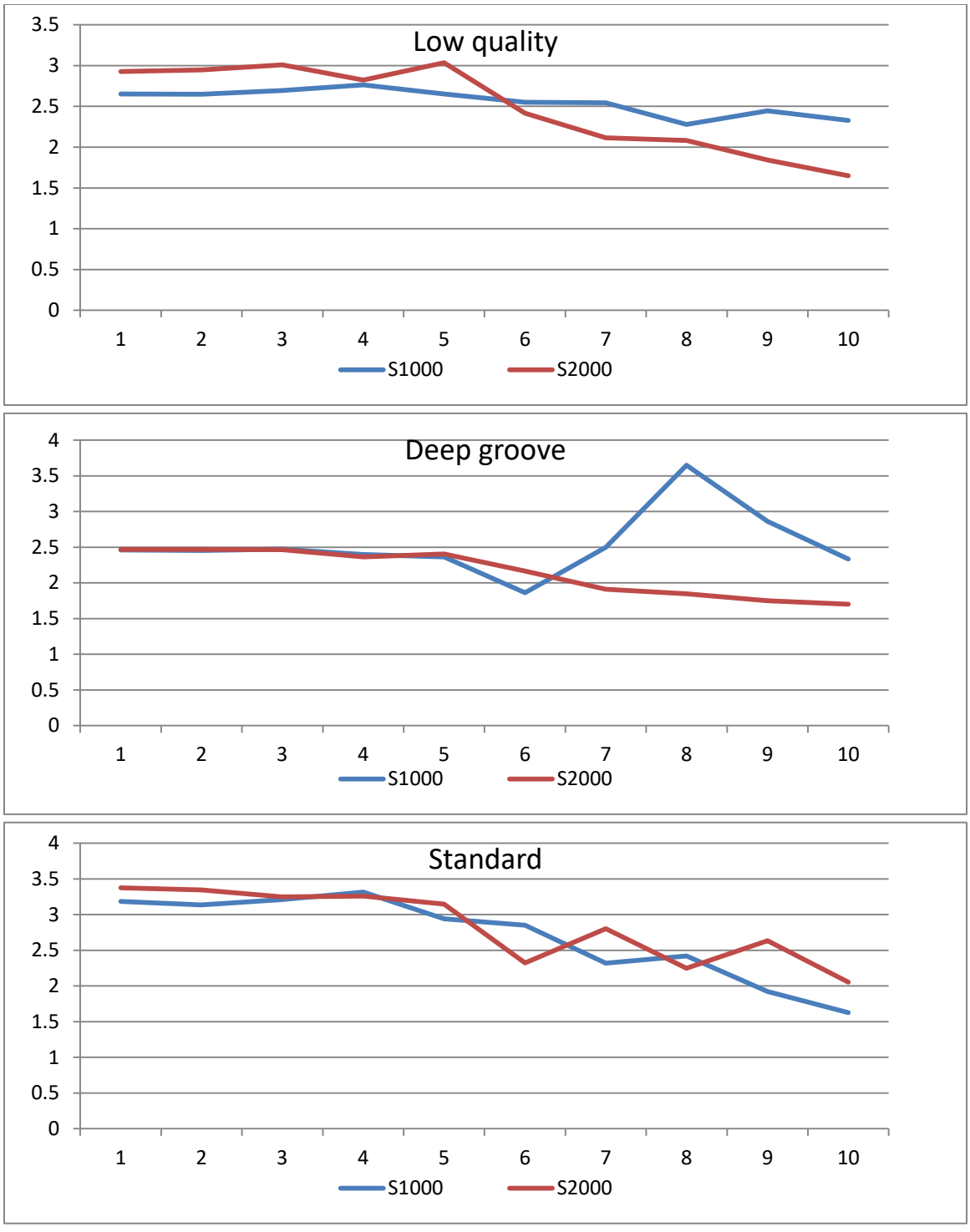

Figure 79: Large bearing at no load crest factor approximations in heavy oil

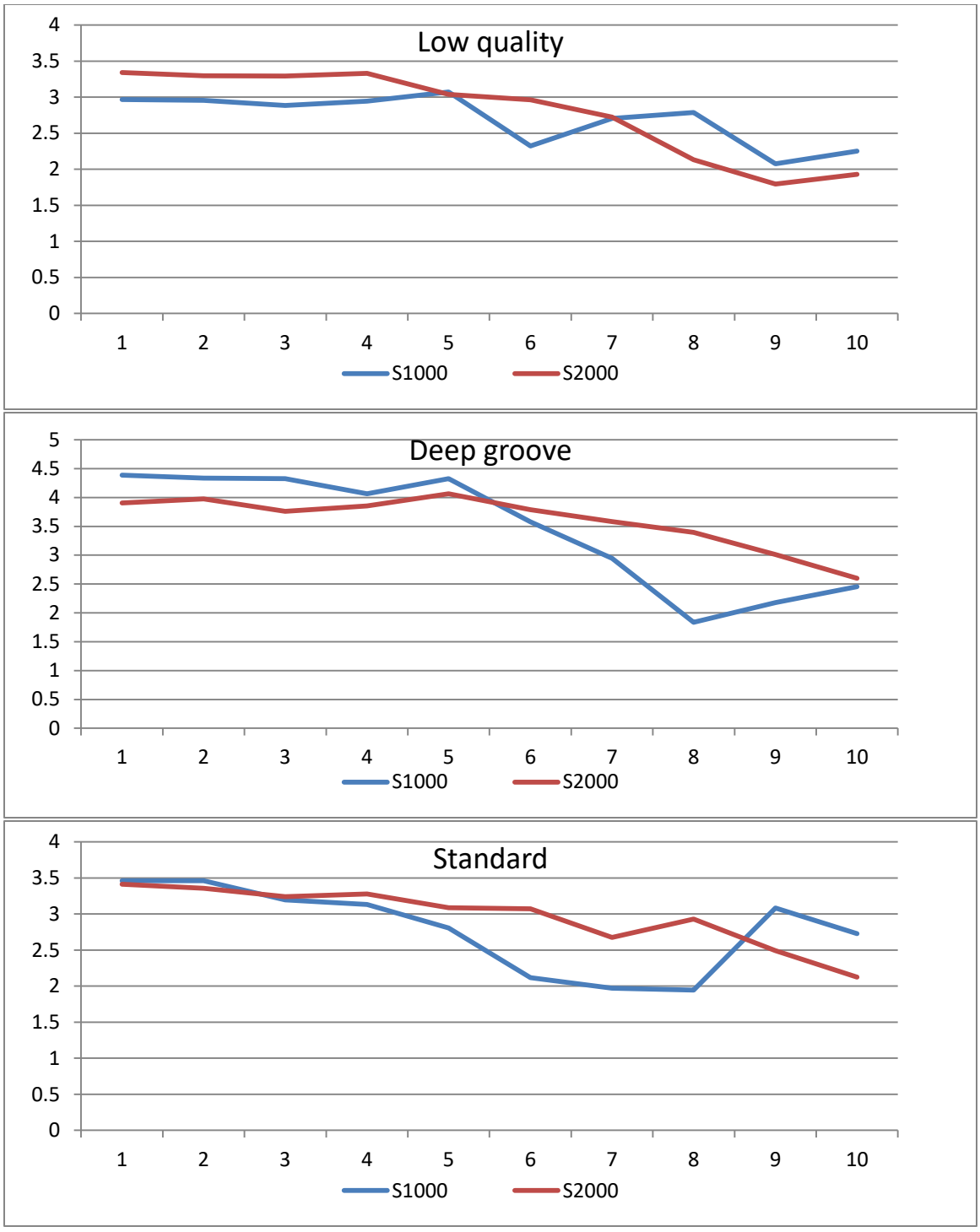

Figure 80: Large bearing at load three crest factor approximations in heavy oil

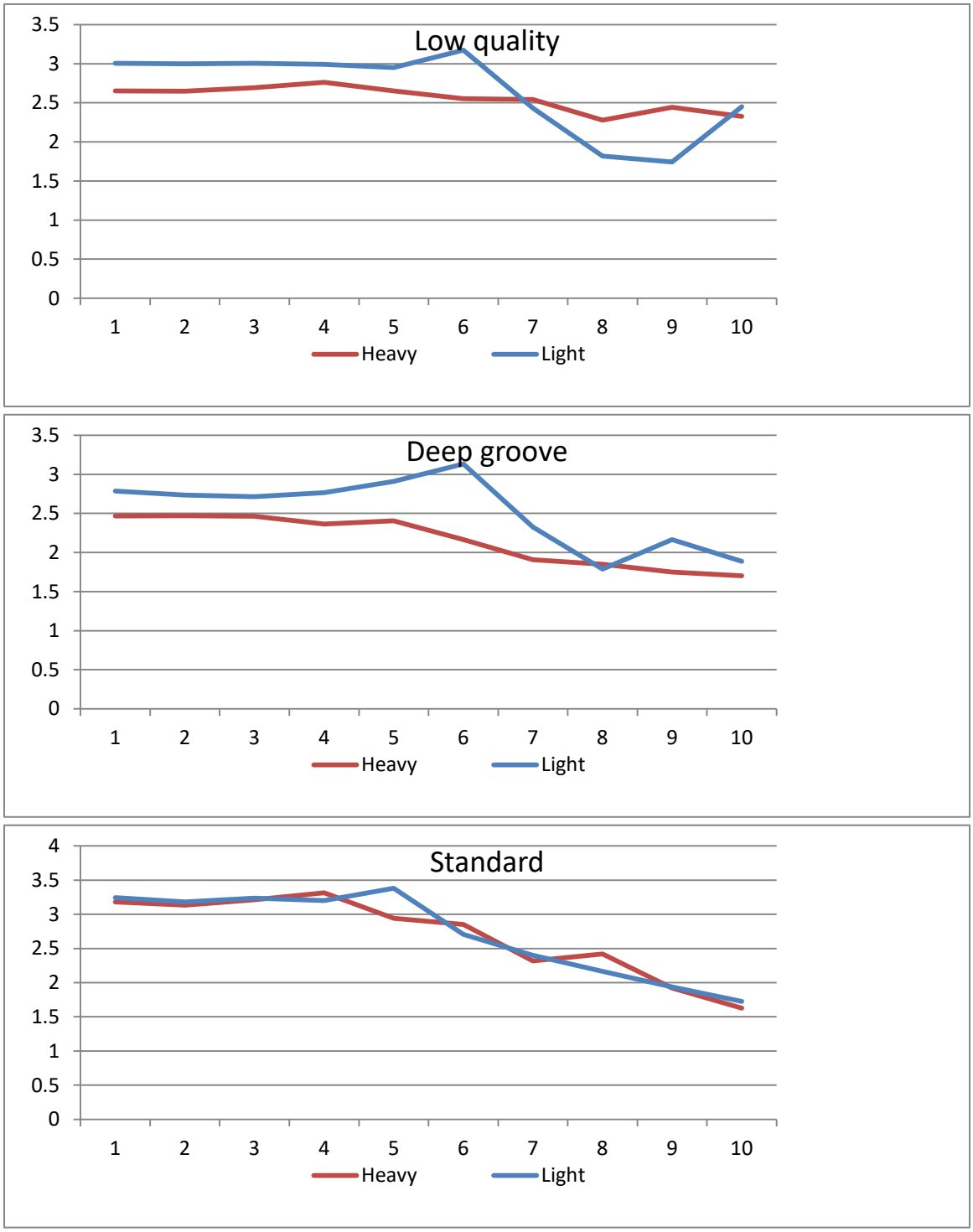

Figure 81: Large bearing at no load crest factor approximations at 1000 rpm

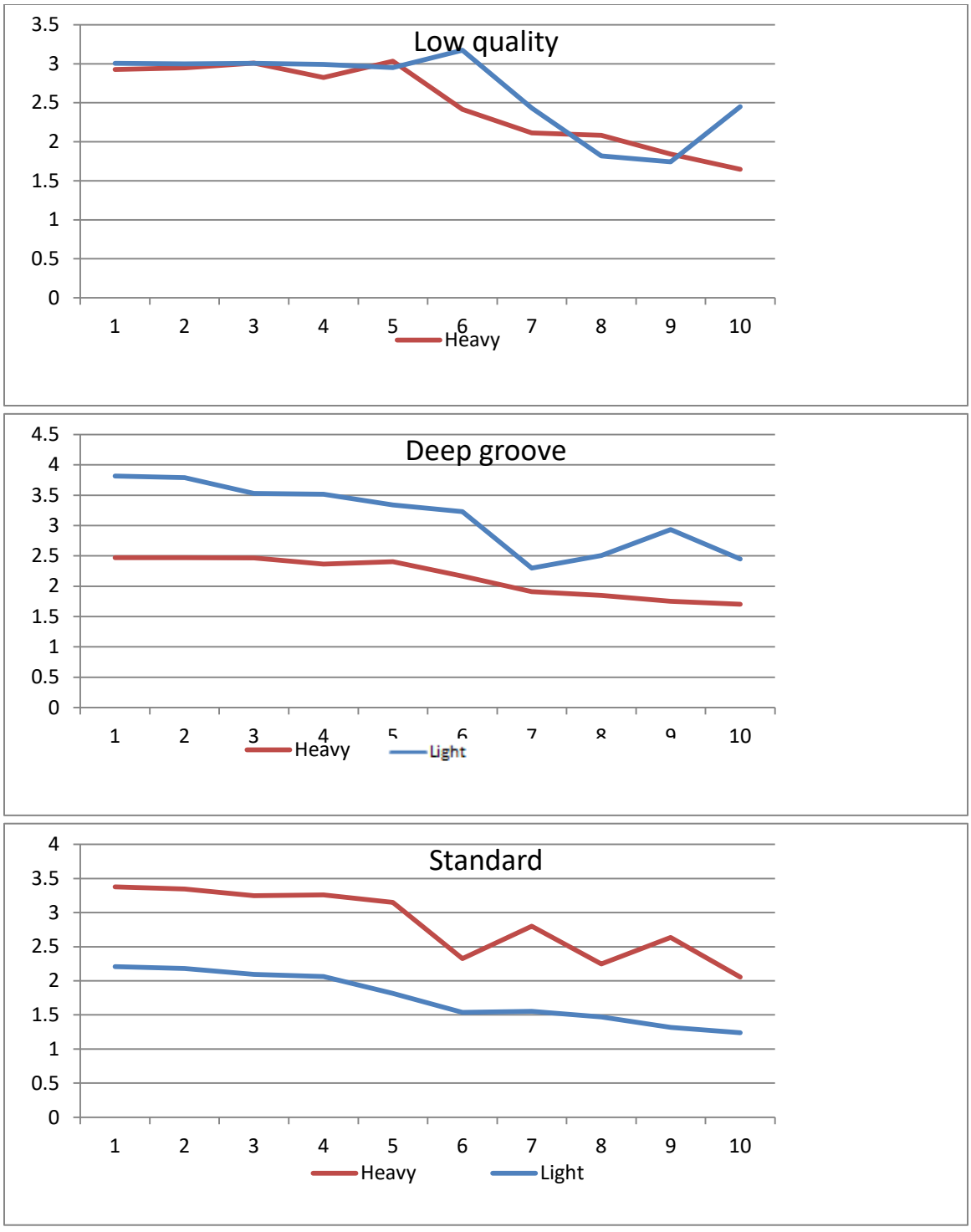

Figure 82: Large bearing at no load crest factor approximations at 2000 rpm

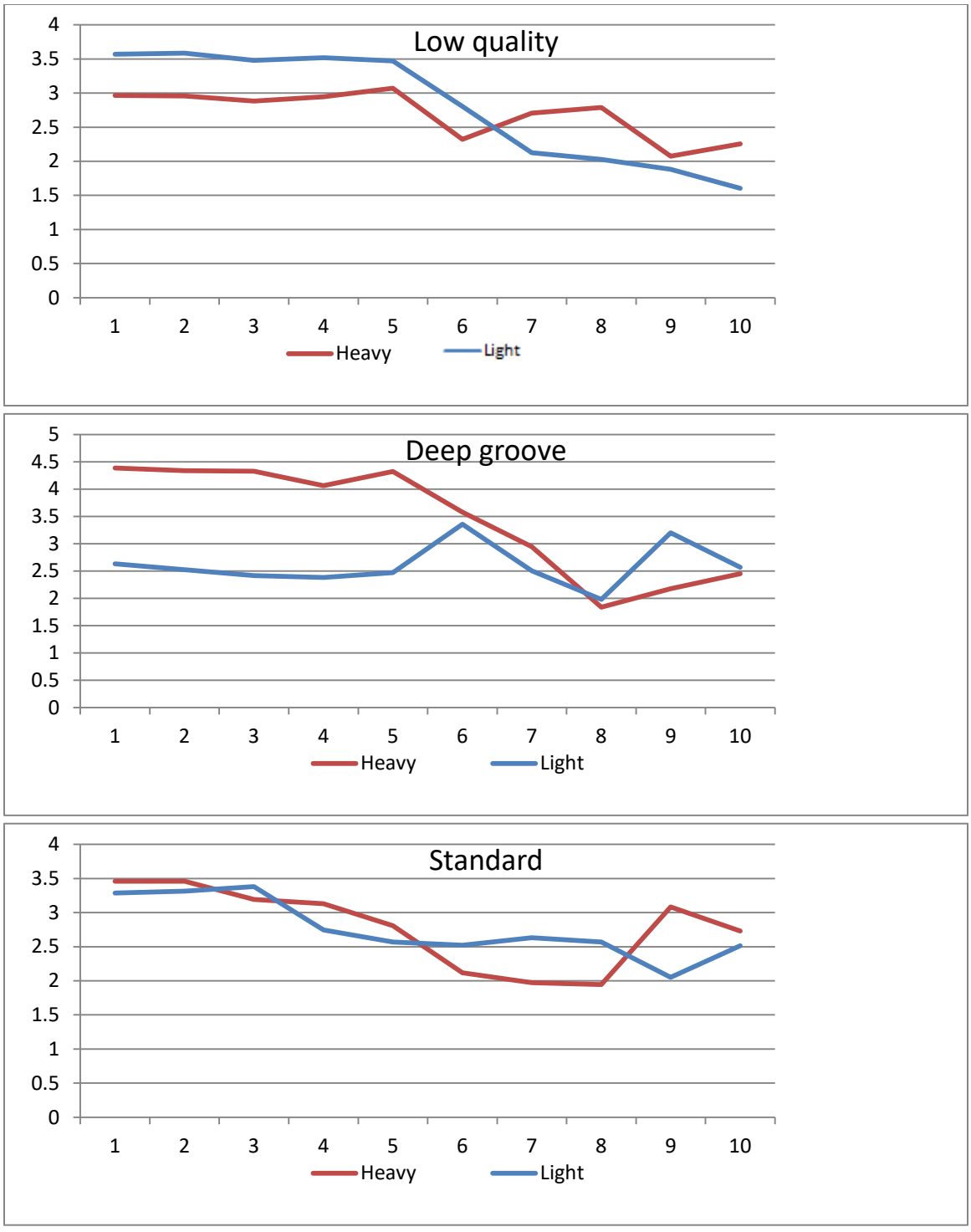

Figure 83: Large bearing at load three crest factor approximations at 1000 rpm

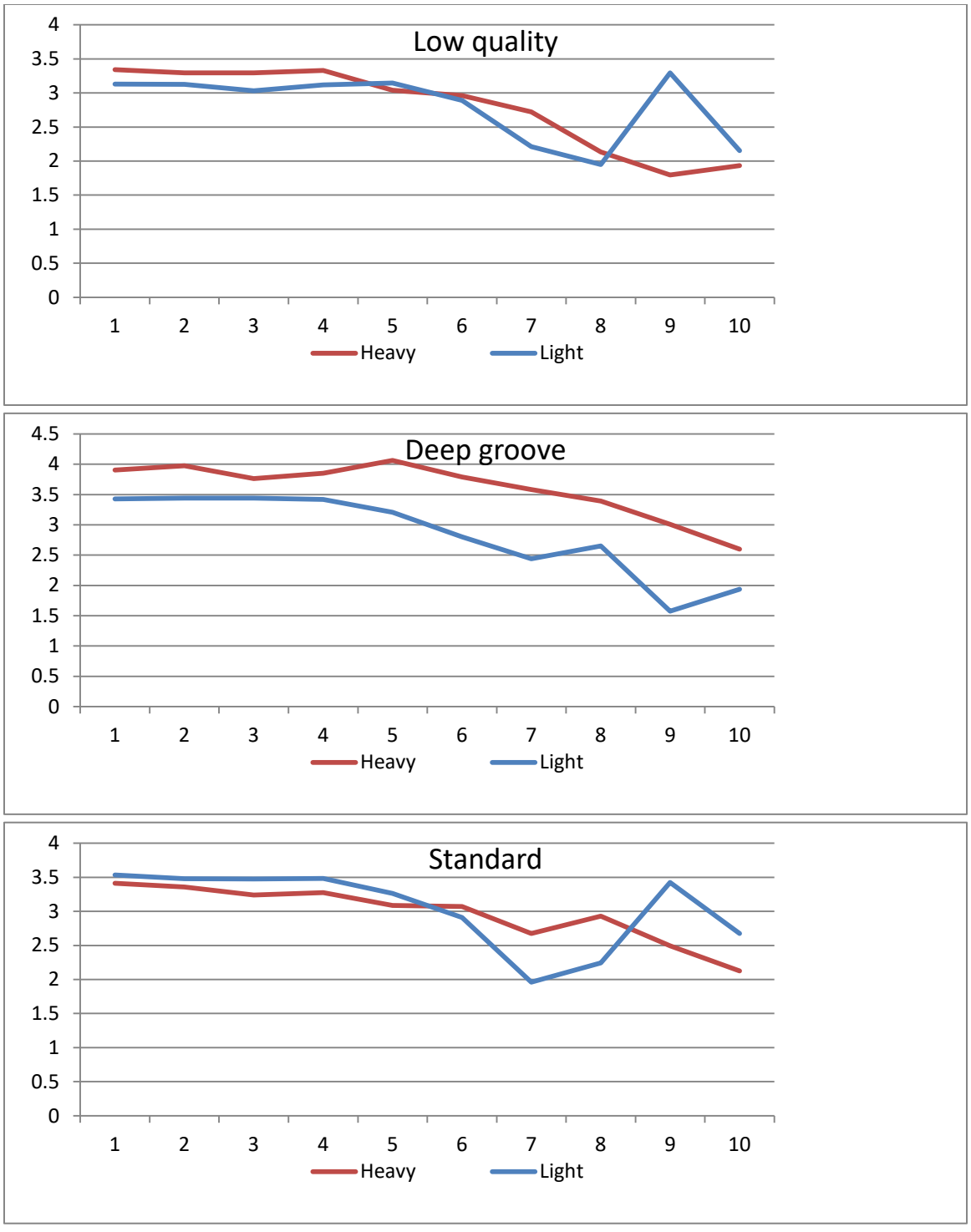

Figure 84: Large bearing at load three crest factor approximations at 2000 rpm

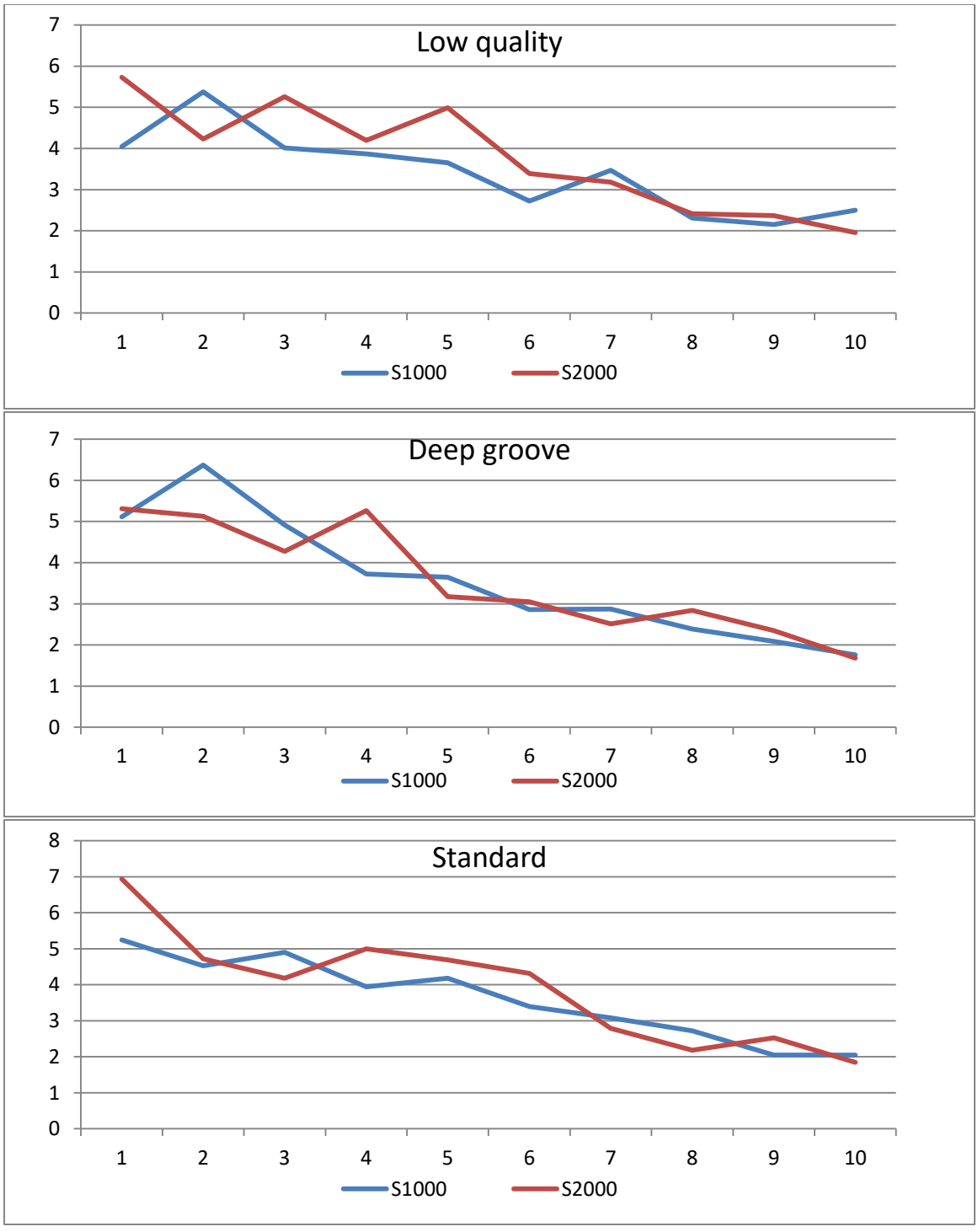

Figure 85: Large bearing at no load crest factor details in heavy oil

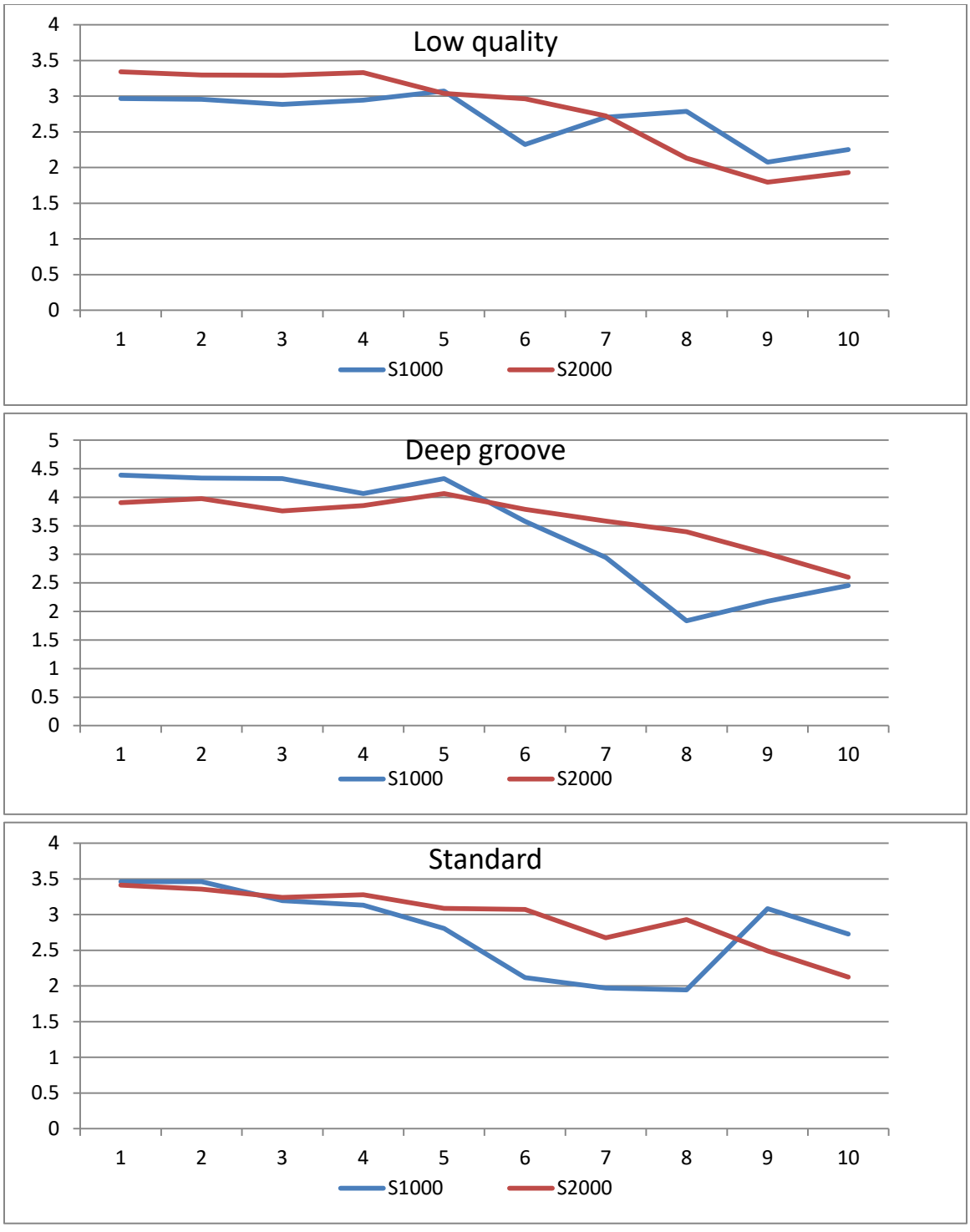

Figure 86: Large bearing at load three crest factor details in heavy oil

Chapter 5

Conclusion

Machinery requires that its rotating parts be properly supported to maintain proper position and absorb axial and radial forces. The designer has a variety options to meet these requirements but only one solution is best for a given set of circumstances. Design considerations pivot heavily on considerations such as cost, availability, ease of maintenance, expected life, etc. Under some circumstances, a designer may find the vibrational energy of a bearing to be unusually important and need recourse to aid in choosing the best bearing type. This study was undertaken to fill a gap in the literature concerning the vibrational energy of new bearings.

Historically, the science of measuring bearing vibration has been reserved for measuring the vibration signal of a defective or aging bearing. This was done to help predict bearing failure and avoid costly repairs. Aging or defective bearings are expected to produce a strong vibrational signal as defective, damaged, or worn areas interact. Conversely, with this study examining new and healthy bearings and it was quickly found that the vibrational emissions were quite weak. The bearing generated portion of a signal was similar to the noise in the signal and the two were difficult to separate form one another. This required modification to the test equipment and adopting more robust analysis methods.

The main conclusions of the test were fairly consistent with what the literature would have predicted based on related testing. In general, as load and speed were increased, the various analysis methods showed a stronger response. The bearing types performed similarly

overall with some important observations being that bearings labeled ‘low quality’ had a similar performance to those considered high quality. Also, the deep groove bearing tended to have a more dramatic reaction to a change in load or speed than other bearings in the test. The literature suggested that lubricating a bearing with higher viscosity oil would stiffen the bearing assembly as a whole and reduce dampening. The end result would be a bearing with stronger vibrational energy emission. This test found no significant difference in the vibration signal of the various bearing types with a change in lubricant viscosity. There are two theories to explain this behavior, one being that the bearings are all new and in a healthy condition and that there is little vibrations that needs to be dampened, the other being that the difference in oil viscosities in the test were too small the equipment used wasn’t sensitive enough to detect a difference in signal strength.

This test focused on a small portion of the bearing population. If deemed beneficial, additional research should be focused on gaining a better understanding of other bearing types (needle, tapered, cylindrical, etc.), materials (plastic, ceramic, etc.) combinations (face to face, back to back, etc.), mountings (self-centering, pillow block, etc.), and loadings (axial, radial, combination, etc.) and mounted (interference fit, retaining ring, etc.).

Appendix A

Sample Results for Small Bearings

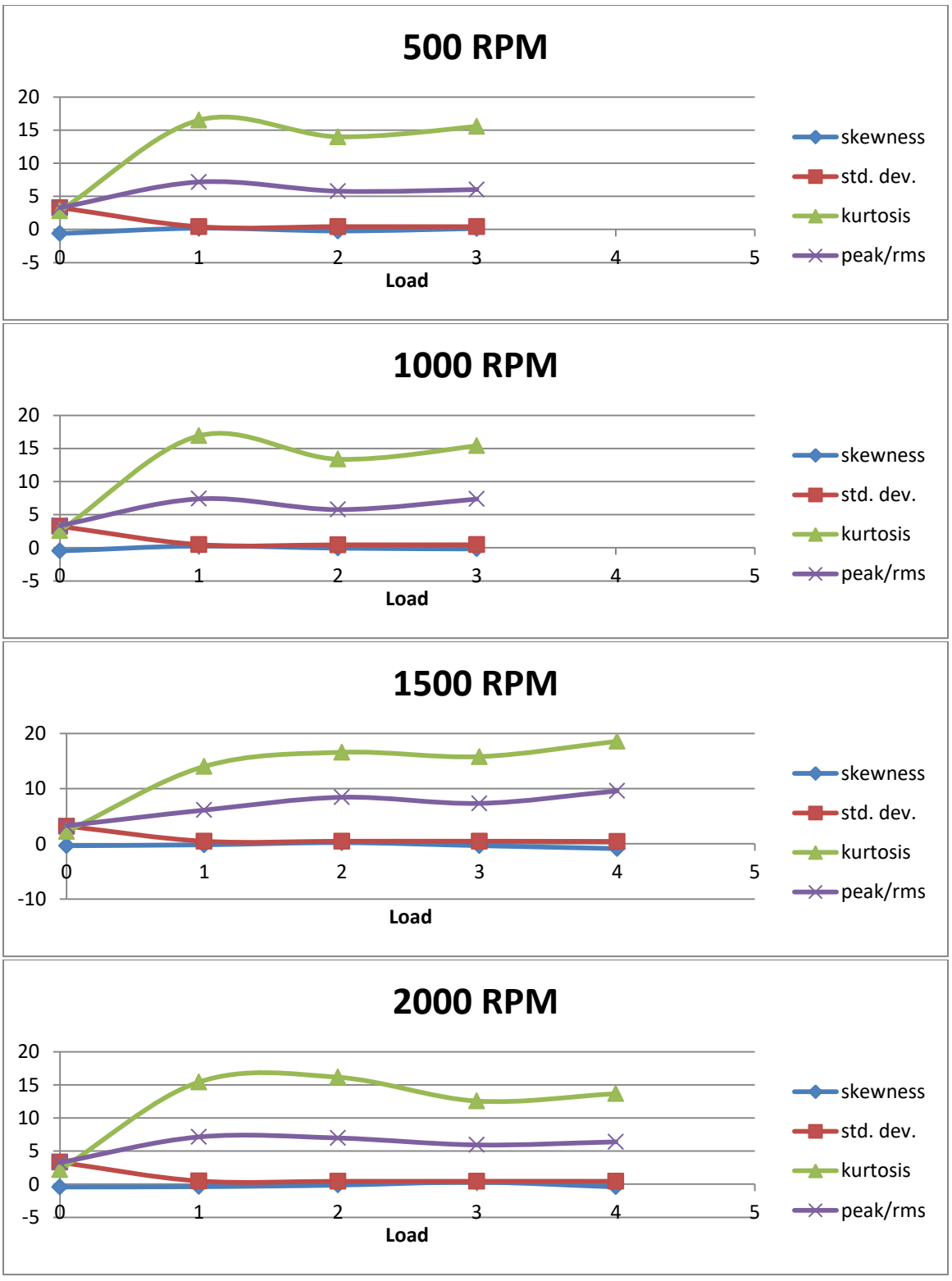

Figure A-1: Small standard bearing accelerometer parameters with thin oil as speed varied

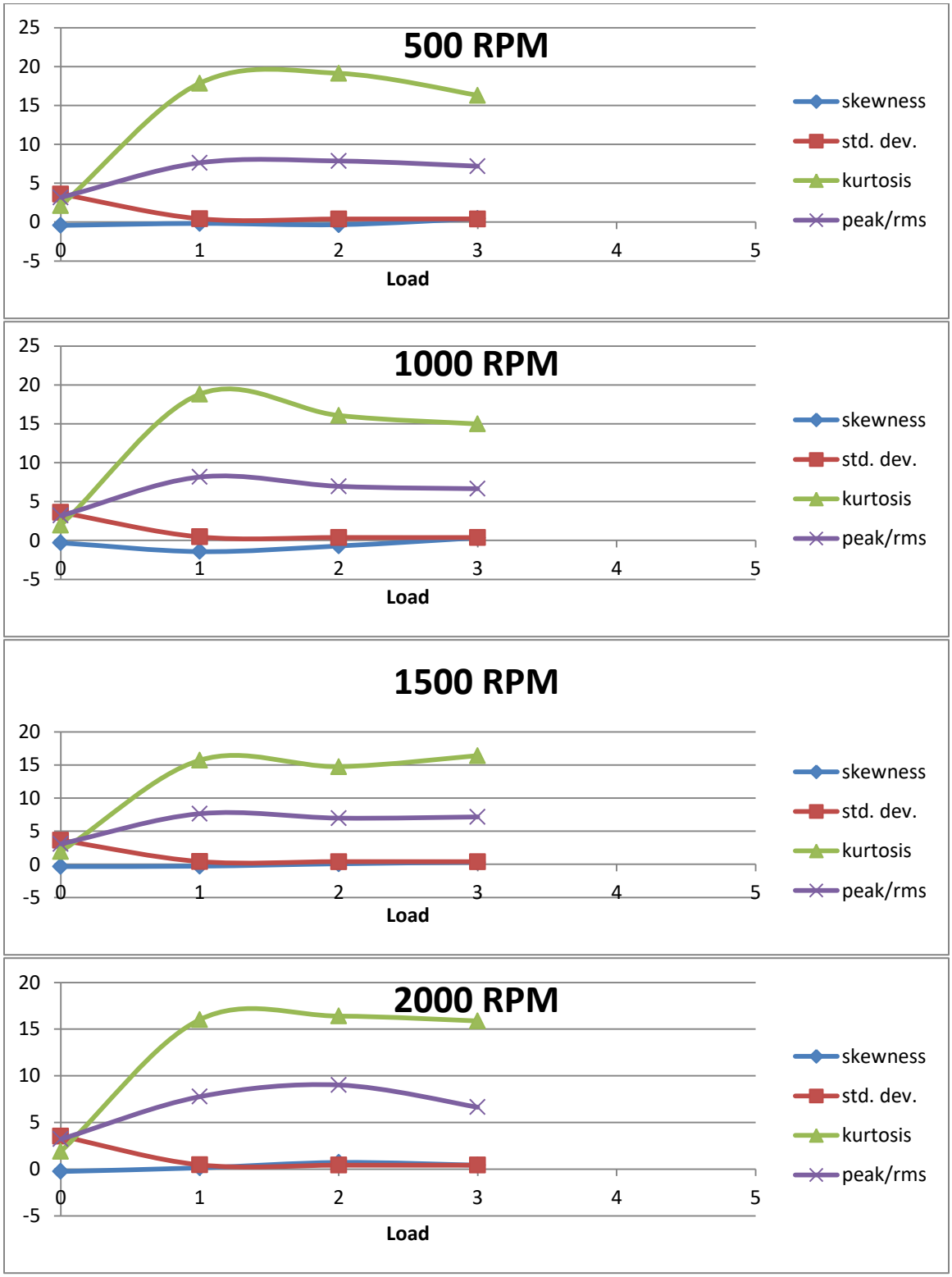

Figure A-2: Small deep groove bearing accelerometer parameters with thin oil as speed varied

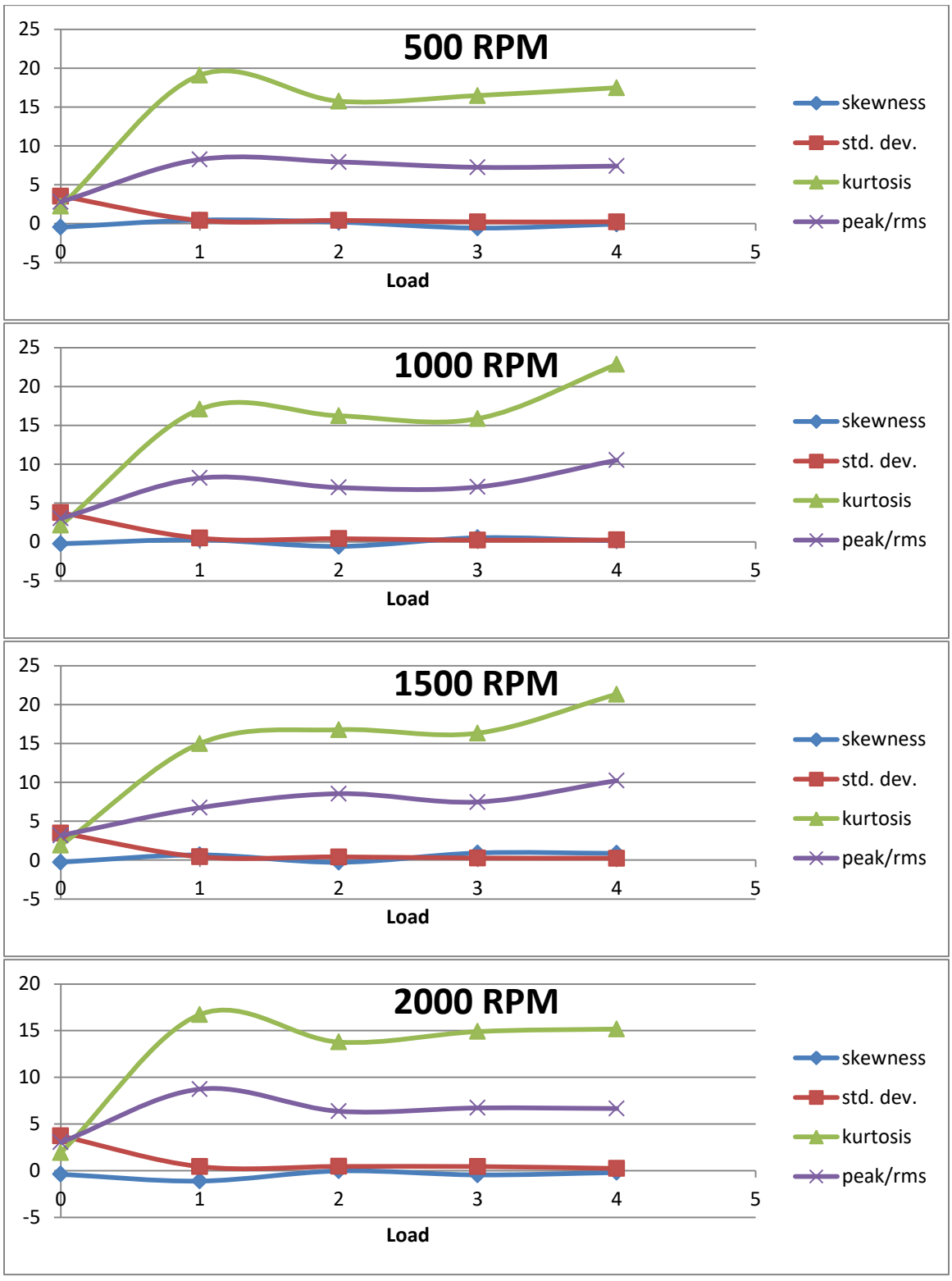

Figure A-3: Small low quality bearing accelerometer parameters with thin oil as speed varied

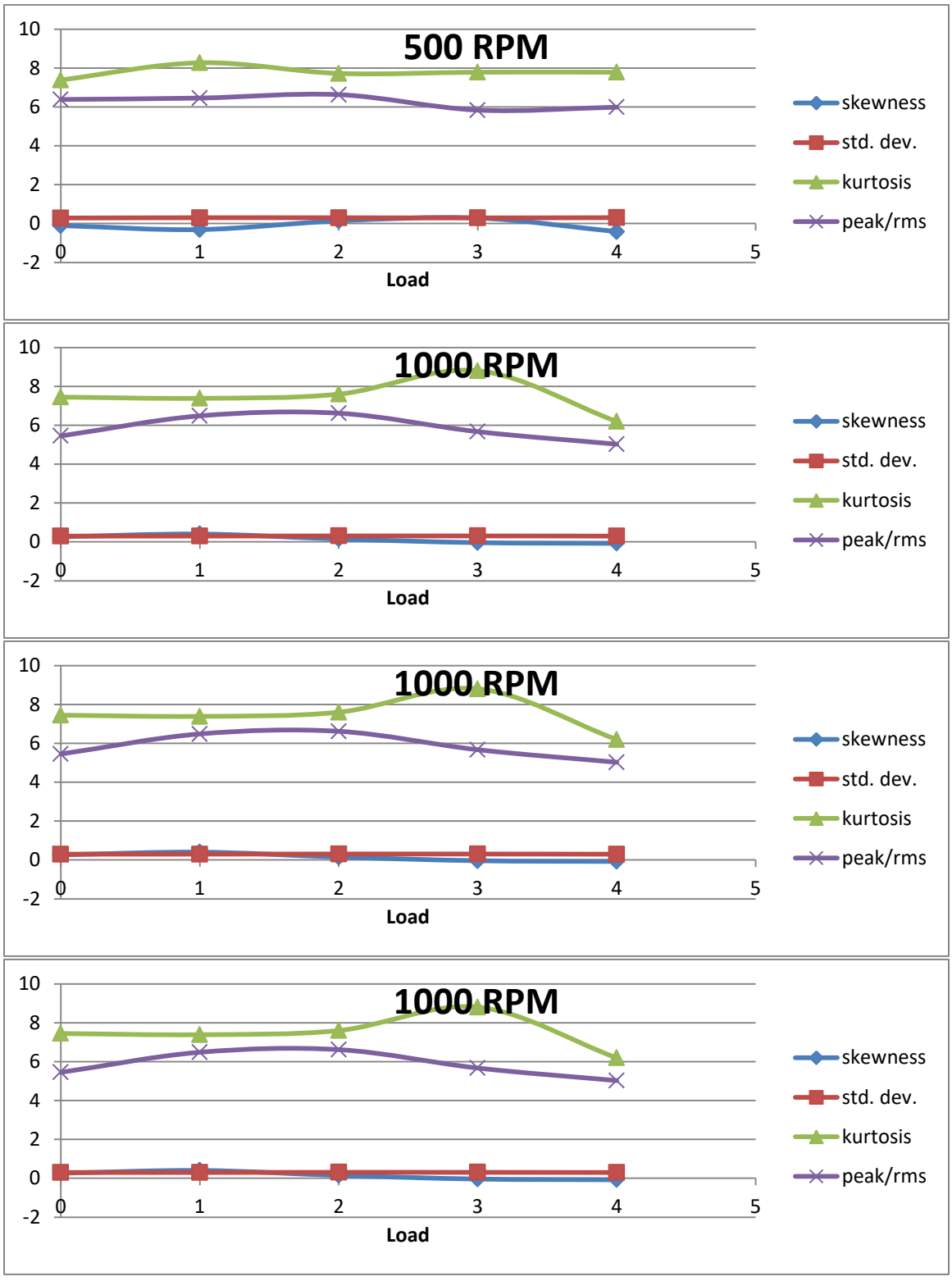

Figure A-4: Large standard bearing accelerometer parameters with thin oil as speed varied

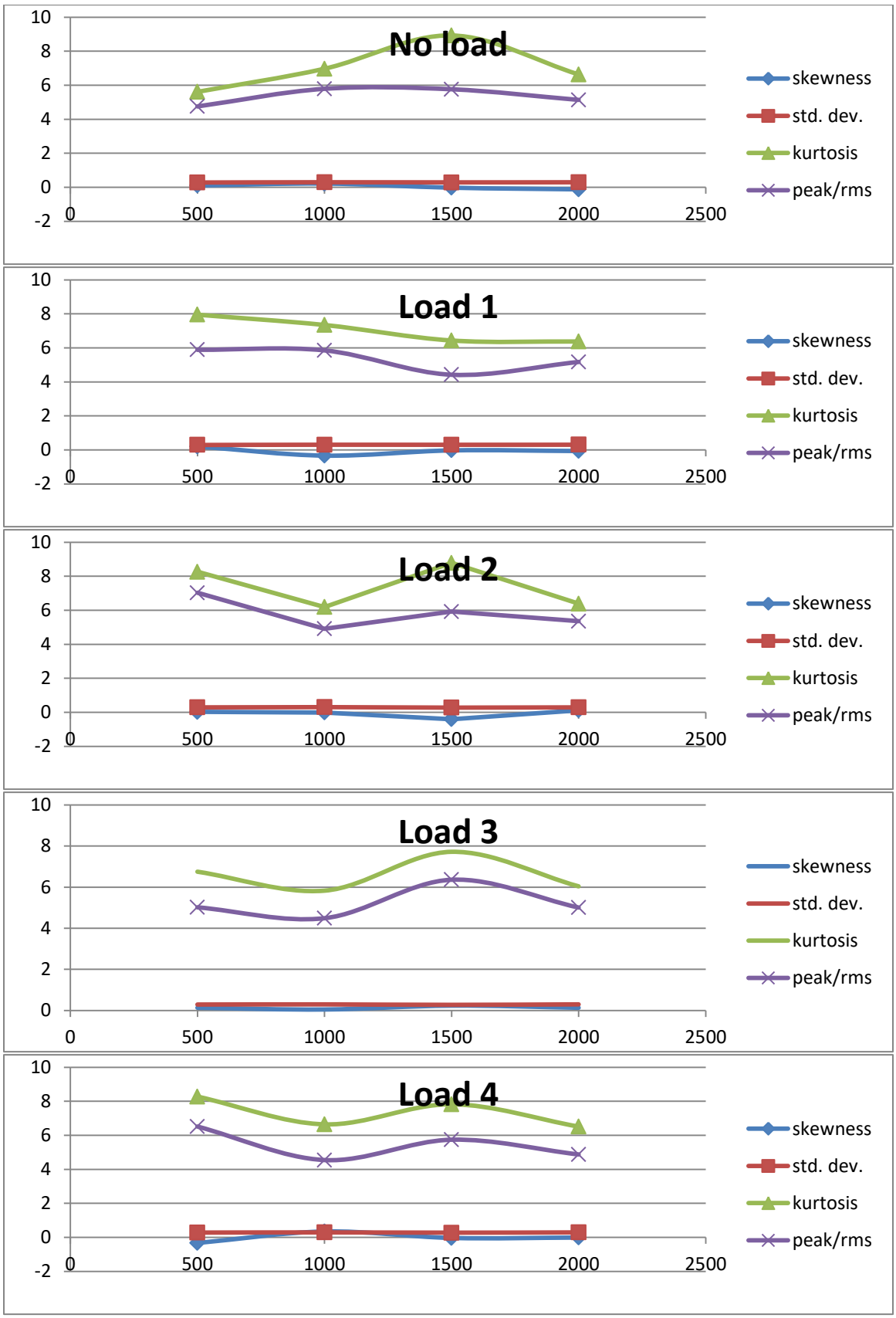

Figure A-5: Large deep groove bearing accelerometer parameters with thin oil as load varied

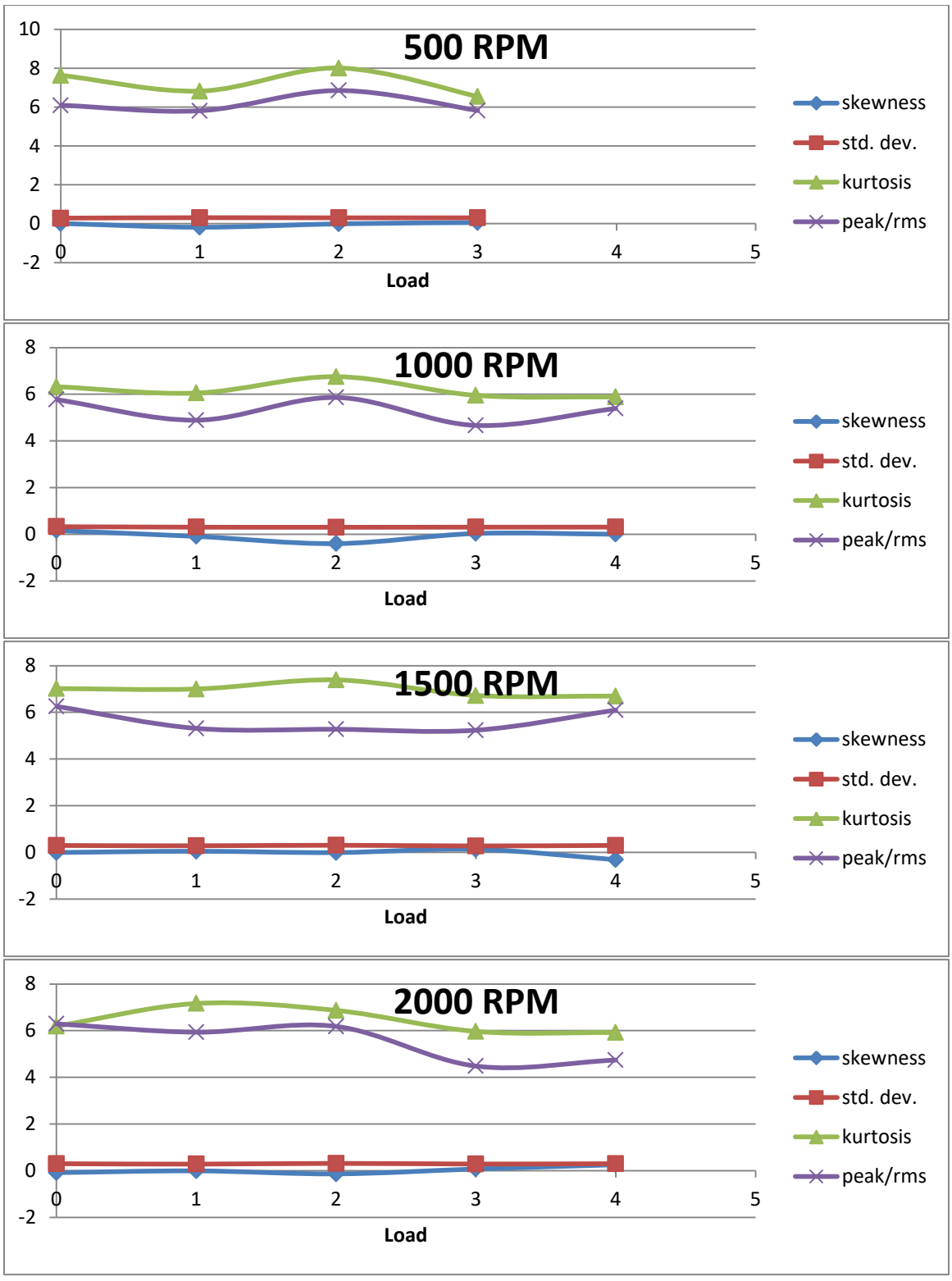

Figure A-6: Large standard bearing accelerometer parameters with thick oil as speed varied

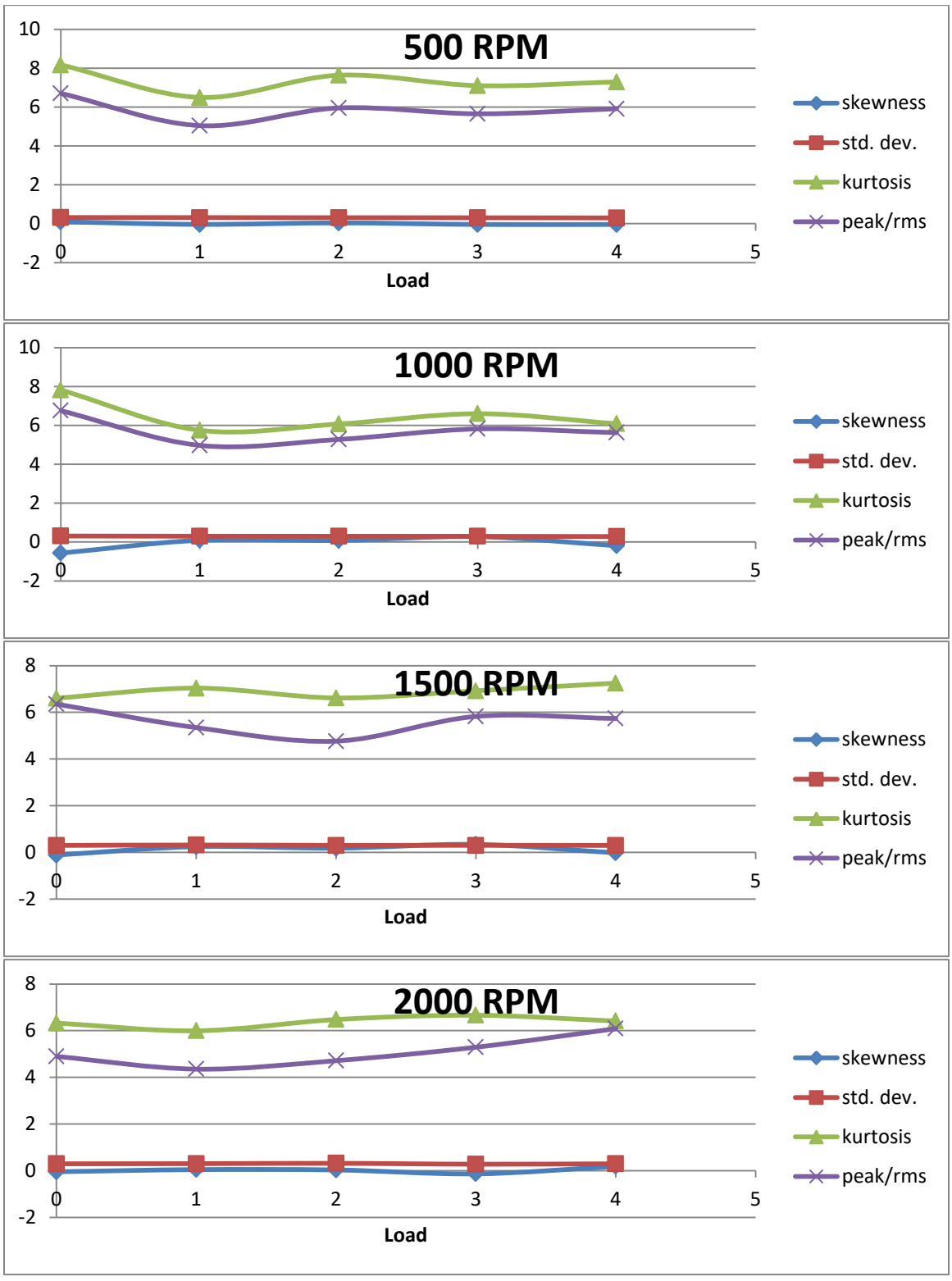

Figure A-7: Large deep groove bearing accelerometer parameters with thick oil as speed varied

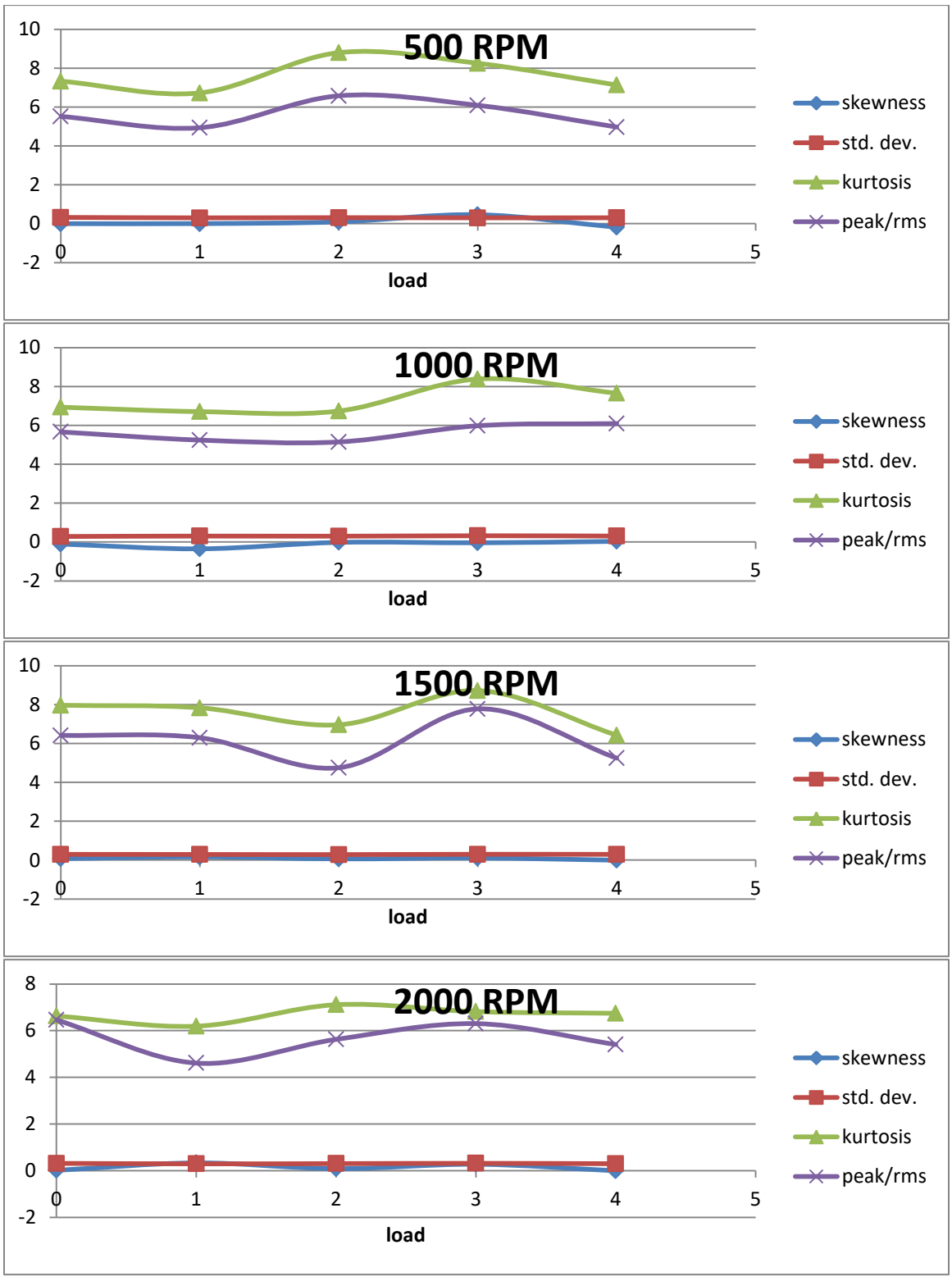

Figure A-8: Large low quality bearing accelerometer parameters with thick oil as speed varied

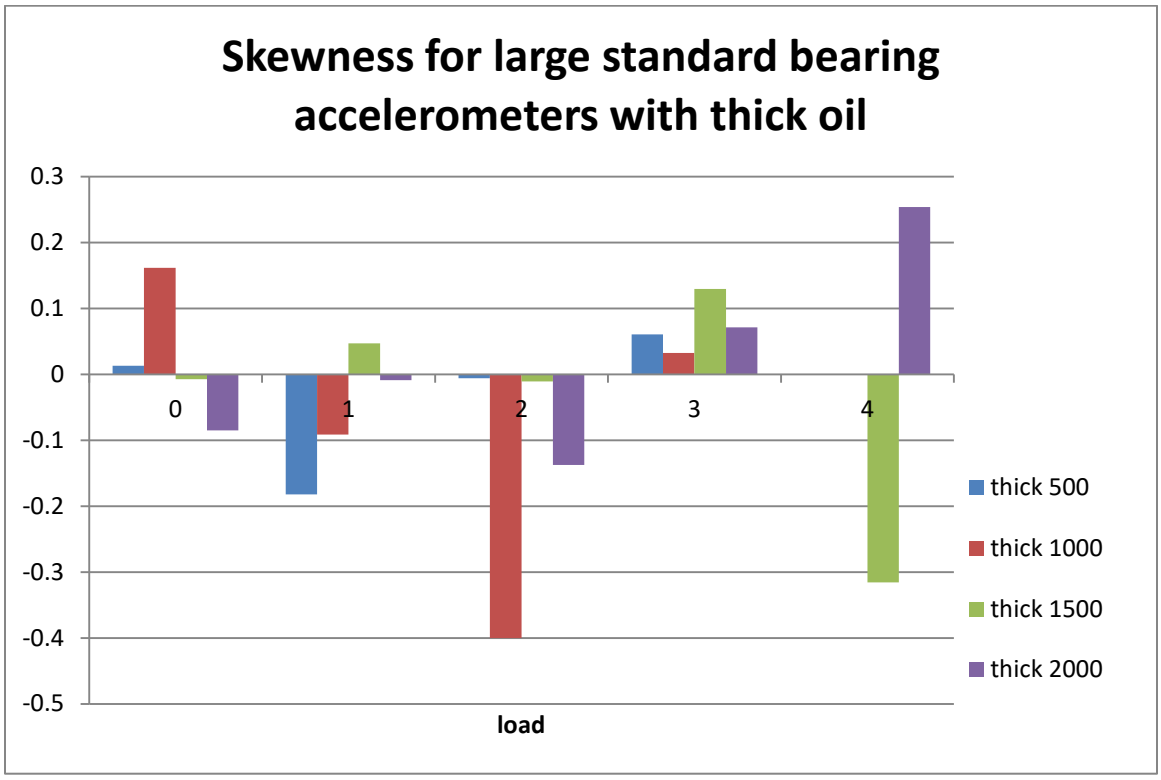

Figure A-9: Skewness for large standard bearing accelerometers with thick oil

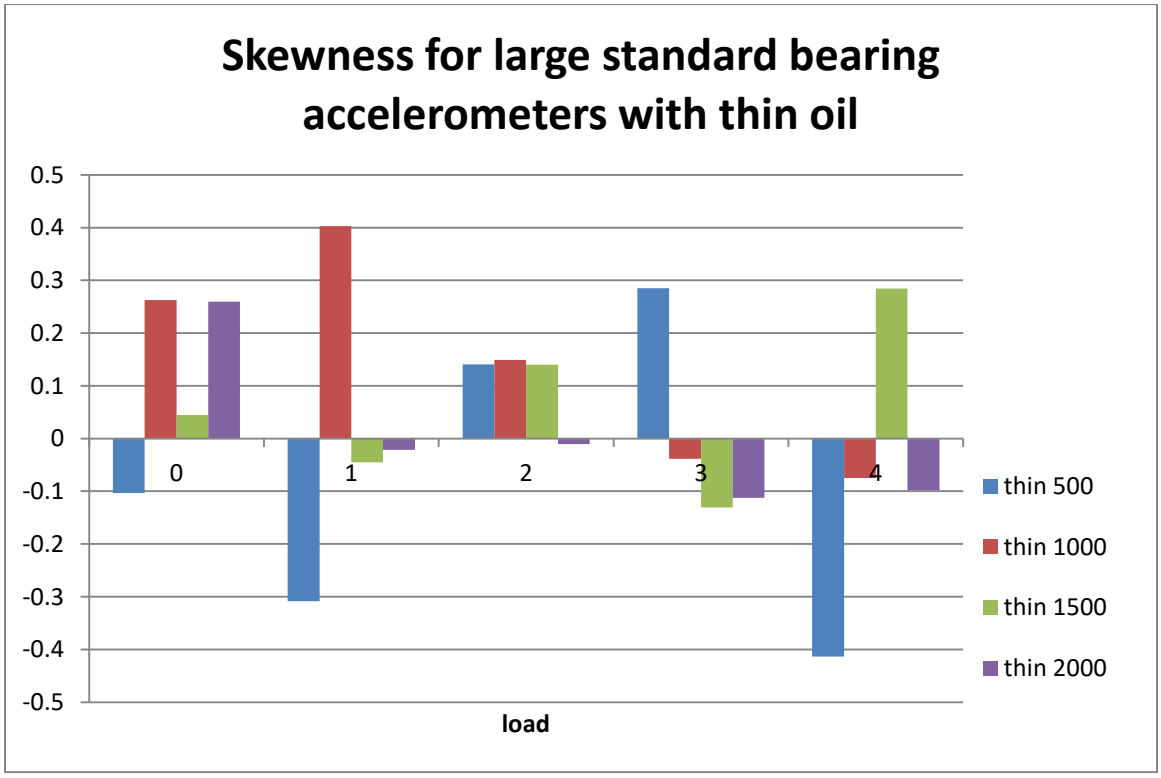

Figure A-10: Skewness for large standard bearing accelerometers with thin oil

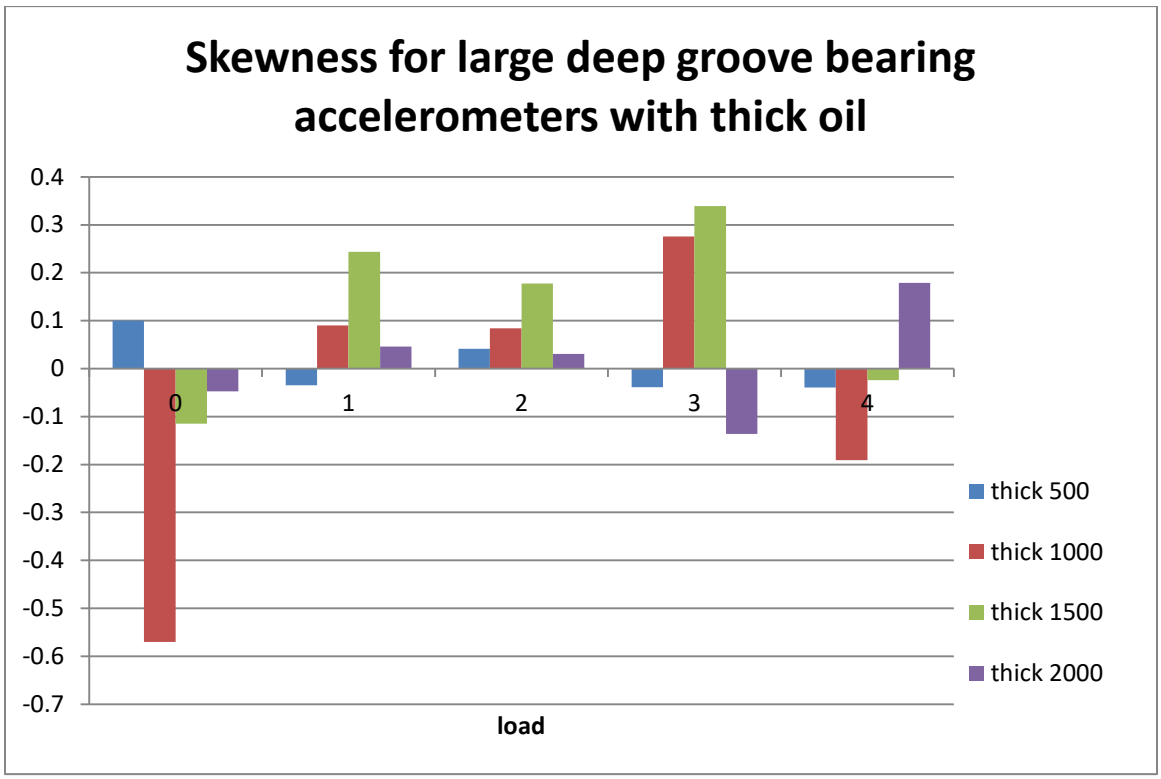

Figure A-11: Skewness for large deep groove bearing accelerometers with thick oil

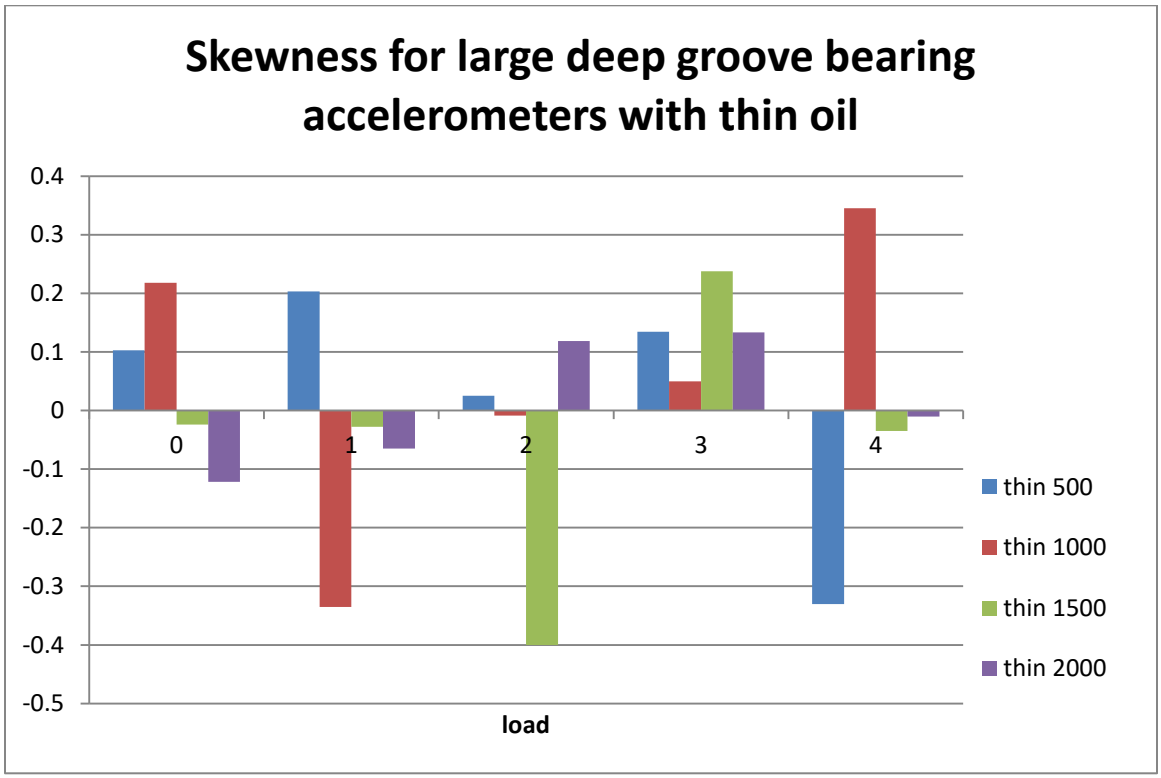

Figure A-12: Skewness for large deep groove bearing accelerometers with thin oil

Appendix B

Remaining Wavelet data not previously shown

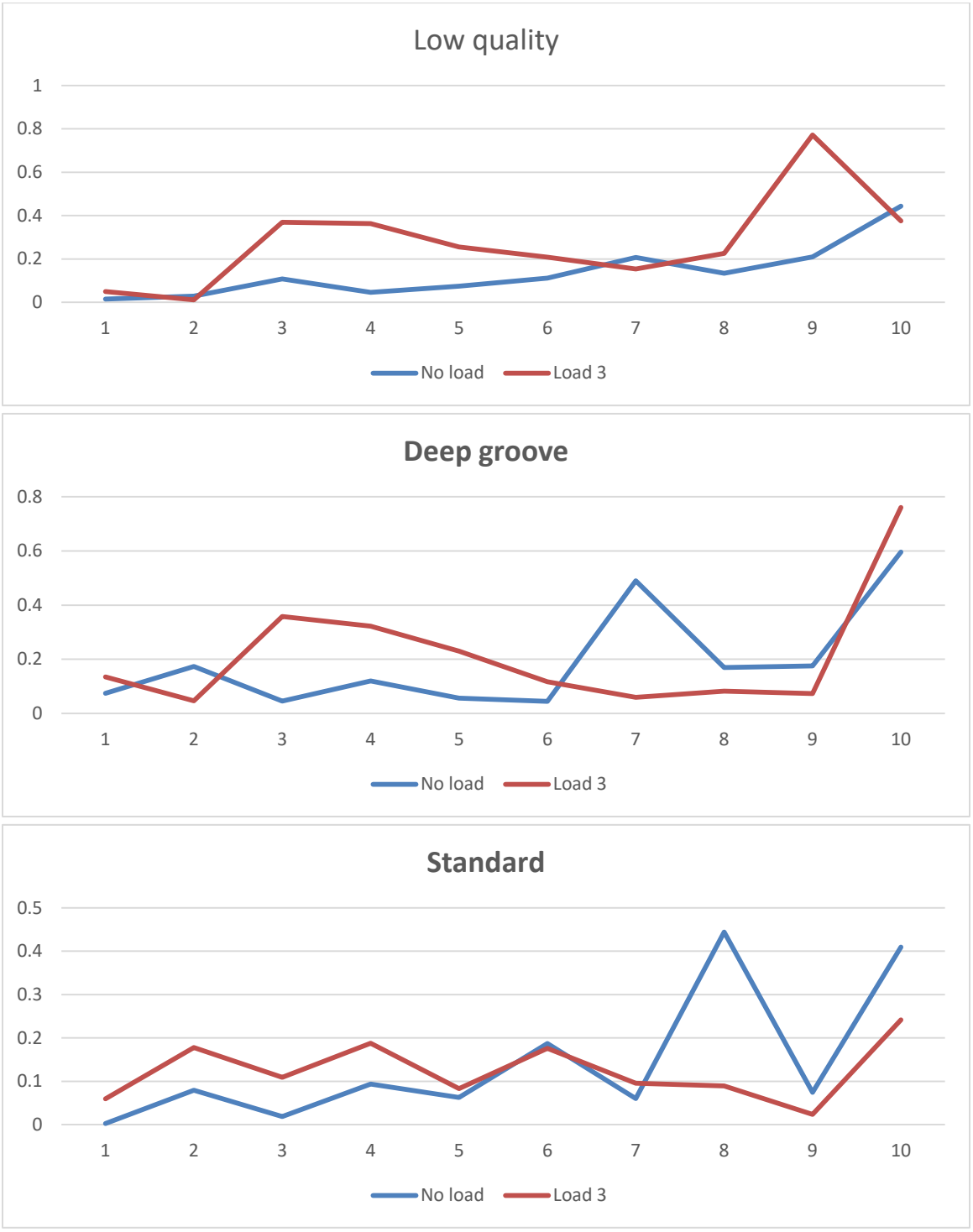

Figure B-1: Large bearing skewness details at 1000 RPM in heavy oil

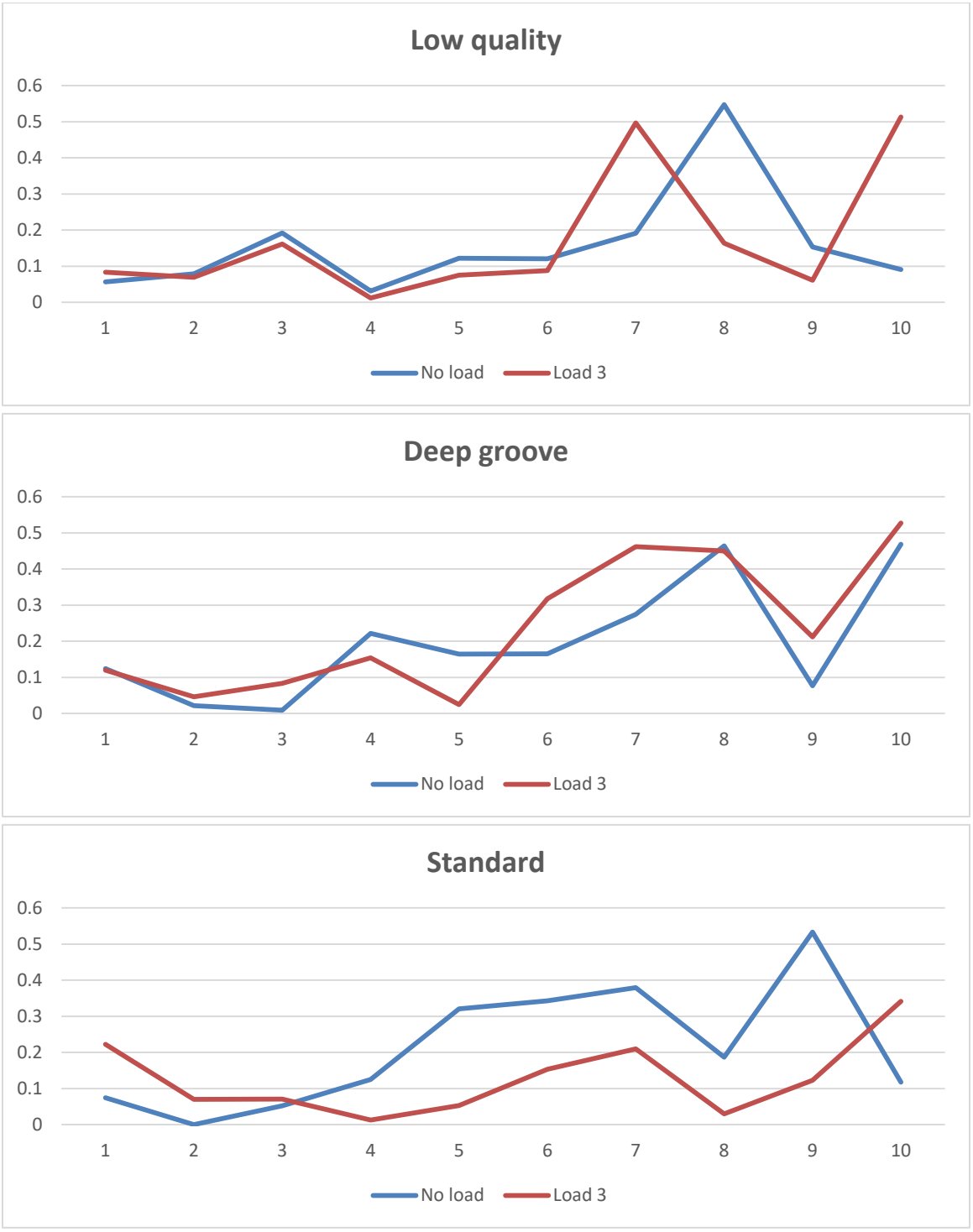

Figure B-2: Large bearing skewness details at 2000 RPM in heavy oil

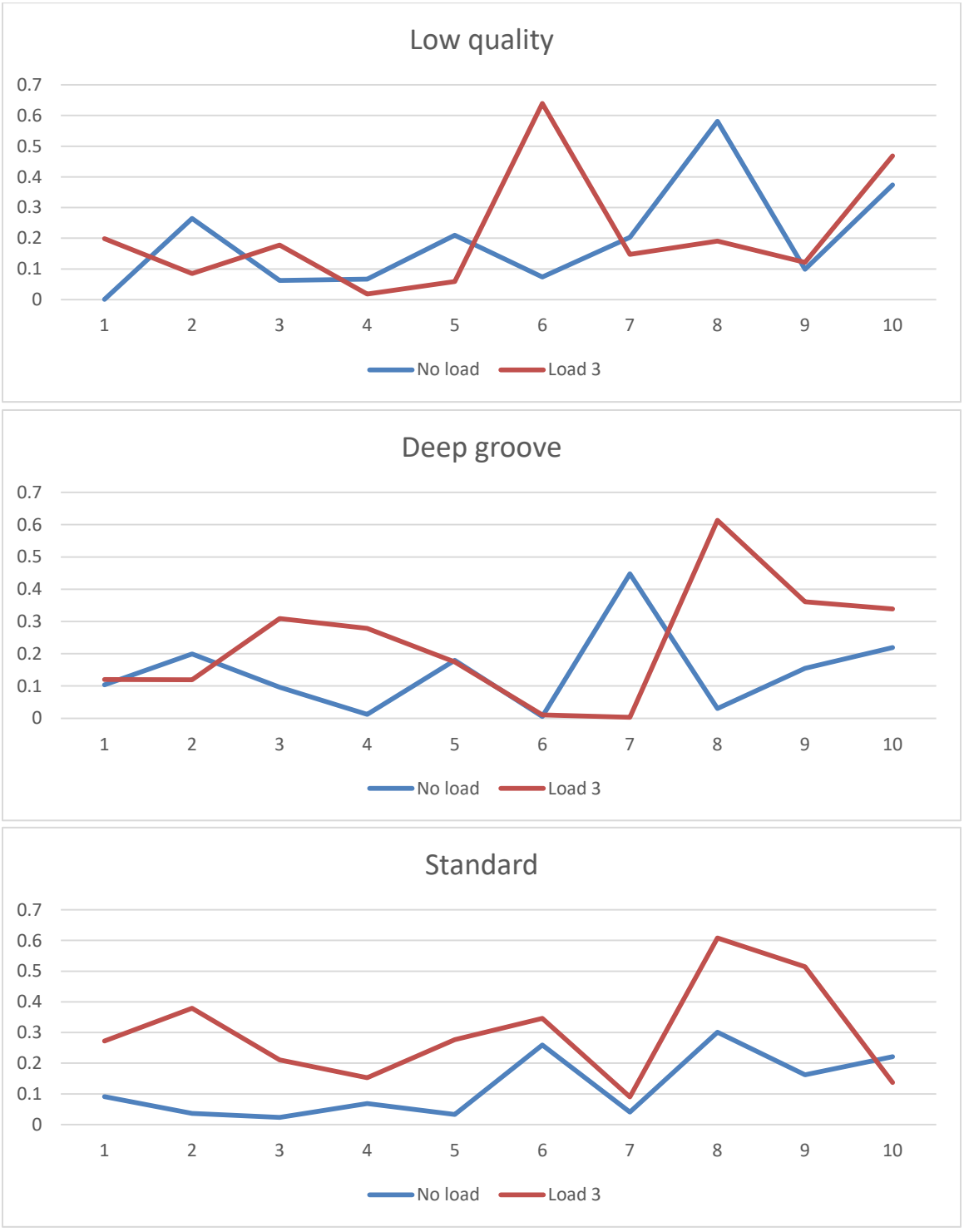

Figure B-3: Large bearing skewness details at 1000 RPM in light oil

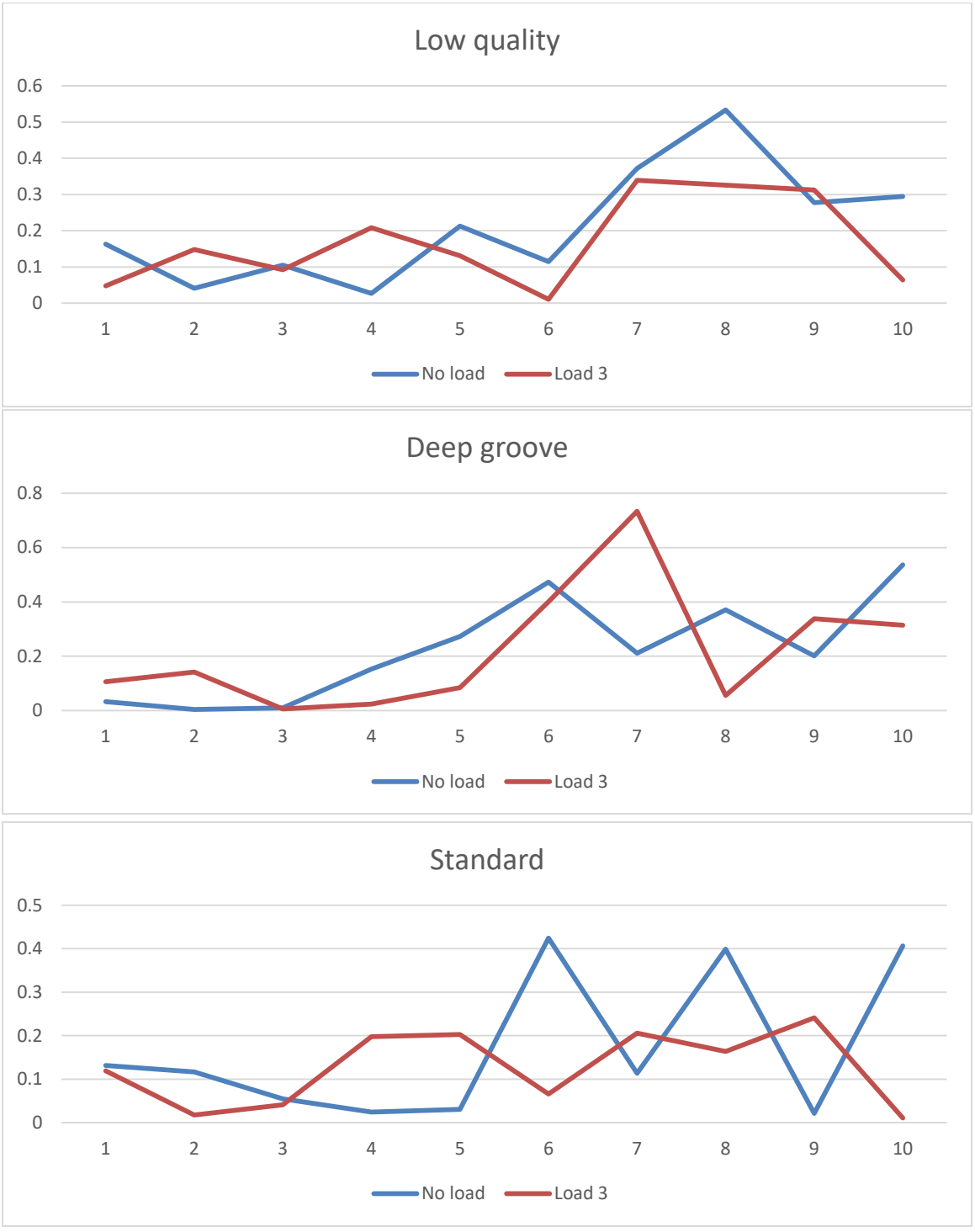

Figure B-4: Large bearing skewness details at 2000 RPM light oil

Bibliography

[1] V. Bucinskas, S. Mirzaei, K. Kirchner, “Some Aspects of Bearing Noise Generation,” *Solid State Phenomenon*, vol. 164, pp. 278-284, 2010

[2] H. Qiu, J. Lee, J. Lin, G. Yu, “Wavelet Filter-based Weak Signature Detection Method and Its Application on Rolling Element Bearing Prognostics,” *Journal of Sound and Vibration*, vol. 289, pp. 1066-1090, 2006

[3] Y. Lei, J. Lin, Z. He, Y. Zi, “Application of an Improved Kurtogram Method for Fault Diagnosis of Rolling Element Bearings,” *Mechanical Systems and Signal Processing*, vol. 25, pp. 1738-1749, 2011

[4] D. Fernandez-Francos, D. Marinez-Rego, O. Fontenla-Romero, A. Alsonso-Betanzos, “Automatic Bearing Fault Diagnostics Based on One-class v-SVM,” *Computer & Industrial Engineering*, vol. 64, pp. 357-365, 2013

[5] X. Bai, Y. Wu, I. Rosca, H. Shi, “Investigation on the Effects of the Ball Diameter Difference in the Sound Radiation of Full Ceramic Bearings,” *Journal of Sound and Vibration,* vol. 450, pp. 2321-250, 2019

[6] V. Augustaitis, V. Bucinskas, “Dependency of Bearing Noise Properties on Surfaces Lubrication,” *Mechanica*, vol. 17(4), pp. 381-386, 2011

[7] h. Shi, K. Zhang, Y. Wu, G. Yue, “Influence of Uneven Loading Condition on the Sound Radiation of Starved Full Ceramic Bearings, “ *Journal of Sound and Vibration,* vol. 461, 2019

[8] Y. Wang, G. Xu, L. Liang, K. Jiang, “Detection of Weak Transient Signals Based on Wavelet Packet Transformation and Manifold Learning for Rolling Element Bearing Fault Diagnostics,” *Mechanical Systems and Signal Processing*, vol. 54-55, pp. 259-276, 2015

[9] R. Randall, J. Antoni, “Rolling Element Bearing Diagnostics – A Tutorial,” *Mechanical Systems and Signal Processing*, vol. 25, pp. 485-520, 2011

[10] J. Liu, “A theoretical Study for the Influence of the Combined Defect on Radial Vibrations of a Ball Bearing,” *Industrial lubrication and Tribology,* vol. 70/2, pp. 339-346, 2018

[11] J. Ban, B. Rho, K, Kim, “A study on the Sound of Roller Bearings Operating Under Radial Load,” *Tribology International,* vol. 40, pp. 21-28, 2007

[12] Z. Zhao, G. Dong, H. Liu, F. Wang, M. Li, M. Jing, “High Frequency Vibration Analysis of Ball Bearings Under Radial Load,” *Journal of Multi-body Dynamics*, vol. 230(4), pp. 579-588, 2016

[13] W. Jacobs, R. Boonen, P. Sas, D. Moens, “The Influence of the Lubricant Film on the Stiffness and Dampening Characteristics of a Deep Groove Ball Bearing,” *Mechanical Systems and Signal Processing,* vol. 42, pp. 235-250, 2014

[14] M. Braun, W. Hannon, “Cavitation Formation and Modeling for Fluid Film Bearings: A Review,” *Journal of Engineering Tribology,* vol. 224, part J, Special Issue Paper 839, 2010

[15] F. Immovilli, M. Cocconcelli, “Experimental Investigation of Shaft Radial Load Effect on Bearing Fault Signatures Detection,” *IEEE transactions on Industry Application,* vol. 53, no. 3, pp. 2721-2728, 2017

[16] A. Sharma, M. Amarnath, P. Kankar, “Feature Extraction and Fault Severity Classification in Ball Bearings,” *Journal of Vibration and Control,* vol. 22(1), pp. 176-172, 2014